

Summer 9-2019

Multimode Nonlinear Vibration Analysis of Stiffened Functionally Graded Double Curved Shells in a Thermal Environment

Boutros Azizi
Embry-Riddle Aeronautical University

Follow this and additional works at: <https://commons.erau.edu/edt>



Part of the [Aerospace Engineering Commons](#)

Scholarly Commons Citation

Azizi, Boutros, "Multimode Nonlinear Vibration Analysis of Stiffened Functionally Graded Double Curved Shells in a Thermal Environment" (2019). *Doctoral Dissertations and Master's Theses*. 469.
<https://commons.erau.edu/edt/469>

This Dissertation - Open Access is brought to you for free and open access by Scholarly Commons. It has been accepted for inclusion in Doctoral Dissertations and Master's Theses by an authorized administrator of Scholarly Commons. For more information, please contact commons@erau.edu.

MULTIMODE NONLINEAR VIBRATION ANALYSIS OF STIFFENED
FUNCTIONALLY GRADED DOUBLE CURVED SHELLS IN A THERMAL
ENVIRONMENT

A Dissertation

Submitted to the Faculty

of

Embry-Riddle Aeronautical University

by

Boutros Azizi

In Partial Fulfillment of the

Requirements for the Degree

of

Doctor of Philosophy in Aerospace Engineering

September 2019

Embry-Riddle Aeronautical University

Daytona Beach, Florida

**MULTIMODE NONLINEAR VIBRATION ANALYSIS OF STIFFENED
FUNCTIONALLY GRADED DOUBLE CURVED SHELLS IN A THERMAL
ENVIRONMENT**

By

Boutros Azizi

This dissertation was prepared under the direction of the candidate's Dissertation Committee Chairman, Dr. Habib Eslami, Department of Aerospace Engineering, and has been approved by the members of the dissertation committee. It was submitted to the Office of the Senior Vice President for Academic Affairs and Provost and was accepted in partial fulfillment of the requirements for the Degree of Doctor of Philosophy in Aerospace Engineering

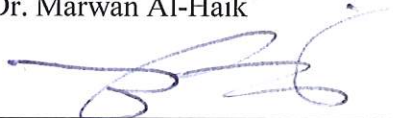
DISSERTATION COMMITTEE


Chairman, Dr. Habib Eslami


Member, Dr. John Ekaterinaris

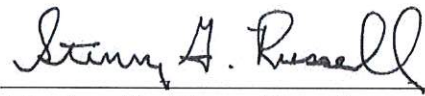

Member, Dr. Jeff Brown

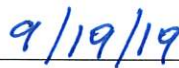

Graduate Program Coordinator,
Dr. Marwan Al-Haik


Dean of College of Engineering,
Dr. Maj Mirmirani

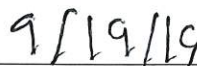

Senior Vice President for Academic
Affairs and Provost, Dr. Lon Moeller


Member, Dr. Ali Tamijani


Member, Dr. Steven Russell


Date


Date


Date

DEDICATION

This dissertation is dedicated to my beloved family. My parents, Joseph and Lamita, and my sisters Lati, Joyce and Joya, for their unconditional love and their endless support and encouragement.

ACKNOWLEDGMENTS

It gives me pleasure to acknowledge the people for all the support and strength they gave me which made this dissertation possible. I like to express the deepest appreciation to my committee chair, Dr. Habib Eslami for his guidance, supervision, and above all, the moral support for the last four years. Throughout my dissertation work, he encouraged me to develop independent thinking and foster a stress-free working relationship which was crucial for the completion of this work.

I want to thank my committee members, Dr. Ali Tamijani, Dr. John Ekaterinaris, Dr. Jeff Brown and Dr. Steven Russell for all their advice and constructive suggestions.

I like to express deep appreciation to my friends, Audrey, Suma, Rossana, Kaveh, Chitrang, Pierrot, Sandeep, Claudia, Madhur and Patricia for their support and encouragement throughout my Ph.D. Program.

I would like to share this achievement with Brooke, my girlfriend, for her love, motivation, support, and faith in me. Finally, I like to thank my relatives for all the support they gave me.

TABLE OF CONTENTS

LIST OF TABLES	vii
LIST OF FIGURES	ix
SYMBOLS.....	xiii
ABBREVIATIONS	xviii
ABSTRACT.....	xix
1. Introduction	1
1.1 Literature Survey	1
1.2 Scope.....	10
2. Functionally Graded Materials Double Curved Shells	13
2.1 Modeling.....	13
2.2 Material Properties.....	14
3. Single Mode Theoretical Formulation	19
3.1 Governing Equations	19
3.2 Constitutive Relations.....	21
3.3 Equations of Motion	26
3.4 Solution Procedures	27
3.4.1 Linear Vibration Analysis Solution	30
3.4.2 The solution of Nonlinear Static Equations.....	30
3.4.3 The solution of Nonlinear Dynamic Equations	31
3.4.4 Amplitude – Frequency Curve.....	32
3.5 Numerical Results Validation and Discussion.....	34
3.5.1 Natural Frequency Results.....	35
3.5.2 Nonlinear Static Analysis Results.....	41
3.5.3 Nonlinear Dynamic Analysis Results	45
3.5.4 Nonlinear Frequency Response	51
4. Temperature Variation And Thermal Buckling	58
4.1 Temperature Variation	58
4.1.1 Uniform Temperature Rise	58
4.1.2 Linear Temperature Rise.....	58
4.1.3 Nonlinear Temperature Rise	59
4.2 Thermal Buckling	60
4.2.1 Buckling Under Uniform Temperature Rise.....	61
4.2.2 Buckling Under Linear Temperature Change Across The Thickness	62
4.2.3 Buckling Under Nonlinear Temperature Change Across the Thickness	63
4.3 Numerical Results.....	64
4.3.1 Critical Buckling Temperature Variation	65
4.3.2 Natural Frequency Results in Thermal Environment	68
4.3.3 Thermomechanical Static Analysis Results.....	70
4.3.4 Amplitude - Frequency Response Under Thermal Load	72
5. Multimode Theoretical Formulation	74

5.1	Kinetic and Elastic Strain Energy	74
5.2	Boundary Conditions	76
5.3	Linear Analysis	79
5.4	Nonlinear Analysis.....	81
5.5	Numerical Results.....	84
5.5.1	Validation of the Multimodal Formulation.....	85
5.5.2	Results and Discussions.....	92
6.	Conclusion And Future Work.....	96
6.1	Conclusion	96
6.2	Future Work	97
	REFERENCES	98
	APPENDIX.....	106

LIST OF TABLES

Table	Page
3.1 Material Properties of the FGM Shell (Reddy & Chin, 1998).....	33
3.2 Comparison of Dimensionless Frequency $\varpi = \omega_{mn}b\sqrt{\rho_m(1 - \nu^2)/E_m}$ for Isotropic Cylindrical Panels ($h = 0.001, R/b = 10$).....	34
3.3 Comparison of Fundamental Natural Frequency Parameter $\varpi = \omega_{mn}h\sqrt{\rho_c/E_c}$	35
3.4 Comparison of Fundamental Natural Frequency Parameter $\varpi = \omega_{mn}h\sqrt{\rho_c/E_c}$ of Stiffened and Un-Stiffened Al/Al ₂ O ₃ Spherical Panels ($a = b = 0.8\text{m}, h = 0.01\text{m}, h_x = h_y = 0.05\text{m}, b_x = b_y = 0.0025\text{m}, d_x = d_y = 0.1\text{m}$).....	36
3.5 Comparison of First 5 Modes Natural Frequency Parameters $\varpi = \omega_{mn}h\sqrt{\rho_c/E_c}$ of Stiffened and Un-Stiffened Al/Al ₂ O ₃ FGM Spherical Shallow Shell ($a = b = 0.8\text{m}, h = 0.01\text{m}, h_x = h_y = 0.05\text{m}, b_x = b_y = 0.0025\text{m}, d_x = d_y = 0.1\text{m}, R_x = R_y = 5\text{m}, K = 1$).	37
3.6 Natural Frequency of a Rectangular Aluminum Plate with Longitudinal, Transversal and Orthogonal Stiffeners ($a/b = 2, h = 0.025\text{m}, h_x = h_y = 0.05\text{m}, b_x = b_y = 0.03\text{m}$).....	38
3.7 Natural Frequency of a Rectangular Al/ZrO ₂ Plate with Longitudinal, Transversal and Orthogonal Stiffeners ($a/b = 2, h = 0.025\text{m}, h_x = h_y = 0.05\text{m}, b_x = b_y = 0.03\text{m}$).....	39
3.8 Comparison of Non-Dimensional Deflection of Simply Supported Plate Under Static Bi-Sinusoidal Transverse Loading ($10h^3E_cw/a^4q_0$).....	40
3.9 Practical Behavior of Amplitude Frequency Curve of Forced Nonlinear Vibration of Stiffened and Unstiffened FGM Spherical Shell.....	54
4.1 Critical Buckling Thermal Load for Stiffened FGM Cylindrical Shell Subjected to Nonlinear Temperature Rise with Temperature Dependent Properties ($R_x = 2, h = 0.01\text{m}$).....	67
4.2 Comparison of Dimensionless Frequencies ($\Omega = \varpi_L(a^2/h)[\rho_0(1 - \nu^2)/E_0]^{1/2}$ for Si ₃ N ₄ /SUS304 Plate Under Thermal Load ($a=b=0.2\text{m}, h=0.3\text{m}$).....	68

Table	Page
5.1 Comparison of Dimensionless In-Plane Frequency $\bar{\omega} = \omega_{mn}a^3\sqrt{\rho h/D}$ for Isotropic Rectangular Plate (h=0.001, R/b=10).....	84
5.2 Comparison of Dimensionless In-Plane Frequency $\bar{\omega} = \omega_{mn}a^3\sqrt{\rho h/D}$ for Isotropic Rectangular Plate (h=0.001, R/b=10).....	85
5.3 Dimensionless in Plane Frequency $\bar{\omega} = \omega_{mn}a^3\sqrt{\rho h/D}$ for Isotropic Rectangular Plate (h=0.001, R/b=10, a/h=30).....	85
5.4 Generalized Coordinates Combination.....	86
5.5 Generalized Coordinated Combination for the FGM Double Curved Shell.....	90

LIST OF FIGURES

Figure	Page
2.1 A double curved shell with configurations and dimensions of transversal stiffeners.....	12
2.2 Effect of power index “K” on the variation in the ceramic volume fraction V_c through the shell thickness	14
2.3 Young’s modulus variations with respect to the dimensionless thickness of the shell for different volume fraction indices ($E_{Al} = 70\text{GPa}$ and $E_{ZrO_2} = 151\text{GPa}$).....	17
3.1 Frequency and mode shapes of a stiffened rectangular Aluminum plate using ABAQUS.....	38
3.2 Frequency and mode shapes of a stiffened rectangular Al/ZrO ₂ plate using ABAQUS.....	39
3.3 Comparisons of nonlinear load-deflection curves with different index K for cylindrical shells ($a/b=1$, $b/h=20$, $h=0.01$, $a/R_y=0.2$).....	41
3.4 Effect of volume fraction exponent K and imperfection μ on the nonlinear response of cylindrical shells ($a/b=1.1$, $b/h=50$, $h=0.01\text{m}$, $a/R_y=0.5$).....	42
3.5 Effect of length to width ratio and imperfection μ on the nonlinear response of cylindrical shells ($b/h=30$, $a/R_y=0.5$, $k=1$).....	42
3.6 Effect of width to thickness ratio and imperfection μ on the nonlinear response of cylindrical shells ($a/b=1$, $a/R_y=0.5$, $K=1$).....	43
3.7 Effect of length to radius ratio and imperfection μ on the nonlinear response of cylindrical panels ($a/b=1$, $b/h=30$, $K=1$).....	44
3.8 Nonlinear responses of stiffened and unstiffened spherical shells ($a=b=0.8\text{m}$, $h=0.01\text{m}$, $q(t)=10^5 \sin(100t)$, $K=1$, $R_x=R_y=5\text{m}$).....	45
3.9 Linear and Nonlinear responses of stiffened and unstiffened spherical shells ($a=b=0.8\text{m}$, $h=0.01\text{m}$, $q(t)=10^5 \sin(100t)$, $K=1$, $R_x=R_y=5\text{m}$).....	45
3.10 Harmonic beat phenomenon of a stiffened spherical shell with different excitation frequencies Ω ($a=b=0.8\text{m}$, $h=0.01\text{m}$, $R_x=R_y=5\text{m}$, $K=1$).....	46

Figure	Page
3.11 Effect of excitation loads on the harmonic beat phenomenon of stiffened spherical shells ($a=b=0.8\text{m}$, $h=0.01\text{m}$, $R_x=R_y=5\text{m}$, $q(t)=Q\sin(2650t)$, $K=1$).....	46
3.12 Effect of power-law index K on the nonlinear response of stiffened cylindrical shell ($a=b=0.8\text{m}$, $q(t)=10^5 \sin(100t)$, $h=0.01\text{m}$, $R_y=5\text{m}$	47
3.13 Effect of width to thickness ratio on the nonlinear response of stiffened cylindrical shell ($a/b=1$, $q(t)=10^5 \sin(100t)$, $h=0.01\text{m}$, $R_y=5\text{m}$, $K=1$)....	48
3.14 Effect of length to width ratio on the nonlinear response of stiffened cylindrical shell ($b/h=80$, $q(t)=10^5 \sin(100t)$, $h=0.01\text{m}$, $R_y=5\text{m}$, $K=1$).	49
3.15 Effect of excitation loads on the nonlinear response of stiffened cylindrical shell ($b/a=1$, $b/h=80$, $\Omega=100 \text{ rad/s}$, $h=0.01\text{m}$, $R_y=5\text{m}$, $K=1$).....	49
3.16 Backbone for a square simply supported immovable Aluminum plate ($a = b = 0.3\text{m}$, $h = 0.001\text{m}$, $E = 70 \text{ GPa}$, $\rho = 2778 \text{ kg/m}^3$, $\nu = 0.3$).....	50
3.17 The frequency-amplitude curve of nonlinear vibration of an immovable Aluminum plate under $F = 1.74\text{N}$ and $\zeta = 0.065$	51
3.18 Backbone curve for square simply-supported immovable SUS304/SI3N4 plate.....	51
3.19 The frequency-amplitude curve of nonlinear vibration of immovable SUS304/SI ₃ N ₄ plate under $\bar{f} = f_b/h\omega^2 = 0.03$ and $\zeta = 0.01$	52
3.20 The frequency-amplitude curve of free nonlinear vibration of stiffened and unstiffened Al/Al ₂ O ₂ spherical shell $R_x = R_y = 5\text{m}$, $a = b = 0.8\text{m}$, $h = 0.025\text{m}$, $K = 1$	53
3.21 The frequency-amplitude curve of forced nonlinear vibration of stiffened and unstiffened Al/Al ₂ O ₂ spherical shell $R_x = R_y = 5\text{m}$, $a = b = 0.8\text{m}$, $h = 0.025\text{m}$, $K = 1$ and $\zeta = 0.01$ under uniformly distributed load $Q = 10^5\text{Pa}$	53
3.22 Effect of volume fraction exponent K on the frequency-amplitude curves of stiffened spherical panels ($R_x=R_y = 5\text{m}$, $a = b = 0.8\text{m}$, $h = 0.025\text{m}$, $Q = 105\text{Pa}$).....	55

Figure	Page
3.23 Effect of radii R_y on the frequency-amplitude curves of stiffened cylindrical shell ($R_x = \infty, a = b = 0.8\text{m}, h = 0.025\text{m}, K = 1, Q = 105\text{Pa}$).....	56
3.24 Effect of excitation loads Q on the frequency-amplitude curves of stiffened spherical shells ($R_x=R_y = 5\text{m}, a = b = 0.8\text{m}, h = 0.025\text{m}, K = 1$).....	56
4.1 Critical buckling under uniform temperature rise vs b/a for $\text{Si}_3\text{N}_4/\text{SUS304}$	64
4.2 Critical buckling under linear temperature rise vs b/a for $\text{Si}_3\text{N}_4/\text{SUS304}$	65
4.3 Critical buckling under nonlinear temperature rise vs b/a for $\text{Si}_3\text{N}_4/\text{SUS304}$	65
4.4 Critical buckling under linear temperature rise vs b/h for $\text{Si}_3\text{N}_4/\text{SUS304}$	66
4.5 Critical buckling under uniform temperature rise vs b/h for $\text{Si}_3\text{N}_4/\text{SUS304}$	69
4.6 Effect of uniform temperature rise Δt on the nonlinear response of cylindrical panels ($a/b=1, b/h=50, a/R_y=0.5, K=1$).....	70
4.7 Effect of uniform temperature rise Δt and imperfection μ on the nonlinear response of $\text{Si}_3\text{N}_4/\text{SUS304}$ cylindrical shell ($a/b=1, b/h=50, a/R_y=0.5, k=1$).....	71
4.8 Backbone curve for square simply supported plate subjected to temperature variations through the thickness $a = b = 0.2\text{m}, h = 0.025\text{m}, K = 2$	72
4.9 The frequency-amplitude curve of nonlinear vibration of simply supported $\text{SUS304}/\text{Si}_3\text{N}_4$ plate ($a = b = 0.2\text{m}, h = 0.025\text{m}$) under $F = 375\text{kN}$ and $\zeta = 0.01$ subjected to temperature variations through the thickness.....	72
5.1 The frequency amplitude curve of nonlinear vibration of free edges stainless steel rectangular plate ($b/a = 1.5, a/h = 30$) under $f = 0.03$ and damping ratio $\zeta = 0.004$ using 24 dof model.....	87

Figure	Page
5.2 The frequency amplitude curve of nonlinear vibration of free edges stainless steel rectangular plate ($b/a = 1.5, a/h = 30$) under dimensionless $f = 0.03$ and damping ratio $\zeta = 0.004$ using 36 dof model	87
5.3 The frequency amplitude curve of nonlinear vibration of the free edges stainless steel rectangular plate ($b/a = 1.5, a/h = 30$) under dimensionless $f = 0.03$ and damping ratio $\zeta = 0.004$ using 44 dof model.....	88
5.4 The frequency amplitude curve of nonlinear vibration of the free edges stainless steel rectangular plate ($b/a = 1.5, a/h = 30$) under dimensionless $f = 0.03$ and damping ratio $\zeta = 0.004$ using 50 dof model.....	88
5.5 Effect of the number of dof model on the nonlinear frequency amplitude response of the free edges stainless steel rectangular plate ($b/a = 1.5, a/h = 30$) under dimensionless $f = 0.03$ and damping ratio $\zeta = 0.004$	89
5.6 The frequency amplitude curve of nonlinear vibration of the simply supported double curved shells with movable edges ($b/a = 1.5, a/h = 30$) under dimensionless $f = 0.0155$ and damping ratio $\zeta = 0.004$	90
5.7 The effect of the number of dof on the frequency-amplitude curve of forced nonlinear vibration of stiffened Al/Al ₂ O ₂ spherical shell $R_x = R_y = 5m, a = b = 0.8m, h = 0.025m, K = 1$ and $\zeta = 0.01$ under uniformly distributed load $Q = 10^5 Pa$	91
5.8 Effect of uniform temperature rise on the frequency response curve of a stiffened spherical shell ($R_x = R_y = 5m, a = b = 0.8m, h = 0.025m, K = 1$ and $\zeta = 0.01$) under uniformly distributed load $Q = 10^5 Pa$	92
5.9 Effect of geometrical imperfection on the frequency response curve of a stiffened spherical shell ($R_x = R_y = 5m, a = b = 0.8m, h = 0.025m, K = 1$ and $\zeta = 0.01$) under uniformly distributed load $Q = 10^5 Pa$	93

SYMBOLS

A	Extensional stiffness matrix
B	Bending-extensional coupling stiffness matrix
D	Bending stiffness matrix
A_s	Transverse shear stiffness matrix
Q_{ij}	Conjugate stiffness matrix
Q_x	Uniformly distributed pressure over the shell in x direction
Q_y	Uniformly distributed pressure over the shell in y direction
Q_z	Uniformly distributed pressure over the shell in z direction
M	Global mass matrix
C	Damping coefficient matrix
K_1	Linear stiffness matrix
K_2	Nonlinear quadratic stiffness matrix
K_3	Nonlinear cubic stiffness matrix
Q	Excitation load
F	Concentrated harmonic force at the center
R_x	Radius of curvature in x direction
R_y	Radius of curvature in y direction
K	Volume fraction index of the shell
K_x	Volume fraction index of the longitudinal stiffener
K_y	Volume fraction index of the transversal stiffener
V_c	Volume fraction of ceramic

V_m	Volume fraction of metal
E	Young's modulus of the shell
E_x	Young's modulus of the longitudinal stiffener
E_y	Young's modulus of the transversal stiffener
G_x	Shear modulus of the longitudinal stiffener
G_y	Shear modulus of the transversal stiffener
J_x	Effective torsional constants of the longitudinal stiffener
J_y	Effective torsional constants of the transversal stiffener
I'_x	Second moment of the area of the longitudinal stiffener
I'_y	Second moment of the area of the transversal stiffener
L_{ij}	Linear operator
NL_i	Nonlinear operator
U_{mn}, V_{mn}, W_{mn}	Generalized coordinates in x direction
T_i	Initial temperature
T_f	Final temperature
T_b	Bottom temperature
T_t	Top temperature
T_m, T_n	Chebyshev polynomials
R^{u,v,w,ψ_x,ψ_y}	Boundary functions
N_{max}	Total number of degree of freedom
d_x	Spacing between tow consecutive longitudinal stiffenres
d_y	Spacing between tow consecutive transversal stiffenres

b_x	Longitudinal stiffener width
b_y	Transversal stiffener width
h_x	Longitudinal stiffener thickness
h_y	Transversal stiffener thickness
e_x	Eccentricity of the longitudinal stiffener
e_y	Eccentricity of the transversal stiffener
k	Thermal conduction coefficient of the shell
k_{sx}	Thermal conduction coefficient of the longitudinal stiffener
k_{sy}	Thermal conduction coefficient of the transversal stiffener
k_s	Shear correction factor
w^*	Initial shell imperfection
m	Metal
c	Ceramic
t	Time
a	Length of the shell
b	Width of the shell
h	Shell thickness
q_0	Amplitude of the excitation
u_0	Middle plane displacement component in x direction
v_0	Middle plane displacement component in y direction
w_0	Middle plane displacement component in z direction
ψ_x	Middle plane rotation of transverse normal about y axis

ψ_y	Middle plane rotation of transverse normal about x axis
ε_x	Normal strain in x direction
ε_y	Normal strain in y direction
γ_{xy}	In plane shear strain
γ_{xz}, γ_{yz}	Transverse shear deformation
α	Thermal expansion coefficient of the shell
α_x	Thermal expansion coefficient of the longitudinal stiffener
α_y	Thermal expansion coefficient of the transversal stiffener
ρ	Mass density of the shell
ρ_{sx}	Mass density of the of the longitudinal stiffener
ρ_{sy}	Mass density of the of the transversal stiffener
ν	Poisson ratio of the shell
ν_{sx}	Poisson ration of the longitudinal stiffener
ν_{sy}	Poisson ration of the transversal stiffener
μ	Imperfection constant
ω	Natural frequency
ζ	Modal damping ratio
ω_{NL}	Nonlinear frequency
ω_L	Linear frequency
ΔT_{cr}	Critical buckling temperature difference
ΔT	Buckling temperature change
\tilde{f}	Harmonic force

δ	Dirac delta function
Ω	Forcing excitation frequency

ABBREVIATIONS

FGM	Functionally Graded Material
CPT	Classical Plate Theory
FSDT	First Order Shear Deformation Theory
TSDT	Third Order Shear Deformation Theory
HSDT	Higher Order Shear Deformation Theory
ODE	Ordinary Differential Equation
PDE	Partial Differential Equation
GDQ	Generalized Differential Quadrature
S8R	8-node Doubly Curved Shell Element
Dof	Degree of Freedom
TD	Temperature Dependent
T-ID	Temperature Independent
2D	Two Dimensional
3D	Three Dimensional

ABSTRACT

The motivation of the current work is to develop a multi-modal analysis of the nonlinear response of stiffened double curved shells made of functionally graded materials under thermal loads. The formulation is based on the first order shear deformation shell theory in conjunction with the von Kármán geometrical nonlinear strain-displacement relationships. The nonlinear equations of motion of stiffened double curved shell based on the extended Sanders's theory were derived using Galerkin's method. The resulting system of infinite nonlinear ordinary differential equations, that includes both cubic and quadratic nonlinear terms, was solved using a nonlinear dynamic software XPPAUT to obtain the force-amplitude relationship. The effect of both, longitudinal and transverse stiffeners, was considered using the Lekhnitsky's technique and the material properties are temperature dependent and vary in the thickness direction according to the linear rule of mixture. In order to obtain accurate natural frequency in thermal environments, critical buckling temperature differences are carried out, resulting in closed form solutions. The effect of temperature's variation as well as power index, functionally graded stiffeners, geometrical parameters, temperature depended materials and initial imperfection on the nonlinear response of the stiffened shell are considered and discussed. This dissertation showed that the nonlinear study of problems of thin-walled structures with even stiffeners is of paramount importance. It was also found that the difference between single-mode and multi-mode analyses could be very significant for nonlinear problems in a thermal environment. Hence, multimode vibration analysis is necessary for structures of this nature.

1. Introduction

For the last few decades, laminated composite materials have been extensively used in aerospace, civil and marine engineering. They are well accepted due to their high strength to weight ratio, high corrosion resistivity, and very good fatigue characteristics. In many cases, the laminated plates undergo extreme high thermal loading and large amplitude vibration, which may lead to delamination, crack initiations create thermal stresses between layers. Their multilayer compositions and bonding phenomenon make them vulnerable to a mismatch of mechanical properties across the interfaces (Reddy, 2000). Recently, functionally graded materials (FGMs), a new type of composite materials, has been introduced to overcome these drawbacks. The concept of functionally graded materials was proposed in 1984 by Japanese materials scientists along with the preparation of a heat resistant material for reactor vessels, aerospace vehicles and other engineering applications (Koizumi, 1997). The material design of FGMs has mechanical properties varying smoothly from a surface made of metal to another made of ceramic at the micron level (Kawasaki & Watanabe, 1997). The main advantage of this continuous variation is to avoid and reduce thermal stresses.

1.1 Literature Survey

In recent years, several studies have been devoted to the dynamical analysis of FGM plates and shells. The effects of aspect ratios, gradient indices and stiffness coefficients of the free vibration of FGM plates using first-order shear deformation theory were studied (Hashemi, Taher, Akhavan, & Omidi, 2010). Six combinations of boundary conditions were studied in their paper. The influence of skew angle on bending and natural frequencies of an FGM shell panel using Reddy's higher-order theory was covered

(Gulshantaj & Chakrabarti, 2013). Higher order shear deformation theory and a meshless approach were adopted by Xiang, Kang and Liu (2014) to calculate the natural frequency of the FGM plates.

Nonlinear transient response of imperfect FGM cylindrical, spherical, paraboloid and hyperboloid shells were studied by Pradyumna and Nanda (2013) using Sander's approximation. The arc length approach combined with the Newton-Raphson's method was used by Zhao and Liew (2009) to study the nonlinear response of FGM shells under thermomechanical loads. The elliptic governing partial differential equation (PDE) was reduced by Kobayashi and Leissa (1995) to an ordinary differential equation (ODE) based on the first shear deformation theory (FSDT) in order to analyze the nonlinear vibration of thick shallow shells.

Cylindrical panels are found mainly in spacecraft, submarine, missile and other aircraft components (e.g. fuselage sections). To study the nonlinear vibration of stainless steel and nickel cylindrical shells, the Sanders-Koiter theory was adopted (Strozzi & Pellicano, 2013). Their study was based on two steps, linear analysis to find the eigenfunctions, and then nonlinear analysis based on the previously calculated functions. The governing equations were derived by Pradhan, Loy, Lam and Reddy (2000) using the Rayleigh method. The natural frequencies of the FGM cylindrical shells were evaluated based on Love's shell theory.

Then Pradhan et al. (2000) extended the previous study to include different volume fraction indices and various boundary conditions. The vibration and buckling analysis of two-layered cylindrical shells made of an inner FGM and outer isotropic layer under static and periodic loads were considered (Sepiani, Rastgoo, Ebrahimi & Arani, 2010).

Their theoretical formulations are based on both FSDT and CPT. The Rayleigh Ritz approach was adopted by Shah, Mahmood and Naeem (2009) to find the linear natural frequencies of FGM thin cylindrical shells. By ignoring the shallowness of cylindrical shells, Bich and Xuan (2012) introduced an improved Donnell shell theory to study the nonlinear vibration of FG circular cylindrical shells. Very good agreement was observed comparing their results by using commercial software.

The natural frequencies and the unstable regions of the FG cylindrical panels under mechanical and thermal loads were studied (Yang & Shen, 2003). The governing equations of motion based on FSDT were discretized by Tornabene, Viola and Inman (2009) into a standard linear eigenvalue problem using generalized differential quadrature (GDQ) to study the vibration of FGM plates and shells. A semi-analytical finite element model based on converting the equations of motion from 3D to 2D was developed by Santos, Soares and Reddy (2009) to study the bending and free vibration of FGM cylindrical shells.

The original 3D foundational equations with variable coefficients were transformed by Cao and Tang (2012) into membrane bending coupling of 2D equations with constant coefficients to study the natural frequencies of FGM cylindrical shells with infinite and finite lengths. A parametric study was conducted by Patel, Gupta, Loknath and Kadu (2005) on the free vibration analysis of FGM elliptical and cylindrical shells using the finite element method based on a higher order displacement model. Embedded thin piezoelectric layers were used by Sheng and Wang (2013) to control the nonlinear vibration of FGM laminated cylindrical shells.

A generalized formulation of doubly curved shells including double radii of curvature has been considered in some papers. A nonlinear finite element method was presented by Singh and Panda (2014) in order to study the nonlinear free vibration analysis of doubly curved composite shell panels. The nonlinear natural frequencies were calculated using a direct iterative method. The nonlinear vibration of clamped FGM doubly curved shallow elliptical shells was studied (Chorfi & Houmat, 2010). The nonlinear dynamic analysis of FGM shallow shells was studied by Tornabene, Liverani and Caligiana (2011) using the generalized differential quadrature method. Equations of motion were solved using the free form meridian. The nonlinear vibration and dynamic buckling of FGM cylindrical and doubly curved shallow shells subjected to mechanical loads were studied by Bich and Long (2010) using classical shell theory. A 2D higher order theory was presented by Matsunaga (2009) to evaluate the natural frequencies, stress distribution, and buckling stresses of simply supported functionally graded shallow shells.

The vibration and dynamic analysis of FGM plates, cylinders and double curved shells along with temperature dependent and independent materials have received positive attention. Transient response of FGM plate in thermal environments was studied by Yang and Shen (2002) using one dimensional differential quadrature technique, Galerkin approach, and the modal superposition method. A geometrically nonlinear analysis of FGM plate was conducted by Zhu, Zhang and Liew (2014) using the local meshless method with moving Kriging interpolation. Nonlinear temperature and heat flux were considered as thermal loadings and Newton-Raphson method was used to solve the nonlinear system of equations.

A three dimensional linear theory of elasticity was presented by Li, Iu and Kou (2009) to study the free vibration simply supported FGM rectangular plates subjected to various temperature forms. Chebyshev polynomials were used to satisfy the essential boundary conditions. A detailed investigation was carried out by Sundararajan, Prakash and Ganapathi (2005) to detect the influence of the skew angle, aspect ratios and plate thickness on the nonlinear free flexural vibration of FGM rectangular plates under thermal load. Lagrange's equations of motion were used to find nonlinear governing equations that were solved using finite element procedure coupled with the direct iteration technique. A displacement based finite element formulation associated with a novel TSDT was presented by Bui et al. (2016) to analyses the static bending deflection and the natural frequencies subjected to high thermal conditions. The nonlinear dynamic response of thick FGM plate subjected to both thermal and damping loads was studied by Duc, Bich and Cong (2016) using the TSDT and stress function.

A higher order finite element formulation for nonlinear transient analysis of FGM curved panels was presented (Pradyumna, Nanda & Bandyopadhyay, 2010). Heat conduction between the top and bottom surfaces was neglected and a parametric study was performed. The post buckling analysis of FGM plate under in plane compressive, thermal and thermomechanical loads were studied by Tung and Duc (2010) using the classical plate theory. The free vibration analysis of four edges simply supported FGM cylindrical shells subjected to thermal loads was studied by Haddadpour, Mahmoudkhani and Navazi (2007) using Love's shell theory and the Karman-Donnell type of kinematic nonlinearity.

The Differential quadrature method combined with iteration approaches was used by Liew, Yang and Wu (2006) in order to evaluate the linear and nonlinear vibration analysis of a three-layer coating FGM substrate cylindrical with different boundary conditions. The nonlinear dynamic analysis of FGM circular cylindrical shell with clamped-clamped boundary condition was studied by Zhang, Hao and Yang (2012) under mechanical and uniform thermal loads. After studying the nonlinear vibration with and without temperature, Shen (2012) and Shen and Wang (2014) evaluated the post-buckling response of FGM cylindrical shells under thermomechanical loads. Then Voight and Mori-Tanaka models were adopted by Shen and Wang (2013), and it has shown to have the same influence as their previous paper.

The Governing equation was based on HSDT and von Karman strain- displacement relationship. The nonlinear response of FGM cylindrical panels was investigated by Duc and Tung (2010) under uniform lateral pressure using the classical shell theory. Across the thickness, linear and nonlinear temperature distribution were considered. The nonlinear dynamic analysis of the FGM double curved thin shell based on classical shell theory was studied (Duc & Quan, 2013a). All the material properties were assumed to be temperature-dependent including the poisson ratio. The nonlinear vibration and dynamic response of FGM double curved shallow shells were investigated by Quan and Duc (2016) under thermal effect. The formulation was based on TSDT. The free vibration of FGM curved panels was analyzed by Kar and Panda (2015) under a thermal environment using the HSDT. All the materials properties are temperature-dependent.

The nonlinear vibration of FGM double curved panels under thermal loads based on HSDT and von Karman strain displacement relationships was studied (Shen, Chen, Guo,

Wu & Huang, 2015). In order to calculate the natural frequencies, the equations of motion were solved by two step perturbation technique. The nonlinear free vibration response of FGM doubly curved panels under heat conduction were studied by Kar and Panda (2017) using the HSDT and Green-Lagrange nonlinearity. Temperature-dependent and independent material properties are evaluated using Voigt's micromechanics model. The buckling and post-buckling of FGM curved panels using HSDT were studied (Tung & Duc, 2014). The shallow panel is subjected to thermal, mechanical and thermomechanical loads. All the materials properties are completely independent of the temperature variation. Buckling and -post-buckling analysis of double curved FGM panels were calculated by Duc and Quan (2012) based on classical shell theory and subjected to thermal and thermomechanical loads.

The nonlinear free and forced vibration and dynamic response of piezoelectric FGM laminated composite shells under electrical, thermal, mechanical and aerodynamic loading were studied (Rafiee, Mohammadi, Sobhani & Yaghoobi, 2013). The governing equations are derived based on improved Donnell shell theory by taking into consideration the physical neutral surface concept. Their previous publication was expended by Kar and Panda (2016) to spherical panels under the same conditions.

Apart from discussing the results related to unstiffened structures, the study of stiffened plates and shells is very significant and should be considered merely because they are more realistic and have been utilized in the aerospace industry. Most of the following studies are based on Lekhnitsky smeared technique. For example, conducted a geometrically nonlinear vibrational analysis of eccentrically stiffened doubly curved functionally graded structure based on (FSDT) under a mechanical load. The nonlinear

dynamic response of the stiffened FGM double curved shallow shells being subjected to both transverse and compressive loads was studied (Duc, 2013).

The classical shell theory and the smeared stiffeners technique were used by Bich, Dung and Nam (2012) to study the nonlinear vibration and dynamic buckling of stiffened functionally graded cylindrical panels. The influence of the volume fraction index and the initial imperfection were taken into account in their study. The vibrational behavior of ring supported functionally graded cylindrical shells was evaluated by Rahimi, Ansari and Hemmatnezhad (2011) based on Sanders' thin shell theory. Ritz method is used to derive the governing equations of motion. The influence of some boundary conditions was considered. A theoretical formulation was adopted by Dung, Duc and Thiem (2017) in terms of displacement components based on Reddy's TSDT to analyze the dynamic response of stiffened cylindrical shells made completely of FGM and filled inside by elastic foundations.

Explicit relations of load-deflection curves and post-buckling of eccentrically stiffened FGM cylindrical panels on elastic foundation subjected to mechanical loads were determined (Duc & Quan, 2014). A semi-analytical approach was presented by Bich, Dung and Nam (2013) to investigate the nonlinear dynamic behavior of orthogonally stiffened functionally graded shallow shells using the classical thin shell theory. The effects of damping, mechanical and critical buckling loads were taken into account in this work. The power law distribution and Mori-Tanaka homogenization scheme were used by Wattanasakulpong and Chaikittiratana (2015) to define the material variational through the shell thickness. In this study, stiffened shells with the various radius of curvatures are considered in the evaluation of the nonlinear frequencies.

The nonlinear dynamic response of reinforced FGM plates with stiffeners using both the Reddy's TSDT and stress function was studied (Cong, Anh & Duc, 2017). Uniform and non-uniform temperature distribution over the thickness were considered. The influence of physical and temperature-dependent materials properties of the plate and stringers on the nonlinear vibration was discussed. The nonlinear vibration and dynamic response of stiffened thick sandwich plate made of functionally graded materials were discussed by Duc et al. (2016) using the first-order shear deformation theory and stress function with full motion equations. The Plate was subjected to both mechanical and thermal loads. The governing equations were established by Duc, Nguyen and Khoa (2017) based on classical shell theory and Airy stress functions.

Then nonlinear vibrational and dynamical equations of eccentrically stiffened Sigmoid power-law distribution FGM elliptical cylindrical shells under thermal loads are solved by Galerkin method and Runge-Kutta numerical technique. The buckling and post-buckling analysis of stiffened double curved thin shallow shells were studied by Duc and Quan (2013b) under thermal effect using based on the CST. Here the functionally graded material's volume fraction is based on a simple power-law distribution.

The Donnell nonlinear strain displacement relations were adopted by Najafizadeh, Hasani and Khazaeinejad (2009) to derive the equilibrium and stability equation of stiffened functionally graded cylindrical shells. The static and dynamic stability and buckling of stiffened FGM double curved shallow shells in thermal environment were studied (Quan & Duc, 2017). Equilibrium, compatibility and motion equations are derived using the third-order shear deformation theory taking into account the thermal stress in both the shells and stiffeners

In all the above papers, nonlinear analysis of stiffened and unstiffened functionally graded materials with or without thermal load were conducted using only a single-mode approximation. Few authors have adapted a multi-modal approach to solving these type of problems. The multi-modal energy approach was adopted by Alijani, Amabili and Nejad (2011) to study the nonlinear vibration of FGM doubly curved shells under thermal effect, using the HSDT. In order to obtain numerical solutions, the Lagrange equation of motion was used to reduce the energy function to a system of infinite nonlinear ordinary differential equations. Moreover, the nonlinear forced vibration of simply supported FGM doubly curved shallow shells based on Donnell's shell theory was studied (Alijani, Amabili, Karagiozis & Nejad, 2011).

A multi-modal discretization, considering nine doubly symmetric modes with respect to the panel center, was used in every nonlinear analysis. The amplitude-frequency response was plotted using the software AUTO 97. To overcome the shortcomings in Glarkin's procedure, Abe and Yamada (2019) used the shooting method to study the one to one internal resonance of the symmetric crossly composite shallow shell. The nonlinear vibration of simply-supported isotropic and multi-laminated cross-ply doubly curved shallow shells was studied (Alhazza, Ahmadian, Inman, Leo & Masoud, 2002). Modal interaction between the first and second modes is investigated by applying the method of multiple scales directly to nonlinear partial differential equations of motion.

1.2 Scope

To the author's knowledge, no one has investigated the effect of the stiffeners on the nonlinear vibrations under thermal load using multimode analysis. The present dissertation consists of two main parts. The purpose of the first part of this analytical

investigation is to study and validate the nonlinear behavior of imperfect simply supported stiffened isotropic and functionally graded double curved shells, subjected to thermal and mechanical load using a single-mode approximation. The formulation is based on the first-order shear deformation shell theory in conjunction with the Von Kármán geometrical nonlinear strain-displacement relationships. Galerkin's method is used to transform the nonlinear equations of motion based on the extended Sanders's theory into a set of nonlinear ordinary differential equations. Longitudinal and transversal stiffeners, in addition to the stiffener's twisting moment are included by using the Lekhnitsky's smeared technique. The material properties are temperature-dependent and change through the thickness according to the linear rule of mixtures. Uniform linear and nonlinear temperature distribution are considered in this dissertation.

Consequently, critical buckling temperature differences are carried out, resulting in closed-form solutions. The resulting equations were solved numerically by using the Fourth Order Runge-Kutta method. A closed-form solution of the amplitude-frequency relationship, based on He's energy technique, is developed for a Duffing equation with strong quadratic and cubic nonlinearities. Several studies with different loads and parameters were conducted to validate the present technique and a good agreement was achieved with results already available in the literature.

In the second part of the dissertation, the numerical analysis of the problem introduced before is carried out based on the multi-modal energy method and nonlinear first-order shear deformation theory. The procedure is undertaken in two steps. First, the shape functions of the displacements and rotations field are expressed in terms of shifted Chebyshev polynomials of the first kind. The integration of these polynomials is

performed using Mathematica software. Then linear analysis are performed by minimization of the Lagrangian function. After using the mode shapes from the linear analysis, the energy functional is reduced to set on infinite strongly nonlinear ODE with both, quadratic and cubic nonlinearities. The amplitude-frequency response is plotted using XPPAUT software.

2. Functionally Graded Materials Double Curved Shells

In this chapter, the variation of the volume fractions of ceramic and metal the shallow eccentrically stiffened double curved shell is discussed. The concentration of metal and ceramic is assumed to change through the thickness of the shells and of the stiffeners based on the power law distribution. Furthermore, the material properties are considered to be temperature dependent.

2.1 Modeling

Consider an eccentrically stiffened double curved shallow shell made from functionally graded materials (FGM). The shallow shell is assumed to have a small rise to span ratio. In general, the middle surface of the shells should be defined by curvilinear coordinates. But that is not the case for shallow shells. Here, the Cartesian coordinates (x, y, z) are established in which (x, y) define the plane of the middle surface and z on the thickness direction $(-h/2 \leq z \leq h/2)$. The Cartesian coordinates, the radius of curvature R_x , the configurations and dimensions of transversal stiffeners are shown in Figure 2.1 below.

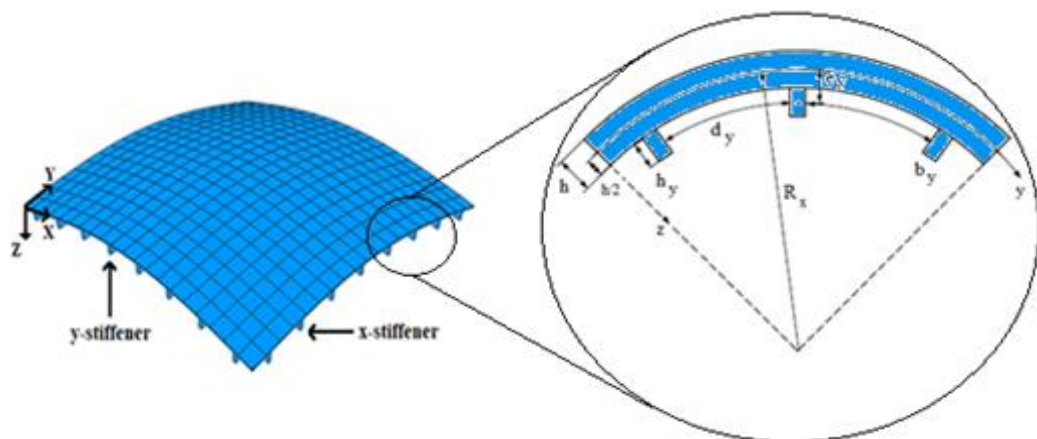


Figure 2.1. A double-curved shell with transversal stiffeners.

It is to be noted that by changing the components of curvatures R_x and R_y , double-curved shells can exhibit different shapes as follow:

- 1) Flat plate: $\frac{1}{R_x} = \frac{1}{R_y} = 0$
- 2) Cylindrical shell: $\frac{1}{R_x} = 0$ or $\frac{1}{R_y} = 0$
- 3) Spherical shell: $\frac{1}{R_x} = \frac{1}{R_y}$
- 4) Hyperbolic paraboloidal shell: $\frac{1}{R_x} = -\frac{1}{R_y}$

For the stiffeners in x and y directions, d_x and d_y are the spacing between two consecutive longitudinal and transversal stiffeners respectively. Also, b_x , b_y represent the width and h_x , h_y represents the thickness. Finally, e_x and e_y are the eccentricities of the stiffeners with respect to the middle surface of the shell.

2.2 Material Properties

Functionally Graded Material consists of a mixture of metal (denoted by “m”) and ceramic (denoted by “c”). The top surface of the shell is considered to be metal and the bottom surface to be ceramic. In order to provide continuity between the shells and the stiffeners, it is assumed that the stiffeners are made of full metal when placed on the metal-rich side of the shell, and made of full ceramic when placed on the ceramic rich side. The volume fractions of ceramic and metal of the FGM shells and stiffeners are assumed to change through the thickness according to the power-law distribution (Reddy & Chin, 1998):

$$V_c(z) = \begin{cases} \left(\frac{2z+h}{2h}\right)^K, & \text{for shells} \quad (0 \leq K \leq \infty) \\ \left(\frac{2z-h}{2h_x}\right)^{K_x}, & \text{for stiffeners in } x \text{ direction} \quad (0 \leq K_x \leq \infty) \\ \left(\frac{2z-h}{2h_y}\right)^{K_y}, & \text{for stiffeners in } y \text{ direction} \quad (0 \leq K_y \leq \infty) \end{cases} \quad (1)$$

$$V_c(z) + V_m(z) = 1 \quad (2)$$

where K, K_x and K_y are the volume fraction indices that define the material distribution and h, h_x and h_y are the total thicknesses of the shells and stiffeners. Figure 2.2 shows the variation of the volume fraction through the thickness with different values of power index K .

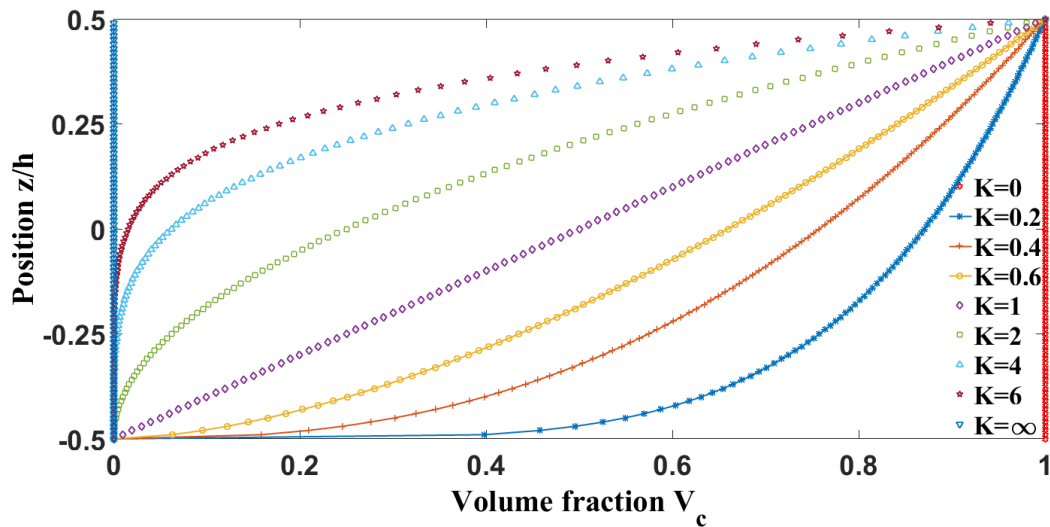


Figure 2.2. Effect of power index “K” on the variation in the ceramic volume fraction V_c through the shell thickness.

In this study, the FGM properties, P , are assumed to be a function of volume fraction and are related to their volume fraction V_c and V_m by the linear rule of mixture (Voigt’s model) as (Reddy & Chin, 1998):

$$P(z, T) = \begin{cases} P_c(z, T)V_c(z, T) + P_m(z, T)V_m(z), & \text{for shells} \\ P_m(z, T)V_c(z) + P_c(z, T)V_m(z), & \text{for stiffeners} \end{cases} \quad (3)$$

where P represents, the young's modulus E , thermal expansion α , thermal conduction coefficient k , and the mass density ρ . Moreover, the material properties of metal and ceramic are temperature dependent and are expressed as the following nonlinear function of temperature (Reddy & Chin, 1998):

$$Pr(z, T) = P_0(P_{-1}T^{-1} + 1 + P_1T^1 + P_2T^2 + P_3T^3) \quad (4)$$

in which $T = T_0 + \Delta T$, $T_0 = 300K$ (room temperature) unless otherwise specified, P_r ("r" can be replaced by "m" or "c"), and $P_0, P_{-1}, P_1, P_2, P_3$ are coefficients characterizing of the constituent materials with temperature-dependent. Substituting equations (1) and (2) into equation (3), the effective FGM mechanical properties are obtained using the following equations:

For Shells:

$$E(z, T) = \begin{cases} E_m(z, T) & \text{as } z = -h/2 \\ E_m(z, T) + \{E_c(z, T) - E_m(z, T)\}V_c(z) & \text{as } -h/2 < z < h/2 \\ E_c(z, T) & \text{as } z = h/2 \end{cases} \quad (5a)$$

$$\alpha(z, T) = \begin{cases} \alpha_m(z, T) & \text{as } z = -h/2 \\ \alpha_m(z, T) + \{\alpha_c(z, T) - \alpha_m(z, T)\}V_c(z) & \text{as } -h/2 < z < h/2 \\ \alpha_c(z, T) & \text{as } z = h/2 \end{cases} \quad (5b)$$

$$k(z, T) = \begin{cases} k_m(z, T) & \text{as } z = -h/2 \\ k_m(z, T) + \{k_c(z, T) - k_m(z, T)\}V_c(z) & \text{as } -h/2 < z < h/2 \\ k_c(z, T) & \text{as } z = h/2 \end{cases} \quad (5c)$$

$$\rho(z, T) = \begin{cases} \rho_m(z, T) & \text{as } z = -h/2 \\ \rho_m(z, T) + \{\rho_c(z, T) - \rho_m(z, T)\}V_c(z) & \text{as } -h/2 < z < h/2 \\ \rho_c(z, T) & \text{as } z = h/2 \end{cases} \quad (5d)$$

$$\nu(z, T) = \begin{cases} \nu_m(z, T) & \text{as } z = -h/2 \\ \nu_m(z, T) + \{(\nu_c(z, T) - \nu_m(z, T))\}V_c(z) & \text{as } -h/2 < z < h/2 \\ \nu_c(z, T) & \text{as } z = h/2 \end{cases} \quad (5e)$$

For stiffeners in x and y directions:

$$E_x(z, T) = \begin{cases} E_c(z, T) & \text{as } z = h/2 \\ E_c(z, T) + \{E_m(z, T) - E_c(z, T)\}V_c(z) & \text{as } h/2 < z < h/2 + h_x \\ E_m(z, T) & \text{as } z = h/2 + h_x \end{cases} \quad (6a)$$

$$E_y(z, T) = \begin{cases} E_c(z, T) & \text{as } z = h/2 \\ E_c(z, T) + \{E_m(z, T) - E_c(z, T)\}V_c(z) & \text{as } h/2 < z < h/2 + h_y \\ E_m(z, T) & \text{as } z = h/2 + h_y \end{cases} \quad (6b)$$

$$\alpha_{sx}(z, T) = \begin{cases} \alpha_c(z, T) & \text{as } z = h/2 \\ \alpha_c(z, T) + \{\alpha_m(z, T) - \alpha_c(z, T)\}V_c(z) & \text{as } h/2 < z < h/2 + h_x \\ \alpha_m(z, T) & \text{as } z = h/2 + h_x \end{cases} \quad (6c)$$

$$\alpha_{sy}(z, T) = \begin{cases} \alpha_c(z, T) & \text{as } z = h/2 \\ \alpha_c(z, T) + \{\alpha_m(z, T) - \alpha_c(z, T)\}V_c(z) & \text{as } h/2 < z < h/2 + h_y \\ \alpha_m(z, T) & \text{as } z = h/2 + h_y \end{cases} \quad (6d)$$

$$k_{sx}(z, T) = \begin{cases} k_c(z, T) & \text{as } z = h/2 \\ k_c(z, T) + \{k_m(z, T) - k_c(z, T)\}V_c(z) & \text{as } h/2 < z < h/2 + h_x \\ k_m(z, T) & \text{as } z = h/2 + h_x \end{cases} \quad (6e)$$

$$k_{sy}(z, T) = \begin{cases} k_c(z, T) & \text{as } z = h/2 \\ k_c(z, T) + \{k_m(z, T) - k_c(z, T)\}V_c(z) & \text{as } h/2 < z < h/2 + h_y \\ k_m(z, T) & \text{as } z = h/2 + h_y \end{cases} \quad (6f)$$

$$\rho_{sx}(z, T) = \begin{cases} \rho_c(z, T) & \text{as } z = h/2 \\ \rho_c(z, T) + \{\rho_m(z, T) - \rho_c(z, T)\}V_c(z) & \text{as } h/2 < z < h/2 + h_x \\ \rho_m(z, T) & \text{as } z = h/2 + h_x \end{cases} \quad (6g)$$

$$\rho_{sy}(z, T) = \begin{cases} \rho_c(z, T) & \text{as } z = h/2 \\ \rho_c(z, T) + \{\rho_m(z, T) - \rho_c(z, T)\}V_c(z) & \text{as } h/2 < z < h/2 + h_y \\ \rho_m(z, T) & \text{as } z = h/2 + h_y \end{cases} \quad (6h)$$

$$v_{sx}(z, T) = \begin{cases} v_c(z, T) & \text{as } z = h/2 \\ v_c(z, T) + \{v_m(z, T) - v_c(z, T)\}V_c(z) & \text{as } h/2 < z < h/2 + h_x \\ v_m(z, T) & \text{as } z = h/2 + h_x \end{cases} \quad (6i)$$

$$v_{sy}(z, T) = \begin{cases} v_c(z, T) & \text{as } z = h/2 \\ v_c(z, T) + \{v_m(z, T) - v_c(z, T)\}V_c(z) & \text{as } h/2 < z < h/2 + h_y \\ v_m(z, T) & \text{as } z = h/2 + h_y \end{cases} \quad (6j)$$

Figure 2.3 shows the variation of modulus of elasticity of Aluminum and Zirconia (Al/ZrO₂) FGM shell with respect to the thickness for different power law indices. It can be seen that the young's modulus is smaller when K's are smaller.

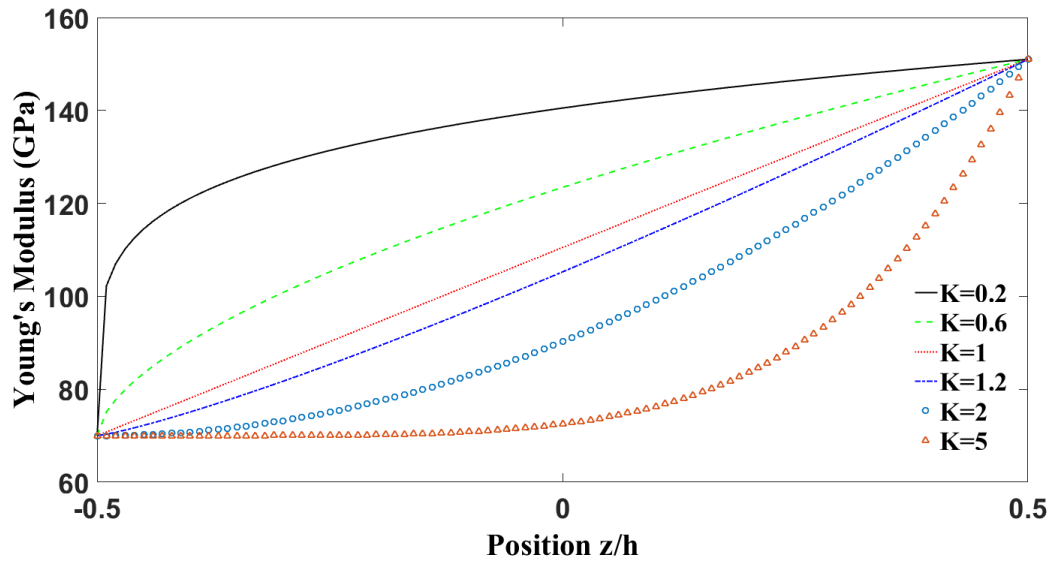


Figure 2.3. Young's modulus variations with respect to the dimensionless thickness of the shell for different volume fraction indices ($E_{Al} = 70\text{GPa}$ and $E_{ZrO_2} = 151\text{GPa}$).

3. Single Mode Theoretical Formulation

In this chapter, static and dynamic analyses of isotropic and FGM simply supported isotropic and FGM stiffened double curved shells are considered. The contribution of the stiffeners are accounted for by using the lekhnitsky smeared stiffeners technique. Fourth Order Runge-Kutta and He's energy method were adopted to investigate the nonlinear dynamic and amplitude frequency responses. The obtained results were validated with previously published papers in this area.

3.1 Governing Equations

Let u_0, v_0, w_0 denote the middle plane displacement components in the x, y, z directions while ψ_x, ψ_y denote the middle plane rotations of transverse normal about the y and x -axes respectively. The displacement field based on the first-order shear deformation theory (FSDT) is defined as (Reddy, 2003):

$$\begin{aligned} u(x, y, z, t) &= u_0(x, y, t) + z\psi_x(x, y, t) \\ v(x, y, z, t) &= v_0(x, y, t) + z\psi_y(x, y, t) \\ w(x, y, z, t) &= w_0(x, y, t) \end{aligned} \quad (7)$$

The FSDT extends the kinematic of the classical plate theory (CPT) by including in its kinematics assumptions, a constant transverse shear deformation through its thickness. To overcome this inconsistency, The FSDT requires a shear correction factor k_s that depends not only on the geometric parameter of a structure but also on the boundary conditions and on the applied load (Reddy, 2003). In the case of isotropic and laminated composite shell, the shear correction factor is $k_s = 5/6$, but in case of functionally graded materials, k_s can be expressed as given (Lee, Zhao & Reddy, 2010):

$$k_s = \frac{5}{6 - \{v_c(z)V_c(z) + v_m(z)V_m(z)\}} \quad (8)$$

A set of simplifying assumptions regarding the behavior of thin elastic shells as given by Reddy (2003) are as follows:

1. The thickness of the shell is very small compared to the width and length of the shell.
2. The transverse normal stress is negligible.
3. The thickness-to-radius ratio of the shell is assumed to be small compared to unity.
4. The second derivatives of membrane displacement are small compared to the second derivatives of the transverse displacement. (Reddy, 2003, p.125)

Based on the above assumptions, and by using the von Kármán type geometrical nonlinearity and Sanders's shell theory, the nonlinear strain-displacement relationship for a double-curved shallow shell is given by (Brush & Almroth, 1975) as:

$$\begin{aligned} \begin{Bmatrix} \varepsilon_x \\ \varepsilon_y \\ \gamma_{xy} \end{Bmatrix} &= \begin{Bmatrix} \varepsilon_x^0 \\ \varepsilon_y^0 \\ \gamma_{xy}^0 \end{Bmatrix} + z \begin{Bmatrix} \kappa_x \\ \kappa_y \\ \kappa_{xy} \end{Bmatrix} = \begin{Bmatrix} \frac{\partial u_0}{\partial x} + \frac{w_0}{R_x} + \frac{\partial w_0}{\partial x} \frac{\partial w^*}{\partial x} + \frac{1}{2} \left(\frac{\partial w_0}{\partial x} \right)^2 \\ \frac{\partial v_0}{\partial y} + \frac{w_0}{R_y} + \frac{\partial w_0}{\partial y} \frac{\partial w^*}{\partial y} + \frac{1}{2} \left(\frac{\partial w_0}{\partial y} \right)^2 \\ \frac{\partial u_0}{\partial y} + \frac{\partial v_0}{\partial x} + \frac{\partial w_0}{\partial x} \frac{\partial w_0}{\partial y} + \\ \frac{\partial w^*}{\partial x} \frac{\partial w_0}{\partial y} + \frac{\partial w_0}{\partial x} \frac{\partial w^*}{\partial y} \end{Bmatrix} + z \begin{Bmatrix} \frac{\partial \psi_x}{\partial x} \\ \frac{\partial \psi_y}{\partial y} \\ \frac{\partial \psi_x}{\partial y} + \\ \frac{\partial \psi_y}{\partial x} \end{Bmatrix} \quad (9) \\ \begin{Bmatrix} \gamma_{xz} \\ \gamma_{yz} \end{Bmatrix} &= \begin{Bmatrix} \gamma_{xz}^0 \\ \gamma_{yz}^0 \end{Bmatrix} = \begin{Bmatrix} \frac{\partial w_0}{\partial x} - \frac{u_0}{R_x} + \frac{\partial w^*}{\partial x} + \psi_x \\ \frac{\partial w_0}{\partial y} - \frac{v_0}{R_y} + \frac{\partial w^*}{\partial y} + \psi_y \end{Bmatrix} \end{aligned}$$

where ε_x and ε_y are the normal strains, γ_{xy} is the in-plane shear strain, γ_{xz} and γ_{yz} are the transverse shear deformation, and w^* the initial shell imperfection which represents a small deviation of the shell middle plane.

3.2 Constitutive Relations

The stress-strain relations by Hooke's law for a functionally graded shell under temperature are defined as (Reddy, 2003):

$$\begin{pmatrix} \sigma_x(z, T) \\ \sigma_y(z, T) \\ \tau_{xy}(z, T) \\ \tau_{yz}(z, T) \\ \tau_{xz}(z, T) \end{pmatrix}^{shell+T} = \begin{pmatrix} Q_{11}(z, T) & Q_{12}(z, T) & 0 & 0 & 0 \\ Q_{21}(z, T) & Q_{22}(z, T) & 0 & 0 & 0 \\ 0 & 0 & Q_{66}(z, T) & 0 & 0 \\ 0 & 0 & 0 & Q_{44}(z, T) & 0 \\ 0 & 0 & 0 & 0 & Q_{55}(z, T) \end{pmatrix} \begin{pmatrix} \varepsilon_x - \alpha_x(z, T)\Delta T(z) \\ \varepsilon_y - \alpha_y(z, T)\Delta T(z) \\ \gamma_{xy} \\ \gamma_{yz} \\ \gamma_{xz} \end{pmatrix} \quad (10)$$

Where

$$Q_{11}(z, T) = Q_{22}(z, T) = \frac{E(z, T)}{1 - \nu^2(z, T)}$$

$$Q_{12}(z, T) = Q_{21}(z, T) = \frac{\nu(z, T)E(z, T)}{1 - \nu^2(z, T)}$$

$$Q_{44}(z, T) = Q_{55}(z, T) = Q_{66}(z, T) = \frac{E(z, T)}{2\{1 + \nu(z, T)\}}$$

It is assumed that the stiffeners are perfectly bonded to the FGM shell, therefore, the normal strain components of the double-curved shell are similar to the skin. Hence, the stress-strain relations of the stiffeners, under temperature, in both x and y directions can be written as:

$$\begin{pmatrix} \sigma_x(z, T) \\ \sigma_y(z, T) \\ \tau_{xy}(z, T) \\ \tau_{yz}(z, T) \\ \tau_{xz}(z, T) \end{pmatrix}^{stiff+T} = \begin{pmatrix} E_x(z, T) & 0 & 0 & 0 & 0 \\ 0 & E_y(z, T) & 0 & 0 & 0 \\ 0 & 0 & 0 & 0 & 0 \\ 0 & 0 & 0 & G_y(z, T) & 0 \\ 0 & 0 & 0 & 0 & G_x(z, T) \end{pmatrix} \begin{pmatrix} \varepsilon_x - \alpha_{sx}(z, T)\Delta T(z) \\ \varepsilon_y - \alpha_{sy}(z, T)\Delta T(z) \\ \gamma_{xy} \\ \gamma_{yz} \\ \gamma_{xz} \end{pmatrix} \quad (11)$$

where $G_x(z, T)$, $G_y(z, T)$ are shear moduli of stiffeners in x and y direction respectively.

For the case of numerous identical and closely spaced stiffeners, the contribution of the stiffeners can be accounted for by using the lekhmitsky smeared stiffeners technique. In other words, the effect of the stiffeners is assumed to be smeared over the skin where the twisting of stiffeners is also included. The forces and moment resultants of the FGM stiffened double-curved shell under temperature are obtained by integrating their normal and shear stresses over its thickness as follow (Birman, 2011):

$$\begin{Bmatrix} N_x \\ N_y \\ N_{xy} \end{Bmatrix} = \int_{-\frac{h}{2}}^{\frac{h}{2}} \begin{Bmatrix} \sigma_x(z, T) \\ \sigma_y(z, T) \\ \tau_{xy}(z, T) \end{Bmatrix}^{Shell+T} dz + \int_{\frac{h}{2}}^{\frac{h}{2}+h_{x,y}} \begin{Bmatrix} \sigma_x(z, T) \\ \sigma_y(z, T) \\ 0 \end{Bmatrix}^{Stiff+T} dz \quad (12a)$$

$$\begin{Bmatrix} M_x \\ M_y \\ M_{xy} \end{Bmatrix} = \int_{-\frac{h}{2}}^{\frac{h}{2}} \begin{Bmatrix} \sigma_x(z, T) \\ \sigma_y(z, T) \\ \tau_{xy}(z, T) \end{Bmatrix}^{Shell+T} z dz + \int_{\frac{h}{2}}^{\frac{h}{2}+h_{x,y}} \begin{Bmatrix} \sigma_x(z, T) \\ \sigma_y(z, T) \\ 0 \end{Bmatrix}^{Stiff+T} z dz \quad (12b)$$

$$\begin{Bmatrix} Q_x \\ Q_y \end{Bmatrix} = k_s \int_{-\frac{h}{2}}^{\frac{h}{2}} \begin{Bmatrix} \tau_{yz}(z, T) \\ \tau_{xz}(z, T) \end{Bmatrix}^{Shell+T} dz + k_s \int_{\frac{h}{2}}^{\frac{h}{2}+h_{x,y}} \begin{Bmatrix} \tau_{yz}(z, T) \\ \tau_{xz}(z, T) \end{Bmatrix}^{Stiff+T} dz \quad (12c)$$

Substituting equations (9), (10), (11) into equations (12 a-c) yield the constitutive relations as follow:

$$\begin{Bmatrix} N_x \\ N_y \\ N_{xy} \\ M_x \\ M_y \\ M_{xy} \end{Bmatrix} = \begin{Bmatrix} A'_{11} & A'_{12} & 0 & B'_{11} & B'_{12} & 0 \\ A'_{21} & A'_{22} & 0 & B'_{21} & B'_{22} & 0 \\ 0 & 0 & A'_{66} & 0 & 0 & B'_{66} \\ B'_{11} & B'_{12} & 0 & D'_{11} & D'_{12} & 0 \\ B'_{21} & B'_{22} & 0 & D'_{21} & D'_{22} & 0 \\ 0 & 0 & B'_{66} & 0 & 0 & D'_{66} \end{Bmatrix} \begin{Bmatrix} \varepsilon_x^0 \\ \varepsilon_y^0 \\ \gamma_{xy}^0 \\ \kappa_x \\ \kappa_y \\ \kappa_{xy} \end{Bmatrix} - \begin{Bmatrix} N_x^T \\ N_y^T \\ N_{xy}^T \\ M_x^T \\ M_y^T \\ M_{xy}^T \end{Bmatrix} \quad (13a)$$

$$\begin{Bmatrix} Q_x \\ Q_y \end{Bmatrix} = k_s \begin{Bmatrix} A'_{55} & 0 \\ 0 & A'_{44} \end{Bmatrix} \begin{Bmatrix} \gamma_{xz}^0 \\ \gamma_{yz}^0 \end{Bmatrix} \quad (13b)$$

where the equivalent-Shell Stiffnesses for a reinforced shell are:

$$\begin{Bmatrix} A'_{11} & A'_{12} & 0 \\ A'_{21} & A'_{22} & 0 \\ 0 & 0 & A'_{66} \end{Bmatrix} = \begin{Bmatrix} A_{11} & A_{12} & 0 \\ A_{21} & A_{22} & 0 \\ 0 & 0 & A_{66} \end{Bmatrix} + \begin{Bmatrix} \frac{E_x A_x}{d_x} & 0 & 0 \\ 0 & \frac{E_y A_y}{d_y} & 0 \\ 0 & 0 & 0 \end{Bmatrix} \quad (14a)$$

$$\begin{Bmatrix} B'_{11} & B'_{12} & 0 \\ B'_{21} & B'_{22} & 0 \\ 0 & 0 & B'_{66} \end{Bmatrix} = \begin{Bmatrix} B_{11} & B_{12} & 0 \\ B_{21} & B_{22} & 0 \\ 0 & 0 & B_{66} \end{Bmatrix} + \begin{Bmatrix} \frac{E_x A_x e_x}{d_x} & 0 & 0 \\ 0 & \frac{E_y A_y e_y}{d_y} & 0 \\ 0 & 0 & 0 \end{Bmatrix} \quad (14b)$$

$$\begin{Bmatrix} D'_{11} & D'_{12} & 0 \\ D'_{21} & D'_{22} & 0 \\ 0 & 0 & D'_{66} \end{Bmatrix} = \begin{Bmatrix} D_{11} & D_{12} & 0 \\ D_{21} & D_{22} & 0 \\ 0 & 0 & D_{66} \end{Bmatrix} + \begin{Bmatrix} \frac{E_x I'_x}{d_x} & 0 & 0 \\ 0 & \frac{E_y I'_y}{d_y} & 0 \\ 0 & 0 & \frac{1}{2} \left(\frac{G_x J_x}{d_x} + \frac{G_y J_y}{d_y} \right) \end{Bmatrix} \quad (14c)$$

$$\begin{Bmatrix} A'_{55} & 0 \\ 0 & A'_{44} \end{Bmatrix} = \begin{Bmatrix} A_{55} & 0 \\ 0 & A_{44} \end{Bmatrix} + \begin{Bmatrix} \frac{G_x A_x}{d_x} & 0 \\ 0 & \frac{G_y A_y}{d_y} \end{Bmatrix} \quad (14d)$$

$$\begin{Bmatrix} N_x^T \\ N_y^T \\ N_{xy}^T \\ M_x^T \\ M_y^T \\ M_{xy}^T \end{Bmatrix} = \begin{Bmatrix} \Phi_{1x}^{T/Shell} + \Phi_{1x}^{T/Stiff} \\ \Phi_{1y}^{T/Shell} + \Phi_{1y}^{T/Stiff} \\ 0 \\ \Phi_{2x}^{T/Shell} + \Phi_{2x}^{T/Stiff} \\ \Phi_{2y}^{T/Shell} + \Phi_{2y}^{T/Stiff} \\ 0 \end{Bmatrix} \quad (14e)$$

and where G_x and G_y are shear moduli, J_x and J_y are the effective torsional constants, I'_x and I'_y are the second moment of the area of the stiffeners with respect to x and y-axis respectively and are expressed as (Nemeth, 2011):

$$G_x = \frac{E_x}{2(1 + \nu)} \quad (15a)$$

$$G_y = \frac{E_y}{2(1 + \nu)} \quad (15b)$$

$$J_x = \frac{d_x (h_x)^3}{3} \left\{ 1 - \frac{64 h_x}{3 \pi^5 d_x} \tanh \left(\frac{\pi d_x}{2 h_x} \right) \right\} \quad (15c)$$

$$J_y = \frac{d_y(h_y)^3}{3} \left\{ 1 - \frac{64h_y}{3\pi^5 d_y} \tanh\left(\frac{\pi d_y}{2h_y}\right) \right\} \quad (15d)$$

$$I'_x = I_x + A_x(e_x)^2 \quad (15e)$$

$$I'_y = I_y + A_y(e_y)^2 \quad (15f)$$

Matrices A, B, A_s and D represent the extensional, bending – extensional coupling, transverse shear and bending stiffness, and are expressed as:

$$(A_{ij}, B_{ij}, D_{ij}) = \int_{-h/2}^{h/2} Q_{ij}(z, T) (1, z, z^2) dz \quad \text{for } i, j = 1, 2, 6 \quad (16a)$$

$$A_{ij}^s = \int_{-h/2}^{h/2} Q_{ij}(z, T) dz \quad \text{for } i, j = 4, 5 \quad (16b)$$

Thermal stresses in both, the shell and the stiffeners are given as follow:

$$\Phi_{1x}^{T/Shell} = \int_{-\frac{h}{2}}^{\frac{h}{2}} \{Q_{11}(z, T)\alpha_x(z, T) + Q_{12}(z, T)\alpha_y(z, T)\} \Delta T(z) dz \quad (17a)$$

$$\Phi_{1y}^{T/Shell} = \int_{-\frac{h}{2}}^{\frac{h}{2}} \{Q_{21}(z, T)\alpha_x(z, T) + Q_{22}(z, T)\alpha_y(z, T)\} \Delta T(z) dz \quad (17b)$$

$$\Phi_{2x}^{T/Shell} = \int_{-\frac{h}{2}}^{\frac{h}{2}} \{Q_{11}(z, T)\alpha_x(z, T) + Q_{12}(z, T)\alpha_y(z, T)\} \Delta T(z) z dz \quad (17c)$$

$$\Phi_{2y}^{T/Shell} = \int_{-\frac{h}{2}}^{\frac{h}{2}} \{Q_{21}(z, T)\alpha_x(z, T) + Q_{22}(z, T)\alpha_y(z, T)\} \Delta T(z) z dz \quad (17d)$$

$$(\Phi_{1x}^{T/Stiff}, \Phi_{2x}^{T/Stiff}) = \left(\frac{b_x}{d_x}\right) \int_{\frac{h}{2}}^{\frac{h}{2}+h_x} E_x(z, T)\alpha_{sx}(z, T)\Delta T(z)(1, z) dz \quad (17e)$$

$$(\Phi_{1y}^{T/Stiff}, \Phi_{2y}^{T/Stiff}) = \left(\frac{b_y}{d_y}\right) \int_{\frac{h}{2}}^{\frac{h}{2}+h_y} E_y(z, T)\alpha_{sy}(z, T)\Delta T(z)(1, z) dz \quad (17f)$$

The expression of the force and moment resultants in equations (13 a-b) can be expanded and written in terms of u_0, v_0, w_0 displacements:

$$\begin{aligned}
N_x &= \left(A_{11} + \frac{E_x A_x}{d_x} \right) \left\{ \frac{\partial u_0}{\partial x} + \frac{w_0}{R_x} + \frac{\partial w_0}{\partial x} \frac{\partial w^*}{\partial x} + \frac{1}{2} \left(\frac{\partial w_0}{\partial x} \right)^2 \right\} + B_{12} \frac{\partial \psi_y}{\partial y} \\
&+ \left(B_{11} + \frac{E_x A_x e_x}{d_x} \right) \frac{\partial \psi_x}{\partial x} + A_{12} \left\{ \frac{\partial v_0}{\partial y} + \frac{w_0}{R_y} + \frac{\partial w_0}{\partial y} \frac{\partial w^*}{\partial y} + \frac{1}{2} \left(\frac{\partial w_0}{\partial y} \right)^2 \right\} \\
&- \Phi_{1x}^{T/Shell} - \Phi_{1x}^{T/Stiff}
\end{aligned} \tag{18a}$$

$$\begin{aligned}
N_y &= \left(A_{22} + \frac{E_y A_y}{d_y} \right) \left\{ \frac{\partial v_0}{\partial y} + \frac{w_0}{R_y} + \frac{\partial w_0}{\partial y} \frac{\partial w^*}{\partial y} + \frac{1}{2} \left(\frac{\partial w_0}{\partial y} \right)^2 \right\} + B_{21} \frac{\partial \psi_x}{\partial x} \\
&+ \left(B_{22} + \frac{E_y A_y e_y}{d_y} \right) \frac{\partial \psi_y}{\partial y} + A_{21} \left\{ \frac{\partial u_0}{\partial x} + \frac{w_0}{R_x} + \frac{\partial w_0}{\partial x} \frac{\partial w^*}{\partial x} + \frac{1}{2} \left(\frac{\partial w_0}{\partial x} \right)^2 \right\} \\
&- \Phi_{1y}^{T/Shell} - \Phi_{1y}^{T/Stiff}
\end{aligned} \tag{18b}$$

$$\begin{aligned}
N_{xy} &= A_{66} \left(\frac{\partial u_0}{\partial y} + \frac{\partial v_0}{\partial x} + \frac{\partial w_0}{\partial x} \frac{\partial w_0}{\partial y} + \frac{\partial w^*}{\partial x} \frac{\partial w_0}{\partial y} + \frac{\partial w_0}{\partial x} \frac{\partial w^*}{\partial y} \right) \\
&+ B_{66} \left(\frac{\partial \psi_x}{\partial y} + \frac{\partial \psi_y}{\partial x} \right)
\end{aligned} \tag{18c}$$

$$\begin{aligned}
M_x &= \left(B_{11} + \frac{E_x A_x e_x}{d_x} \right) \left\{ \frac{\partial u_0}{\partial x} + \frac{w_0}{R_x} + \frac{\partial w_0}{\partial x} \frac{\partial w^*}{\partial x} + \frac{1}{2} \left(\frac{\partial w_0}{\partial x} \right)^2 \right\} + D_{12} \frac{\partial \psi_y}{\partial y} \\
&+ \left(D_{11} + \frac{E_x I'_x}{d_x} \right) \frac{\partial \psi_x}{\partial x} + B_{12} \left\{ \frac{\partial v_0}{\partial y} + \frac{w_0}{R_y} + \frac{\partial w_0}{\partial y} \frac{\partial w^*}{\partial y} + \frac{1}{2} \left(\frac{\partial w_0}{\partial y} \right)^2 \right\} \\
&- \Phi_{2x}^{T/Shell} - \Phi_{2x}^{T/Stiff}
\end{aligned} \tag{18d}$$

$$\begin{aligned}
M_y &= \left(B_{22} + \frac{E_y A_y e_y}{d_y} \right) \left\{ \frac{\partial v_0}{\partial y} + \frac{w_0}{R_y} + \frac{\partial w_0}{\partial y} \frac{\partial w^*}{\partial y} + \frac{1}{2} \left(\frac{\partial w_0}{\partial y} \right)^2 \right\} + D_{21} \frac{\partial \psi_x}{\partial x} \\
&+ \left(D_{22} + \frac{E_y I'_y}{d_y} \right) \frac{\partial \psi_y}{\partial y} + B_{21} \left\{ \frac{\partial u_0}{\partial x} + \frac{w_0}{R_x} + \frac{\partial w_0}{\partial x} \frac{\partial w^*}{\partial x} + \frac{1}{2} \left(\frac{\partial w_0}{\partial x} \right)^2 \right\} \\
&- \Phi_{2y}^{T/Shell} - \Phi_{2y}^{T/Stiff}
\end{aligned} \tag{18e}$$

$$\begin{aligned}
M_{xy} &= B_{66} \left(\frac{\partial u_0}{\partial y} + \frac{\partial v_0}{\partial x} + \frac{\partial w_0}{\partial x} \frac{\partial w_0}{\partial y} + \frac{\partial w^*}{\partial x} \frac{\partial w_0}{\partial y} + \frac{\partial w_0}{\partial x} \frac{\partial w^*}{\partial y} \right) \\
&+ \left\{ D_{66} + \frac{1}{2} \left(\frac{G_x J_x}{d_x} + \frac{G_y J_y}{d_y} \right) \right\} \left(\frac{\partial \psi_x}{\partial y} + \frac{\partial \psi_y}{\partial x} \right)
\end{aligned} \tag{18f}$$

$$Q_x = k_s \left(A_{55} + \frac{G_x A_x}{d_x} \right) \left(\frac{\partial w_0}{\partial x} - \frac{u_0}{R_x} + \frac{\partial w^*}{\partial x} + \psi_x \right) \tag{18g}$$

$$Q_y = k_s \left(A_{44} + \frac{G_y A_y}{d_y} \right) \left(\frac{\partial w_0}{\partial y} - \frac{v_0}{R_y} + \frac{\partial w^*}{\partial y} + \psi_y \right) \quad (18h)$$

3.3 Equations of Motion

The nonlinear equations of motion of imperfect eccentrically stiffened functionally graded double curved shell based on Sanders's shell theory that accounts for the shear deformation are expressed as follow (Reddy, 2003):

$$\frac{\partial N_x}{\partial x} + \frac{\partial}{\partial y} (N_{xy} + C_0 M_{xy}) + \frac{Q_x}{R_x} = I_0 \left(\frac{\partial^2 u_0}{\partial t^2} \right) + I_1 \left(\frac{\partial^2 \psi_x}{\partial t^2} \right) \quad (19a)$$

$$\frac{\partial}{\partial x} (N_{xy} - C_0 M_{xy}) + \frac{\partial N_y}{\partial y} + \frac{Q_y}{R_y} = I_0 \left(\frac{\partial^2 v_0}{\partial t^2} \right) + I_1 \left(\frac{\partial^2 \psi_y}{\partial t^2} \right) \quad (19b)$$

$$\begin{aligned} \frac{\partial Q_x}{\partial x} + \frac{\partial Q_y}{\partial y} - \frac{N_x}{R_x} - \frac{N_y}{R_y} + \frac{\partial}{\partial x} \left\{ N_x \left(\frac{\partial w_0}{\partial x} + \frac{\partial w^*}{\partial x} \right) + N_{xy} \left(\frac{\partial w_0}{\partial y} + \frac{\partial w^*}{\partial y} \right) \right\} + Q_z \\ + \frac{\partial}{\partial y} \left\{ N_{xy} \left(\frac{\partial w_0}{\partial x} + \frac{\partial w^*}{\partial x} \right) + N_y \left(\frac{\partial w_0}{\partial y} + \frac{\partial w^*}{\partial y} \right) \right\} = I_0 \left(\frac{\partial^2 w_0}{\partial t^2} \right) + 2\epsilon I_0 \frac{\partial w_0}{\partial t} \end{aligned} \quad (19c)$$

$$\frac{\partial M_x}{\partial x} + \frac{\partial M_{xy}}{\partial y} - Q_x = I_1 \left(\frac{\partial^2 u_0}{\partial t^2} \right) + I_2 \left(\frac{\partial^2 \psi_x}{\partial t^2} \right) \quad (19d)$$

$$\frac{\partial M_y}{\partial y} + \frac{\partial M_{xy}}{\partial x} - Q_y = I_1 \left(\frac{\partial^2 v_0}{\partial t^2} \right) + I_2 \left(\frac{\partial^2 \psi_y}{\partial t^2} \right) \quad (19e)$$

Where $C_0 = \frac{1}{2} \left(\frac{1}{R_x} - \frac{1}{R_y} \right)$ and Q_x, Q_y and Q_z are uniformly distributed pressures over the shell surface in x,y, and z-direction. I_0, I_1, I_2 are calculated by:

$$I_i = \int_{-\frac{h}{2}}^{\frac{h}{2}} \rho(z, T) z^i dz + \left(\frac{b_x^T}{d_x^T} \right) \int_{\frac{h}{2}}^{\frac{h}{2} + h_x^T} \rho_{sx}(z, T) z^i dz + \left(\frac{b_y^T}{d_y^T} \right) \int_{\frac{h}{2}}^{\frac{h}{2} + h_y^T} \rho_{sy}(z, T) z^i dz \quad (20)$$

for $i, j = 0, 1, 2$

To investigate the dynamic movement of the stiffened double-curved shell under temperature, the governing equations are required to be written in terms of displacements.

By substituting equations (18 e-h) into equations (19 a-e), one can obtain:

$$\begin{aligned}
&L_{11}(u_0) + L_{12}(v_0) + L_{13}(w_0) + L_{14}(\psi_x) + L_{15}(\psi_y) + L_{16}(w^*) + NL_1(w_0) \\
&+ NL_2(w_0, w^*) = I_0 \left(\frac{\partial^2 u_0}{\partial t^2} \right) + I_1 \left(\frac{\partial^2 \psi_x}{\partial t^2} \right)
\end{aligned} \tag{21a}$$

$$\begin{aligned}
&L_{21}(u_0) + L_{22}(v_0) + L_{23}(w_0) + L_{24}(\psi_x) + L_{25}(\psi_y) + L_{26}(w^*) + NL_3(w_0) \\
&+ NL_4(w_0, w^*) = I_0 \left(\frac{\partial^2 v_0}{\partial t^2} \right) + I_1 \left(\frac{\partial^2 \psi_y}{\partial t^2} \right)
\end{aligned} \tag{21b}$$

$$\begin{aligned}
&L_{31}(u_0) + L_{32}(v_0) + L_{33}(w_0) + L_{34}(\psi_x) + L_{35}(\psi_y) + L_{36}(w^*) + L_{37}(\Phi) \\
&+ NL_5(w_0) + NL_6(u_0, w_0) + NL_7(v_0, w_0) + NL_8(\psi_x, w_0) + NL_9(\psi_y, w_0) \\
&+ NL_{10}(w_0, w^*) + NL_{11}(u_0, w^*) + NL_{12}(v_0, w^*) + NL_{13}(\psi_x, w^*) \\
&+ NL_{14}(\psi_y, w^*) + Q_z = I_0 \left(\frac{\partial^2 w_0}{\partial t^2} \right) + 2\epsilon I_0 \frac{\partial w_0}{\partial t}
\end{aligned} \tag{21c}$$

$$\begin{aligned}
&L_{41}(u_0) + L_{42}(v_0) + L_{43}(w_0) + L_{44}(\psi_x) + L_{45}(\psi_y) + L_{46}(w^*) + NL_{15}(w_0) \\
&+ NL_{16}(w_0, w^*) = I_1 \left(\frac{\partial^2 u_0}{\partial t^2} \right) + I_2 \left(\frac{\partial^2 \psi_x}{\partial t^2} \right)
\end{aligned} \tag{21d}$$

$$\begin{aligned}
&L_{51}(u_0) + L_{52}(v_0) + L_{53}(w_0) + L_{54}(\psi_x) + L_{55}(\psi_y) + L_{56}(w^*) + NL_{17}(w_0) \\
&+ NL_{18}(w_0, w^*) = I_1 \left(\frac{\partial^2 v_0}{\partial t^2} \right) + I_2 \left(\frac{\partial^2 \psi_y}{\partial t^2} \right)
\end{aligned} \tag{21e}$$

where L_{ij} ($i = 1,2,3,4,5; j = 1,2,3,4,5,6$) are the linear operator and NL_i ($i =$

$1,2, \dots, 18$), are the nonlinear operators and are given in the Appendix.

3.4 Solution Procedures

It can be seen that equations (21 a-e) show highly coupling between displacements and rotations. To solve the coupled equations, some trigonometric series are used. Suppose that all four edges are simply supported and restrained from moving, in other words, all edges are immovable, then the following conditions are encountered (Chia, 1980):

$$\begin{aligned}
 u_0 = v_0 = 0 & & \text{at } x = 0, \frac{a}{2}, a \\
 w_0 = \psi_y = M_x = \partial^2 w_0 / \partial x^2 = 0 & & \text{at } x = 0, a
 \end{aligned} \tag{22a}$$

$$\begin{aligned}
 u_0 = v_0 = 0 & & \text{at } y = 0, \frac{b}{2}, b \\
 w_0 = \psi_x = M_y = \partial^2 w_0 / \partial y^2 = 0 & & \text{at } y = 0, b
 \end{aligned} \tag{22b}$$

The geometric boundary conditions given by equations (22 a-b) are satisfied identically by employing the following doubly Fourier series equations:

$$u_0(x, y, t) = \sum_{m=1}^M \sum_{n=1}^N U_{mn}(t) \sin\left(\frac{2m\pi x}{a}\right) \sin\left(\frac{n\pi y}{b}\right) \tag{23a}$$

$$v_0(x, y, t) = \sum_{m=1}^M \sum_{n=1}^N V_{mn}(t) \sin\left(\frac{m\pi x}{a}\right) \sin\left(\frac{2n\pi y}{b}\right) \tag{23b}$$

$$w_0(x, y, t) = \sum_{m=1}^M \sum_{n=1}^N W_{mn}(t) \sin\left(\frac{m\pi x}{a}\right) \sin\left(\frac{n\pi y}{b}\right) \tag{23c}$$

$$\psi_x(x, y, t) = \sum_{m=1}^M \sum_{n=1}^N X_{mn}(t) \cos\left(\frac{m\pi x}{a}\right) \sin\left(\frac{n\pi y}{b}\right) \tag{23d}$$

$$\psi_y(x, y, t) = \sum_{m=1}^M \sum_{n=1}^N Y_{mn}(t) \sin\left(\frac{m\pi x}{a}\right) \cos\left(\frac{n\pi y}{b}\right) \tag{23e}$$

$$w^*(x, y, t) = \sum_{m=1}^{\infty} \sum_{n=1}^{\infty} \mu h \sin\left(\frac{m\pi x}{a}\right) \sin\left(\frac{n\pi y}{b}\right) \tag{23f}$$

where m and n denote the number of half-waves in x and y directions, respectively. The terms $U_{mn}(t)$, $V_{mn}(t)$, $W_{mn}(t)$, $X_{mn}(t)$ and $Y_{mn}(t)$ are the generalized coordinates, which are the unknown functions of time “ t ,” and the coefficient “ μ ” is the imperfection constant ($0 \leq \mu \leq 1$). Furthermore, the external force Q_z for the static case can be expressed in the form of double trigonometric series as follow (Brush & Almroth, 1975):

$$Q_z(x, y) = \sum_{m=1}^M \sum_{n=1}^N q_{zmn} \sin\left(\frac{m\pi x}{a}\right) \sin\left(\frac{n\pi y}{b}\right) \quad (24)$$

The coefficients q_{zmn} for the case of uniformly distributed load are defined as:

$$q_{zmn} = \begin{cases} \frac{16q_0}{mn\pi^2} & \text{for } m, n \text{ odd} \\ 0 & \text{for } m, n \text{ even} \end{cases} \quad (25)$$

Where q_0 , is the amplitude of the excitation. For the case of sinusoidal distributed load:

$$q_{zmn} = q_0 \text{ for } m = n = 1 \quad (26)$$

Finally, for the case of concentrated load:

$$q_{zmn} = \frac{4q_0}{ab} \text{ for } m = n = 1 \quad (27)$$

Substituting equations (23 a-d) and equation (24) into equations of motion (21 a-e) and then applying single-mode Galerkin's method, five equations in terms of the time-dependent variables $U_{mn}(t)$, $V_{mn}(t)$, $W_{mn}(t)$, $X_{mn}(t)$ and $Y_{mn}(t)$ are obtained as follows:

$$\begin{aligned} & l_{11}U_{mn}(t) + l_{12}V_{mn}(t) + l_{13}W_{mn}(t) + l_{14}X_{mn}(t) + l_{15}Y_{mn}(t) + l_{16}\mu h \\ & + l_{17}\{W_{mn}^2(t) + 2\mu h W_{mn}(t)\} = I_0\ddot{U}_{mn}(t) + I_1\ddot{X}_{mn}(t) \end{aligned} \quad (28a)$$

$$\begin{aligned} & l_{21}U_{mn}(t) + l_{22}V_{mn}(t) + l_{23}W_{mn}(t) + l_{24}X_{mn}(t) + l_{25}Y_{mn}(t) + l_{26}\mu h \\ & + l_{27}\{W_{mn}^2(t) + 2\mu h W_{mn}(t)\} = I_0\ddot{V}_{mn}(t) + I_1\ddot{Y}_{mn}(t) \end{aligned} \quad (28b)$$

$$\begin{aligned} & l_{31}U_{mn}(t) + l_{32}V_{mn}(t) + l_{33}W_{mn}(t) + l_{34}X_{mn}(t) + l_{35}Y_{mn}(t) + l_{36}\mu h \\ & + l_{37}(W_{mn}(t) + \mu h)U_{mn}(t) + l_{38}(W_{mn}(t) + \mu h)V_{mn}(t) + l_{39}(W_{mn}(t) \\ & + \mu h)X_{mn}(t) + l_{310}(W_{mn}(t) + \mu h)Y_{mn}(t) + l_{311}W_{mn}(t)W_{mn}(t) \\ & + l_{312}\{W_{mn}(t) + \mu h\}\{W_{mn}(t) + 2\mu h\}W_{mn}(t) + l_{313}(\Phi) + q_{zmn}(t) \\ & = I_0\ddot{W}_{mn}(t) + 2\epsilon I_0\dot{W}_{mn}(t) \end{aligned} \quad (28c)$$

$$\begin{aligned}
& l_{41}U_{mn}(t) + l_{42}V_{mn}(t) + l_{43}W_{mn}(t) + l_{44}X_{mn}(t) + l_{45}Y_{mn}(t) + l_{46}\mu h \\
& + l_{47}\{W_{mn}^2(t) + 2\mu h W_{mn}(t)\} = I_1\ddot{U}_{mn}(t) + I_2\ddot{X}_{mn}(t)
\end{aligned} \tag{28d}$$

$$\begin{aligned}
& l_{51}U_{mn}(t) + l_{52}V_{mn}(t) + l_{53}W_{mn}(t) + l_{54}X_{mn}(t) + l_{55}Y_{mn}(t) + l_{56}\mu h \\
& + l_{57}\{W_{mn}^2(t) + 2\mu h W_{mn}(t)\} = I_1\ddot{V}_{mn}(t) + I_2\ddot{Y}_{mn}(t)
\end{aligned} \tag{28e}$$

3.4.1 Linear Vibration Analysis Solution

By taking the linear terms of equations (28 a-e), and neglect the effect of damping and imperfection, the above equations of motion can be written in a matrix form as:

$$\begin{bmatrix} l_{11} & l_{12} & l_{13} & l_{14} & l_{15} \\ l_{21} & l_{22} & l_{23} & l_{24} & l_{25} \\ l_{31} & l_{32} & l_{33} & l_{34} & l_{35} \\ l_{41} & l_{42} & l_{43} & l_{44} & l_{45} \\ l_{51} & l_{52} & l_{53} & l_{54} & l_{55} \end{bmatrix} \begin{Bmatrix} U_{mn}(t) \\ V_{mn}(t) \\ W_{mn}(t) \\ X_{mn}(t) \\ Y_{mn}(t) \end{Bmatrix} + \begin{bmatrix} I_0 & 0 & 0 & I_1 & 0 \\ 0 & I_0 & 0 & 0 & I_2 \\ 0 & 0 & I_0 & 0 & 0 \\ I_1 & 0 & 0 & I_1 & 0 \\ 0 & I_1 & 0 & 0 & I_1 \end{bmatrix} \begin{Bmatrix} \ddot{U}_{mn}(t) \\ \ddot{V}_{mn}(t) \\ \ddot{W}_{mn}(t) \\ \ddot{X}_{mn}(t) \\ \ddot{Y}_{mn}(t) \end{Bmatrix} = \begin{Bmatrix} 0 \\ 0 \\ 0 \\ 0 \\ 0 \end{Bmatrix} \tag{29}$$

For calculating the natural frequency under thermal load, assuming the generalized coordinate are of the form:

$$\begin{aligned}
U_{mn}(t) = U_{mn}e^{i\omega t}; V_{mn}(t) = V_{mn}e^{i\omega t}; W_{mn}(t) = W_{mn}e^{i\omega t}; X_{mn}(t) = \\
X_{mn}e^{i\omega t} \text{ and } Y_{mn}(t) = Y_{mn}e^{i\omega t}
\end{aligned} \tag{30}$$

where ω , is the natural frequency. In addition, substituting assumptions (30) into equation (29) and solving the resultant determinant, leads to five frequencies. The smallest one of which is called the fundamental frequency.

3.4.2 The solution of Nonlinear Static Equations

Consider the FGM double-curved shell with all four edges simply supported and subjected to uniform external transverse load without any imperfection, damping effects and inertial forces. After considering the assumptions above, the static deflection is determined by setting all the time derivative terms in equations (28 a, b, d, and e) through (28e) equal to zero and solving the resulting equations in terms of displacement

components U_{mn} , V_{mn} , X_{mn} and Y_{mn} . Then substituting the results into equation (28c) without the time derivatives (static equation), to obtain the static-deflection curves of the eccentrically FGM double curved shells:

$$\begin{aligned} & \{P_1 + P_6(\mu h) + P_8(\mu h)^2\}W_{mn} + \{P_2 + P_7(\mu h)\}W_{mn}^2 + P_3W_{mn}^3 \\ & + \{P_4(\mu h) + P_5(\mu h)^2\} + P_9(\Phi) = q_{zmn} \end{aligned} \quad (31)$$

Note that q_{zmn} in equation (31) is not a function of time. It is given either by equation (26) or by equation (27). All the P's are symbolic equations in the function of the linear operators l_{ij} .

3.4.3 The solution of Nonlinear Dynamic Equations

For this case, Bich, Duc and Quan (2014) and Kobayashi and Leissa (1995) investigated the effect of inertia terms on nonlinear vibration. It was shown that neglecting both, the in-plane and rotational inertia terms, did not cause significant errors. Hence, solving equations (28a), (28b), (28d) and (28e) for $U_{mn}(t)$, $V_{mn}(t)$, $X_{mn}(t)$ and $Y_{mn}(t)$, then substituting the results into equations (28c) the nonlinear dynamic response of stiffened FGM double curved shallow shell, also known as the extended duffing equation is obtained. Note that the original Duffing equation contains only cubic nonlinear term, whereas the extended Duffing equation problem the governing nonlinear differential equation of motion includes the second order term, quadratic term in addition to the cubic term as:

$$\begin{aligned} & M\ddot{W}_{mn}(t) + C\dot{W}_{mn}(t) + \{P_1 + P_6(\mu h) + P_8(\mu h)^2\}W_{mn}(t) \\ & + \{P_2 + P_7(\mu h)\}W_{mn}^2(t) + P_3W_{mn}^3(t) + \{P_4(\mu h) + P_5(\mu h)^2\} \\ & + P_9(\Phi) = q_{zmn}(t) \end{aligned} \quad (32)$$

where M is the global mass, C is the damping coefficient, $\{P_1 + P_6(\mu h) + P_8(\mu h)^2\}$ is the linear stiffness, $\{P_2 + P_7(\mu h)\}$ and P_3 are the nonlinear quadratic and cubic stiffness

respectively, $\{P_4(\mu h) + P_5(\mu h)^2\}$ is the imperfection coefficients, and P_9 is the thermal coefficient of the stiffened shell. For the case of a perfect structure, the extended duffing equation above becomes:

$$M\ddot{W}_{mn}(t) + C\dot{W}_{mn}(t) + P_1W_{mn}(t) + P_2W_{mn}^2(t) + P_3W_{mn}^3(t) + P_9(\Phi) = q_{zmn}(t) \quad (33)$$

Nonlinear response of equations (32) and (33) are investigated using Fourth Order

Runge-Kutta combined with the following initial conditions:

$$W(0) = 0, \frac{\partial W(0)}{\partial t} = 0$$

3.4.4 Amplitude – Frequency Curve

The nonlinear amplitude frequency response of the stiffened double curved shell is studied. The harmonic balance method was is applied using single and multi-harmonic terms. And the he's energy balance is considered to obtain a closed-form solution for the strongly nonlinear Duffing equation.

3.4.4.1 Nonlinear Forced Vibration for Isotropic Shells

Nonlinear vibration of the stiffened FGM double-curved shell is considered under a uniformly distributed pressure $q_{zmn}(t)$. To obtain a closed-form frequency-amplitude response of nonlinear forced vibration, the harmonic balance method is applied. Only a single harmonic term is used for isotropic shells. The excitation is assumed to be harmonic of the form $q_{zmn}(t) = q_{zmn}\cos(\Omega t)$. The response is assumed to be $W(t) = A\cos(\Omega t + \phi)$. Using single-mode Galerkin's method by multiplying equation (32) by $\cos(\Omega t + \phi)$ and $\sin(\Omega t + \phi)$, respectively then integrating both results over the period $T = 2\pi/\Omega$ of nonlinear oscillation, the equation of the amplitude-frequency curve of nonlinear forced vibration with imperfection is expressed as:

$$\left(P_1A + P_6A(\mu h) + P_8A(\mu h)^2 + \frac{3P_3}{4}A^3 - AM\Omega^2\right)^2 + (C\Omega A)^2 = (q_{zmn})^2 \quad (34)$$

For the case of perfect shell, the forced nonlinear amplitude-frequency curve above becomes:

$$\left(P_1A + \frac{3P_3}{4}A^3 - AM\Omega^2\right)^2 + (C\Omega A)^2 = (q_{zmn})^2 \quad (35)$$

3.4.4.2 Nonlinear Free Vibration of Isotropic Shell

Nonlinear free vibration is expressed when the damping coefficient is neglected ($C = 0$) and no external loads exist ($q_{zmn} = 0$) in equation (34) above. In this case, the frequency-amplitude nonlinear free vibration of an imperfect curve is given as follow:

$$\Omega^2 = \frac{P_1}{M} + \frac{P_6(\mu h)}{M} + \frac{P_8(\mu h)^2}{M} + \frac{3P_3}{4M}A^2 \quad (36)$$

For the case of a perfect shell, the free nonlinear amplitude-frequency curve above becomes:

$$\Omega^2 = \frac{K_1}{M} + \frac{3P_3}{4M}A^2 \quad (37)$$

3.4.4.3 Nonlinear Forced Vibration of FGM Shell

In order to find a closed-form solution for the strongly nonlinear Duffing equation above, He's energy balance method is adopted (He, 2006). A variational principle of extended Duffing equation (32) is calculated, then a Hamiltonian is developed. From which the frequency response is obtained by adopting the collocation method (Quan & Duc, 2016). The amplitude-frequency relationship can be expressed as:

$$\frac{3P_3}{16}A^3 + \left(\frac{P_2}{3} - \frac{P_2}{6\sqrt{2}}\right)A^2 + \left(0.25P_1 - \frac{C\pi\Omega}{4} - 0.25\Omega^2\right)A = q_{zmn} \quad (40)$$

3.5 Numerical Results Validation and Discussion

In this section, natural frequency, nonlinear static and dynamic analysis of simply-supported stiffened and unstiffened functionally graded materials double-curved shell with different geometric parameters and material power-law indices under different mechanical loads are analyzed and validated. Throughout this chapter, the metal-ceramic FGM shell is considered to be made of either, Aluminum and Alumina (Al/Al_2O_2) or Stainless steel and Silicon Nitride ($SUS304/Si_3N_4$).

Table 3.1

Material Properties of the FGM Shell (Reddy & Chin, 1998).

Materials	Properties	P_{-1}	P_0	P_1	P_2	P_3
<i>SUS304</i> (metal TID T=300 K)	$E_m(GPa)$	0	201.04	3.079E-4	-6.534E-7	0
	$\alpha_c(1/k)$	0	12.33E-6	8.086E-4	0	0
	$k(W/mK)$	0	15.379	-1.264E-3	2.092E-6	-7.223E-10
	$\rho(Kg/m^3)$	0	8166	0	0	0
<i>Al</i> (metal TID T=300 K)	$E_m(GPa)$	0	70	0	0	0
	$\alpha_c(1/k)$	0	23E-6	0	0	0
	$k(W/mK)$	0	204	0	0	0
	$\rho(Kg/m^3)$	0	2778	0	0	0
<i>Si₃N₄</i> (ceramic TID T=300 K)	$E_m(GPa)$	0	348.43	-3.07E-4	2.16E-7	-8.946E-11
	$\alpha_c(1/k)$	0	5.8723E-6	9.095E-4	0	0
	$k(W/mK)$	0	13.723	-1.032E-3	5.466E-7	-7.876E-11
	$\rho(Kg/m^3)$	0	2370			
<i>Al₂O₂</i> (ceramic TID T=300 K)	$E_m(GPa)$	0	380	0	0	0
	$\alpha_c(1/k)$	0	7.4E-6	0	0	0
	$k(W/mK)$	0	10.4	0	0	0
	$\rho(Kg/m^3)$	0	3800	0	0	0
<i>ZrO₂</i> (ceramic TID T=300 K)	$E_m(GPa)$	0	151	0	0	0
	$\alpha_c(1/k)$	0	10E-6	0	0	0
	$k(W/mK)$	0	2.09	0	0	0
	$\rho(Kg/m^3)$	0	3000	0	0	0

The material properties of the selected FGMs are listed in Table 3.1. It should be noted that the thermal load is not going to be considered in this chapter. The reason is that thermal buckling analysis should be studied and discussed first due to the nature of the boundary conditions adopted here (immobile simply supported). Therefore, the thermal load effect will be evaluated in chapter 4 instead.

3.5.1 Natural Frequency Results

As part of the validation of the present method, a comparison of the dimensionless frequency for the isotropic cylindrical shell is investigated in Table 3.2. The obtained values and compared with the theoretical results of Kobayashi and Leissa (1995) based on first-order shear deformation theory, Shen (2012) based on a higher-order shear deformation shell theory and a three dimensional theory developed by Chern and Chao (2000) for a variety of simply supported shallow panels. The parameters used are: $R = 10b$ and $h = 0.001m$ while the width to thickness ratios are taken to be 10 and 100 and the length to width ratios was increased from 0.5 to 2 by 0.5 increment.

Table 3.2

Comparison of Dimensionless Frequency $\varpi = \omega_{mn}b\sqrt{\rho_m(1-\nu^2)/E_m}$ for Isotropic Cylindrical Panels ($h=0.001$, $R/b=10$).

b/h	Theory	a/b			
		0.5	1.0	1.5	2.0
10	FSDT	1.3360	0.5563	0.4044	0.3505
	HSDT	1.3153	0.5524	0.4022	0.3488
	3D	1.3174	0.5505	0.3998	0.3461
	Present	1.3195	0.5532	0.4026	0.3490
100	FSDT	0.1615	0.0743	0.0505	0.0404
	HSDT	0.1615	0.0743	0.0505	0.0404
	3D	0.1606	0.0736	0.0491	0.0392
	Present	0.1615	0.0743	0.0505	0.0404

A comparison of the dimensionless frequency of simply supported Aluminum and Alumina ($\text{Al}/\text{Al}_2\text{O}_2$) double curved shallow shells for various volume fraction indices and radii of curvature are calculated in Table 3.3. The obtained results are compared with those presented by Bich et al. (2013) based classical thin shell theory, by Chorfi and Houmat (2010) used the first-order shear deformation theory, and by Quan and Duc (2016) accorded to the higher-order shear theory.

Table 3.3

Comparison of Fundamental Natural Frequency Parameter $\varpi = \omega_{mn}h\sqrt{\rho_c/E_c}$ for $\text{Al}/\text{Al}_2\text{O}_3$ FGM Double Curved Shallow Shells ($a/b=1$, $b/h=10$).

Structures	a/R _x	b/R _y	Theory	k			
				0	0.5	1	4
Plate	0	0	CLPT	0.0597	0.0506	0.0456	0.0396
			FSDT	0.0581	0.0502	0.0446	0.0387
			HSDT	0.0615	0.0519	0.0466	0.0404
			Present	0.0588	0.0492	0.0430	0.0381
Cylindrical Shell	0	0.5	CLPT	0.0648	0.0553	0.0501	0.0430
			FSDT	0.0632	0.0543	0.0501	0.0422
			HSDT	0.0662	0.0581	0.0525	0.0462
			Present	0.0622	0.0535	0.0485	0.0413
Spherical Shell	0.5	0.5	CLPT	0.0779	0.0676	0.0617	0.0520
			FSDT	0.0767	0.0668	0.0611	0.0513
			HSDT	0.0783	0.0691	0.0632	0.0529
			Present	0.0757	0.0658	0.0604	0.0507

The fundamental natural frequencies of stiffened and un-stiffened $\text{Al}/\text{Al}_2\text{O}_3$ FGM spherical panels are shown in Table 3.4 below. The stiffeners are made of Alumina ceramic and the Poisson's ratio is chosen to be 0.3. A good agreement can be witnessed with comparison to those obtained by Bich et al. (2013) based on the classical plate theory. The natural frequencies of the stiffened spherical shells are greater than those of un-stiffened shells. The natural frequencies are obviously dependent on the volume

fraction index as shown in the table. They decrease as the power indices increase. This is very reasonable since the values of the elasticity modulus decrease as K increase.

Table 3.4

Comparison of Fundamental Natural Frequency Parameter $\bar{\omega} = \omega_{mn}h\sqrt{\rho_c/E_c}$ of Stiffened and Un-Stiffened Al/Al₂O₃ Spherical Panels ($a = b = 0.8m, h = 0.01m, h_x = h_y = 0.05m, b_x = b_y = 0.0025m, d_x = d_y = 0.1m$).

$R_x=R_y$	K	Un-Stiffened		Stiffened	
		CPT	Present	CPT	Present
3	0.2	0.0207	0.0206	0.0217	0.0217
	1	0.0180	0.0179	0.0196	0.0199
	5	0.0141	0.0140	0.0169	0.0174
	10	0.0129	0.0128	0.0162	0.0165
5	0.2	0.0132	0.0131	0.0171	0.0172
	1	0.0114	0.0113	0.0161	0.0166
	5	0.0090	0.0089	0.0149	0.0153
	10	0.0083	0.0082	0.0147	0.0151
10	0.2	0.0081	0.0081	0.0152	0.0153
	1	0.0069	0.0069	0.0148	0.0151
	5	0.0056	0.0056	0.0144	0.0149
	10	0.0053	0.0053	0.0144	0.0149
∞ (plate)	0.2	0.0054	0.0054	0.0150	0.0152
	1	0.0045	0.0045	0.0149	0.0151
	5	0.0039	0.0039	0.0148	0.0151
	10	0.0037	0.0037	0.0148	0.0151

Next, the first five natural frequencies parameters of stiffened and unstiffened FGM spherical shell are calculated and listed in Table 3.5. It is seen that the values are not significantly different as compared with the results of Bich, Dung and Nam (2013) based on the classical plate theory, and Bich, Duc and Quan (2014) added the first-order shear deformation theory to the previous problem.

Table 3.5

Comparison of First 5 Modes Natural Frequency Parameters $\varpi = \omega_{mn}h\sqrt{\rho_c/E_c}$ of Stiffened and Un-Stiffened Al/Al₂O₃ FGM Spherical Shallow Shell ($a = b = 0.8\text{m}$, $h = 0.01\text{m}$, $h_x = h_y = 0.050\text{m}$, $b_x = b_y = 0.0025\text{m}$, $d_x = d_y = 0.1\text{m}$, $R_x = R_y = 5\text{m}$, $K = 1$)

Mode	(m,n)	Un-Stiffened			Stiffened		
		CPT	FSDT	Present	CPT	FSDT	Present
1	(1,1)	0.0113	0.0112	0.0112	0.0160	0.0158	0.0160
2	(1,2) and (2,1)	0.0152	0.0151	0.0152	0.0421	0.0422	0.0423
3	(2,2)	0.0206	0.0206	0.0207	0.0581	0.0583	0.0584
4	(1,3) and (3,1)	0.0245	0.0245	0.0246	0.0909	0.0902	0.0912
5	(2,3) and (3,2)	0.0307	0.0306	0.0308	0.1002	0.0997	0.1007

To illustrate the accuracy of the proposed approach of stiffened isotropic and FGM double curved shallow shell based on Lekhnitsky smeared stiffeners technique, the first three natural frequencies (rad/s) of stiffened and un-stiffened aluminum and zirconia Al/ZrO₂ FGM rectangular panels are calculated and shown in Table 3.6 and Table 3.7 respectively.

The stiffeners are made of Aluminum and the Poisson's ratio is chosen to be 0.3 for simplicity. The results are compared with the FEM solutions obtained by ABAQUS software using the 8-node doubly curved shell element (S8R). A stepwise approximation is applied to model the material property gradations of the rectangular FGM. To accomplish the convergence of the results, the thickness is divided into 160 layers where the stiffness matrix for each layer is calculated and then assigned at the centroid of each specific layer. Figure 3.1 and Figure 3.2 show the mode shapes of the aluminum and FGM plate with different stiffeners configurations.

Table 3.6

Natural Frequency of a Rectangular Aluminum Plate with Longitudinal, Transversal and Orthogonal Stiffeners ($a/b = 2, h = 0.025\text{m}, h_x = h_y = 0.05\text{m}, b_x = b_y = 0.03\text{m}$).

Mode (m,n)	1 (1,1)			2 (1,2)			3 (1,3)		
	ABAQUS	Present	% Diff	ABAQUS	Present	% Diff	ABAQUS	Present	% Diff
Un-Stiffened	74.295	74.46	0.22	118.62	119.035	0.35	192.65	193.16	0.26
X-Dir (3 stringers)	74.924	74.679	0.32	165.05	166.19	0.68	228	229.16	0.50
Y-Dir (3 stringers)	118.33	120.879	2.13	147.58	149.615	1.36	206.07	207.899	0.88
X-Y Dir (3 x 3 stringer)	113.66	115.087	1.24	184.5	185.535	0.56	328.06	331.821	1.14
X-Dir (7 stringers)	75.56	74.83	0.97	184	182.07	1.05	212.6	212.97	0.17
Y-Dir (7 stringer)	142.32	142.8	0.33	166.74	166.199	0.32	218.16	216.52	0.75
X-Y Dir (7 x 7 stringer)	130.08	129.432	0.5	210.33	208.17	1.03	372.94	370.191	0.74
X-Y Dir (5x 3 stringer)	126.11	126.74	0.5	191.66	191.968	0.16	329.08	331.674	0.78
X-Y Dir (7 x 4 stringer)	133.93	133.93	0	201.4	200.938	0.23	341.87	344.69	0.82

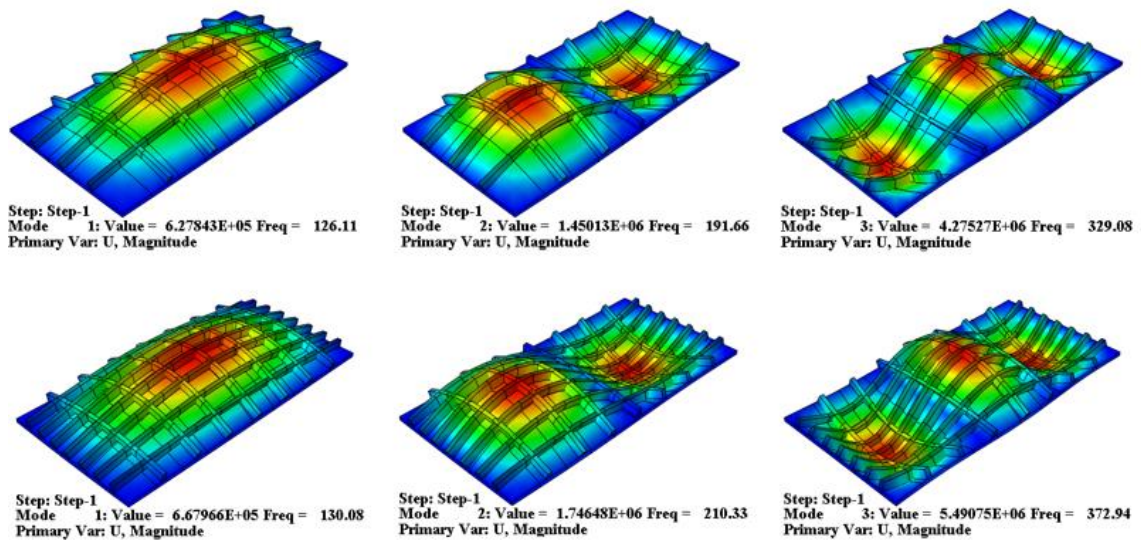


Figure 3.1. Frequency and mode shapes of a stiffened rectangular Aluminum plate using ABAQUS.

Table 3-7

Natural Frequency of a Rectangular Al/ZrO₂ Plate with Longitudinal, Transversal and Orthogonal Stiffeners($a/b = 2$, $h = 0.025\text{m}$, $h_x = h_y = 0.05\text{m}$, $b_x = b_y = 0.03\text{m}$).

Mode (m,n)	1 (1,1)			2 (1,2)			3 (1,3)		
	ABAQUS	Present	% Diff	ABAQUS	Present	% Diff	ABAQUS	Present	% Diff
Un-Stiffened	101.61	102.132	0.51	161.99	163.287	0.79	263.36	265	0.62
X-Dir (3 stringers)	201.5	208.883	3.6	235.61	228.954	6.17	275.4	304.185	9.93
Y-Dir (3 stringers)	111.44	109.477	1.77	274.91	260.416	0.91	319.91	319.12	0.24
X-Y Dir (3 x 3 stringer)	195.13	195.316	0.09	318.35	302.02	2.98	518.02	539.966	4.14
X-Dir (7 stringers)	245.94	245.861	0.03	276.54	241.709	2.55	308.07	312.74	1.5
Y-Dir (7 stringer)	115.84	110.021	5.15	295.65	273.233	0.61	314.66	311.902	0.88
X-Y Dir (7 x 7 stringer)	225.27	222.69	1.15	364.69	320.646	0.71	565.99	570.705	0.82
X-Y Dir (5x 3 stringer)	219.03	219.838	0.36	334.08	273.233	1.2	341.53	334.869	1.96
X-Y Dir (7 x 4 stringer)	232.36	231.151	0.52	351.81	287.137	2.92	305.13	295.781	3.11

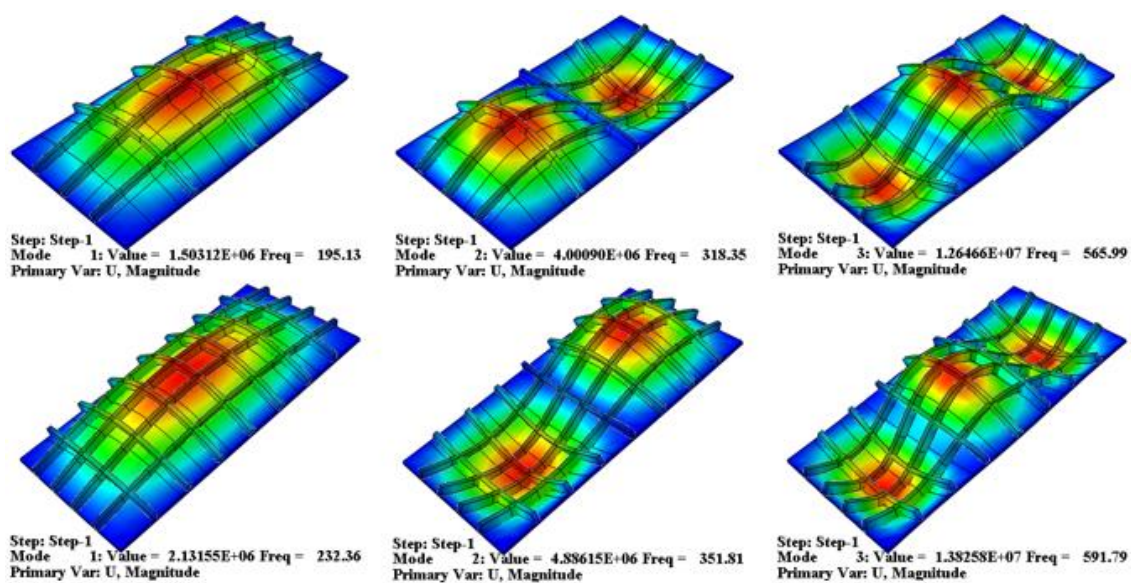


Figure 3.2. Frequency and mode shapes of a stiffened rectangular Al/ZrO₂ plate using ABAQUS.

3.5.2 Nonlinear Static Analysis Results

To validate the results of the present formulation for the case of nonlinear static analysis of mechanically loaded FGM doubly curved shell, a simply supported shell made of Aluminum (Al) and Zirconia (ZrO_2) with different power index K is considered. As the first example, the FGM square plate is subjected to bi-sinusoidal transverse loading. The table shows the non-dimensional deflection of a plate formulated based on classical plate theory (CPT) and first order shear deformation (FSDT) both obtained by Carrera et al. (2011), and higher order shear theory (Parandvar & Farid, 2016). It can be seen that our results are in an excellent agreement with the one based on FSDT in the following Table 3.8.

Table 3.8

Comparison of Non-Dimensional Deflection of the Simply Supported Plate Under Static Bi-Sinusoidal Transverse Loading ($10h^3 E_c w/a^4 q_0$).

K	Theory	a/h		
		4	10	100
1	CPT	0.5623	0.5623	0.5623
	FSDT	0.7291	0.5889	0.5625
	HSDT	0.7251	0.5864	0.5539
	Present	0.7291	0.5889	0.5625
4	CPT	0.8281	0.8281	0.8281
	FSDT	1.1125	0.8736	0.8286
	HSDT	1.1547	0.8777	0.8172
	Present	1.1125	0.8736	0.8286
10	CPT	0.9354	0.9354	0.9354
	FSDT	1.3178	0.9966	0.9360
	HSDT	1.3846	1.0043	0.9247
	Present	1.3178	0.9966	0.9396

Then, the nonlinear load-deflection curves are compared with Zhao and Liew (2009) results based on a modified version of Sander's nonlinear shell theory. The Poisson ratio is chosen to be 0.3 and the material properties are listed in Table 3.1 above. As shown in Figure 3.3, an excellent agreement was met when the present results were compared with (Zhao & Liew, 2009) results.

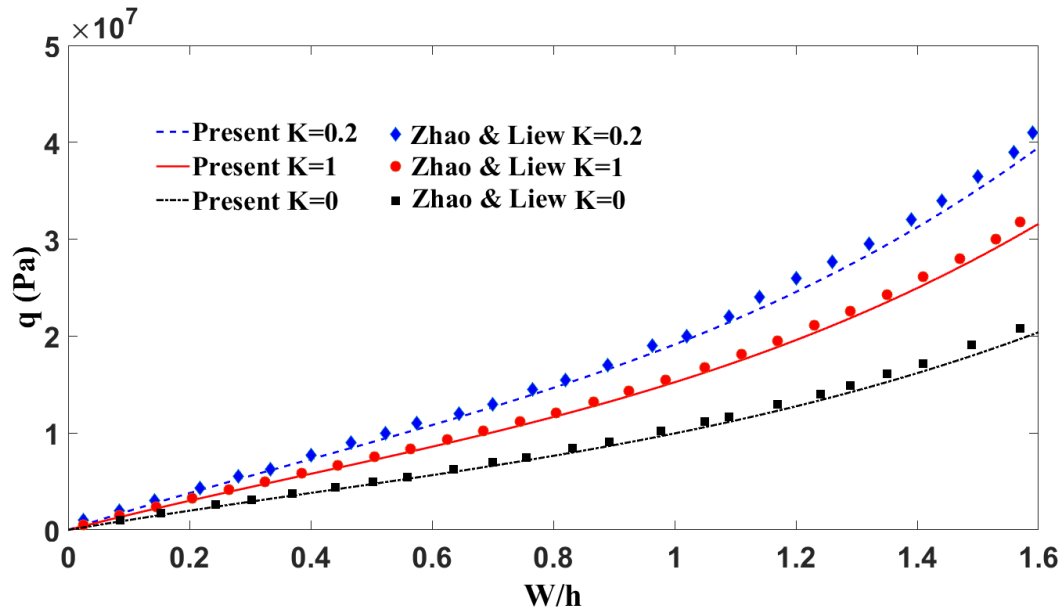


Figure 3.3. Comparisons of nonlinear load-deflection curves with different index K for cylindrical shells ($a/b=1$, $b/h=20$, $h=0.01$, $a/R_y = 0.2$).

Next, a parametric study is conducted on perfect and imperfect Al/ZrO₂ cylindrical shell for different materials and geometric properties. A smooth snap-through behavior of the curved shell is shown in Figure 3.4. It can be seen that for a fixed value of the force q , as the volume fraction indices decreases, the magnitude of the deflection, W/h decreases, the graphs become less nonlinear and more stable and the snap-through response becomes smoother. This is because the concentration of ceramic in the shell increases compared to metal, hence the young's modulus becomes larger. This means that the shell becomes stiffer and therefore, a load of the higher magnitude should be exerted in order to achieve the same nonlinear deflection. Also, it can be noticed that for an imperfectly

curved shell, higher applied mechanical loads are needed to reach the same maximum amplitude as the perfect plate.

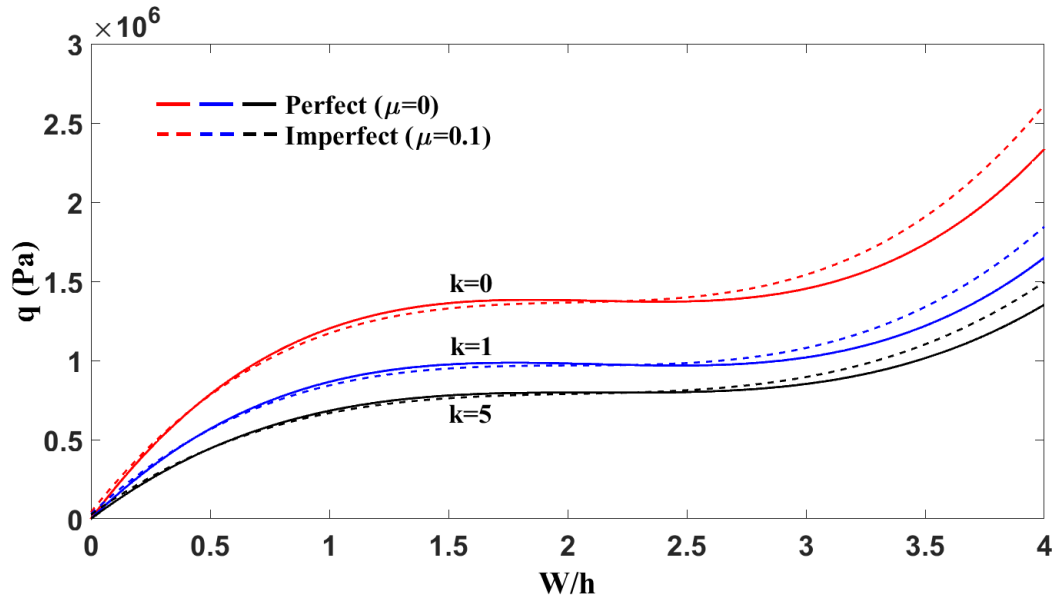


Figure 3.4. Effect of volume fraction exponent K and imperfection μ on the nonlinear response of cylindrical shells ($a/b=1.1$, $b/h=50$, $h=0.01\text{m}$, $a/R_y = 0.5$).

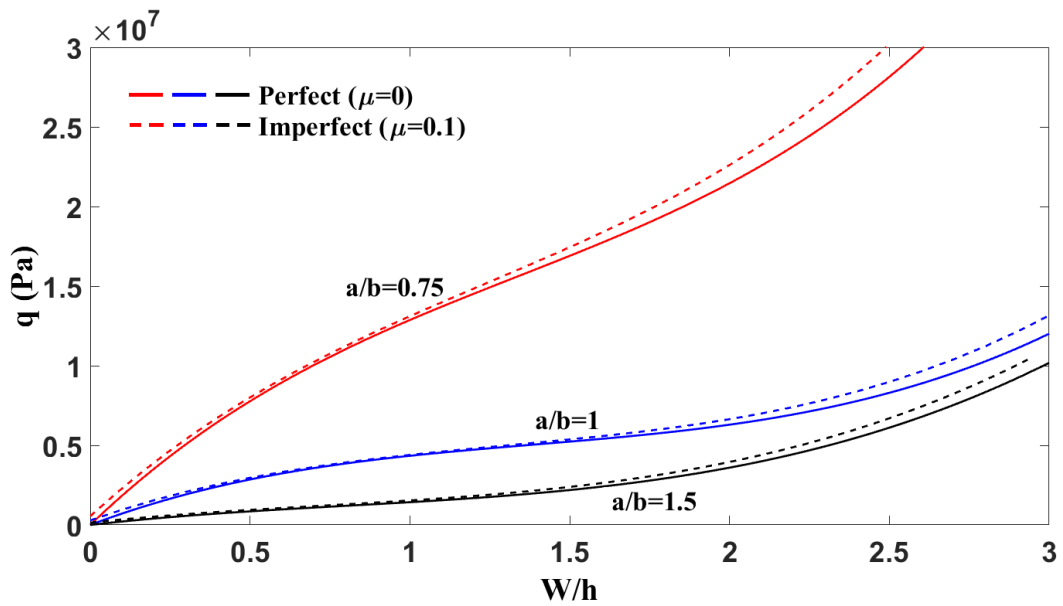


Figure 3.5. Effect of length to width ratio and imperfection μ on the nonlinear response of cylindrical shells ($b/h=30$, $a/R_y = 0.5$, $k=1$).

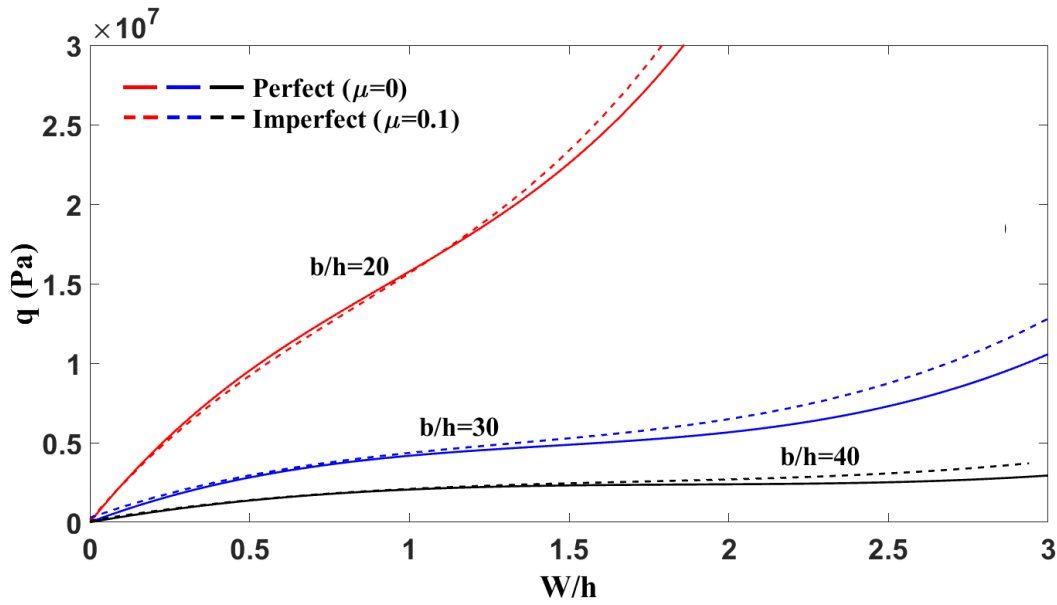


Figure 3.6. Effect of width to thickness ratio and imperfection μ on the nonlinear response of cylindrical shells ($a/b=1$, $a/R_y = 0.5$, $K=1$).

Figure 3.6 illustrates the effect of length to width ratio and width to thickness ratio respectively on nonlinear behavior of FGM cylindrical shell for $K=1$. From both Figure 3.6 and Figure 3.6, it is observed that the load-carrying capacity of the shell increased as the aspect ratio decreased. Moreover, the nonlinear behavior of the curved shell becomes more stable for larger value of a/b and b/h , since the shell thickness increase and hence becomes stiffer.

It is shown in Figure 3.7, that a snap through phenomena was exhibited for $a/R_y = 0.75$ and 1. It can also be seen that when the length to the radius of curvature ratios decreased, the load-carrying capacity increased, and the curve became more stable. It is due to the fact that when the radii of curvature increase, the curved shell becomes shallower and therefore, stiffer and more stable.

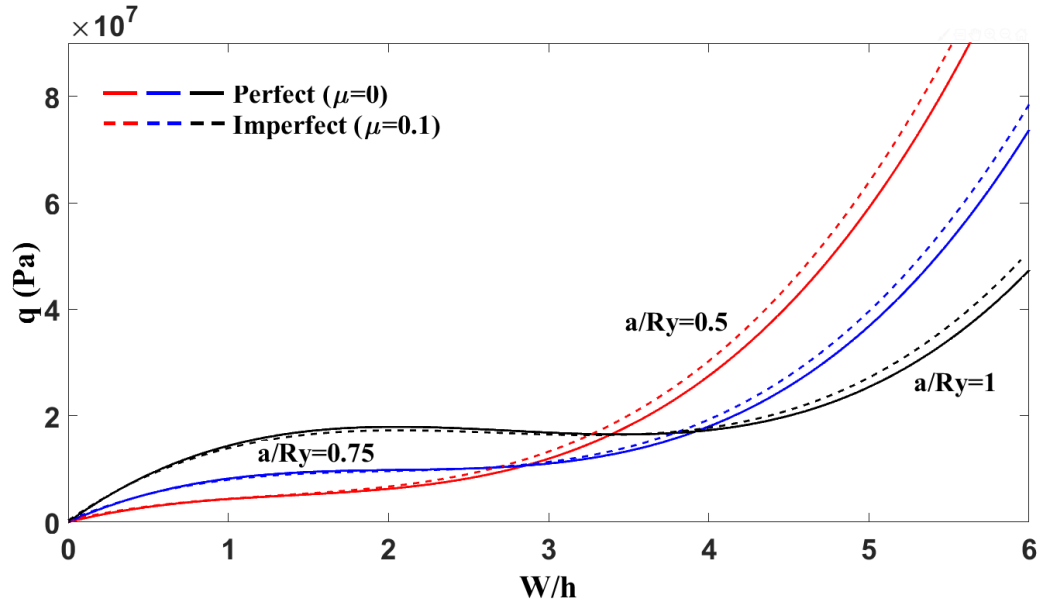


Figure 3.7. Effect of length to radius ratio and imperfection μ on the nonlinear response of cylindrical panels ($a/b=1$, $b/h=30$, $K=1$).

3.5.3 Nonlinear Dynamic Analysis Results

In this section, two cases were considered in order to illustrate the proposed formulation of the nonlinear dynamic analysis of an eccentrically stiffened doubly curved shallow shell made of FGM subjected to a mechanical load. The first and the second numerical examples will be presented for stiffened and un-stiffened spherical and cylindrical shells, respectively. The shell is made of Aluminum and Alumina and the stiffeners are made of Alumina. Both longitudinal and transversal stiffeners are assumed identical. The nonlinear response is solved by using Runge-Kutta fourth order with 3000 steps to reach convergence. The results of the present nonlinear responses of stiffened and un-stiffened spherical panels under sinusoidal mechanical excitation $q(t) = 10^5 \sin(100t)$ is compared with those of Bich (2013) based on the classical thin shell theory with geometrical nonlinearity. An excellent agreement can be seen in

Figure 3.8 below. These results show that the stiffeners strongly decrease the vibration amplitude. Also, it can be seen that the response is not nonlinear and this is

because the excitation frequency ($\Omega=100$ rad/s) is very small compared to the natural frequency ($\Omega=2643.25$ rad/s). Figure 3.9 shows the difference between the linear and nonlinear solution. It is clear that the chosen excitation frequency does not exhibit high geometric nonlinearity.

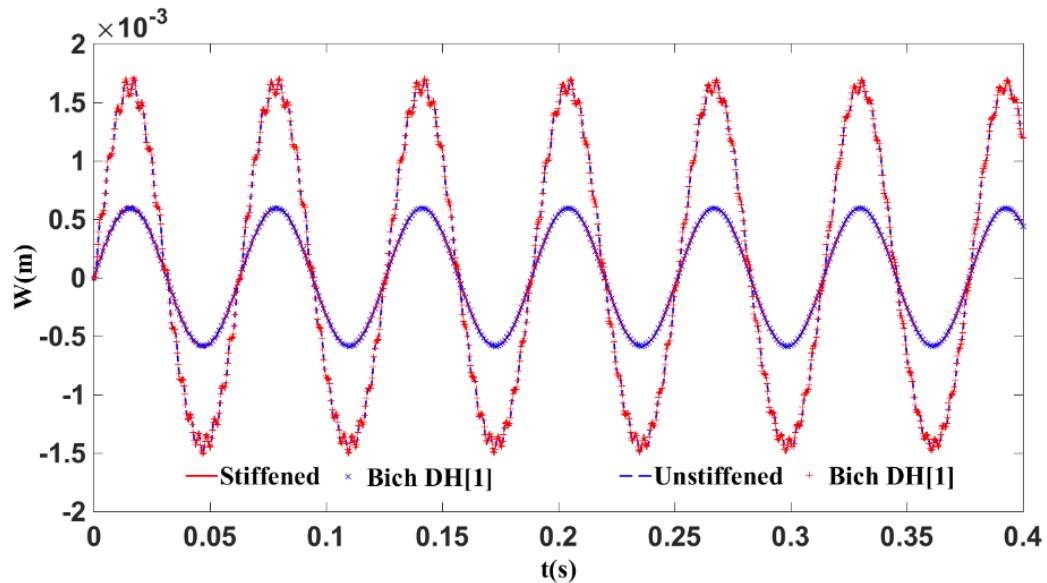


Figure 3.8. Nonlinear responses of stiffened and unstiffened spherical shells ($a=b=0.8$ m, $h=0.01$ m, $q(t)=10^5 \sin(100t)$, $K=1$, $R_x=R_y=5$ m).

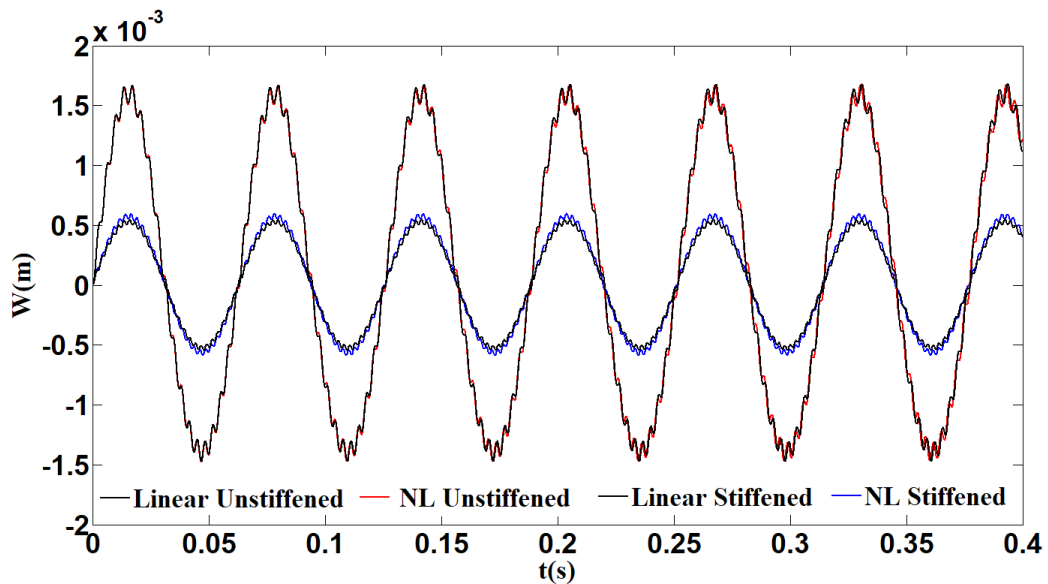


Figure 3.9. Linear and Nonlinear responses of stiffened and unstiffened spherical shells ($a=b=0.8$ m, $h=0.01$ m, $q(t)=10^5 \sin(100t)$, $K=1$, $R_x = R_y = 5$ m).

When the forcing frequencies approach the natural ones, a very important phenomenon called harmonic beating phenomenon occurs. It is created by the interference of two sinusoidal waves at the same point in space. Sometimes they add each other and sometimes they destroy and cancel each other, resulting in a rapid oscillating accompanied by a very slow varying amplitude.

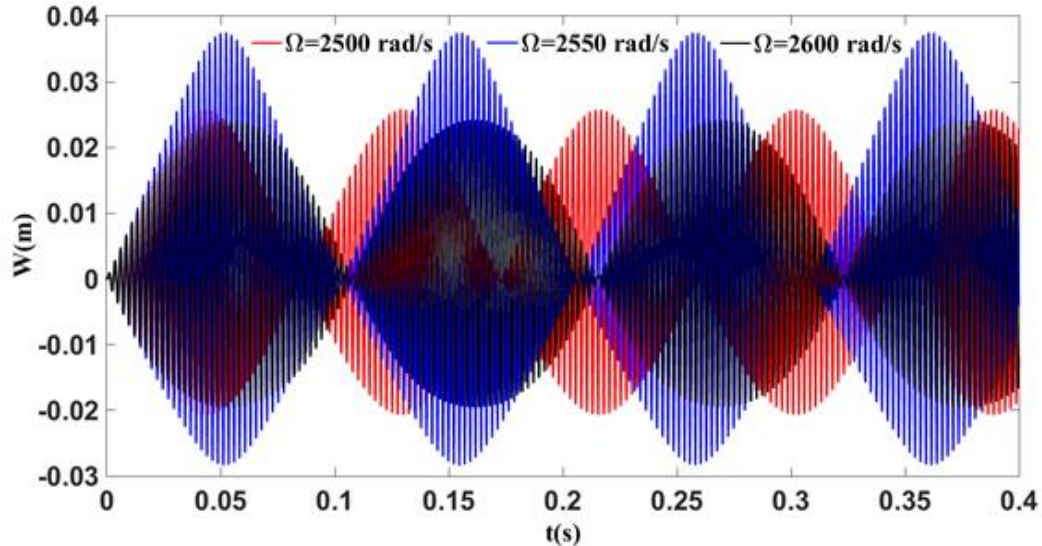


Figure 3.10. Harmonic beat phenomenon of a stiffened spherical shell with different excitation frequencies Ω ($a=b=0.8\text{m}$, $h=0.01\text{m}$, $R_x = R_y = 5\text{m}$, $K=1$, $Q=10^5 \text{ N/m}^2$).

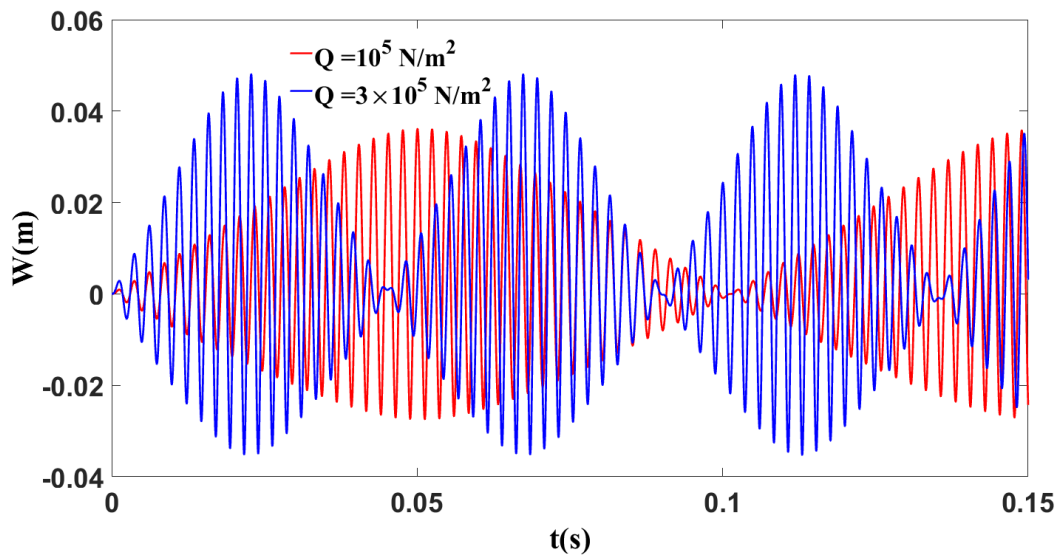


Figure 3.11. Effect of excitation loads on the harmonic beat phenomenon of stiffened spherical shells ($a=b=0.8\text{m}$, $h=0.01\text{m}$, $R_x = R_y = 5\text{m}$, $q(t)=Q\sin(2650t)$, $K=1$).

Figure 3.10 shows that the amplitude of beats increases rapidly while the response time decreases when choosing two external frequencies (2600rad/s, and 2650rad/s) close to the natural frequency 2643.25rad/s of the studied stiffened spherical shell. The amplitude of harmonic beat increases and the response time decreases when the applied excitation force increases like in Figure 3.11.

The second part of the nonlinear dynamic analysis section consists of a parametric study on a stiffened cylindrical shell subjected to a mechanical load. Same mechanical and dimensional properties as the spherical shell are used in this part. The effect of the volume fraction index K on the nonlinear dynamic response of the stiffened cylindrical shell with $R=5\text{m}$, $h=0.01\text{m}$ is shown in Figure 3.12.

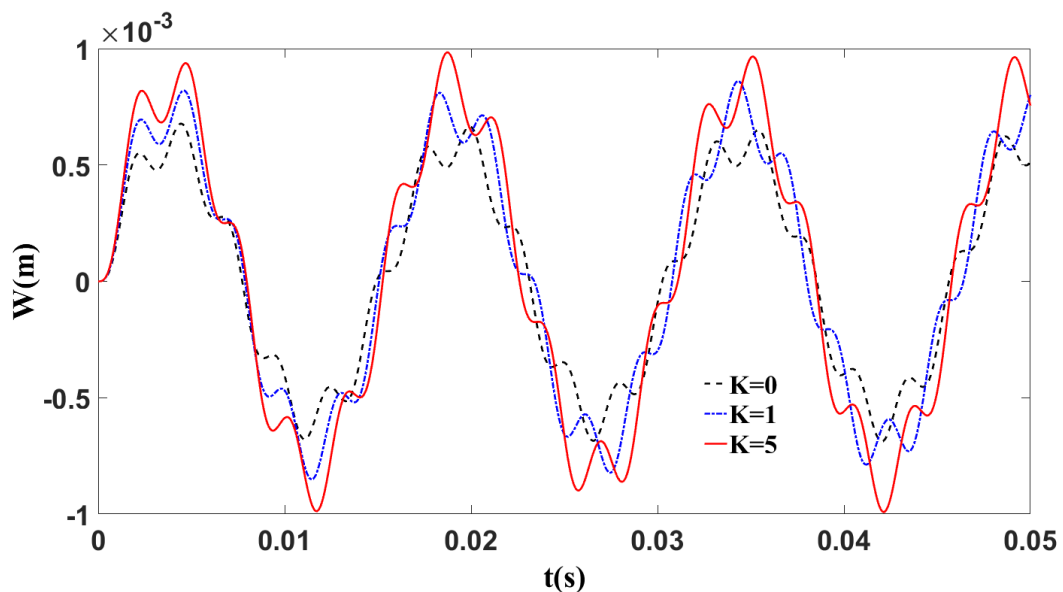


Figure 3.12. Effect of power law index K on the nonlinear response of stiffened cylindrical shell ($a=b=0.8\text{m}$, $q(t)=10^5 \sin(100t)$, $h=0.01\text{m}$, $R_y=5\text{m}$).

Also, this graph shows that the deflection curve increases with time as the power index increases ($K=0,1,5$). This is because the concentration of the metal (Al) in the functionally graded materials increases with the increase in K values according to the rule of mixture. Since the modulus of elasticity of the aluminum is smaller compared to the

Alumina (70 GPa comparing to 380 GPa), it yields a lower material stiffness therefore, a higher deflection. Figure 3.13 shows the effect of width to thickness ratio on the time deflection curve of the stiffened cylindrical shell. It can be observed clearly that as the value of b/h ratio increases, the load-carrying capacity decreases.

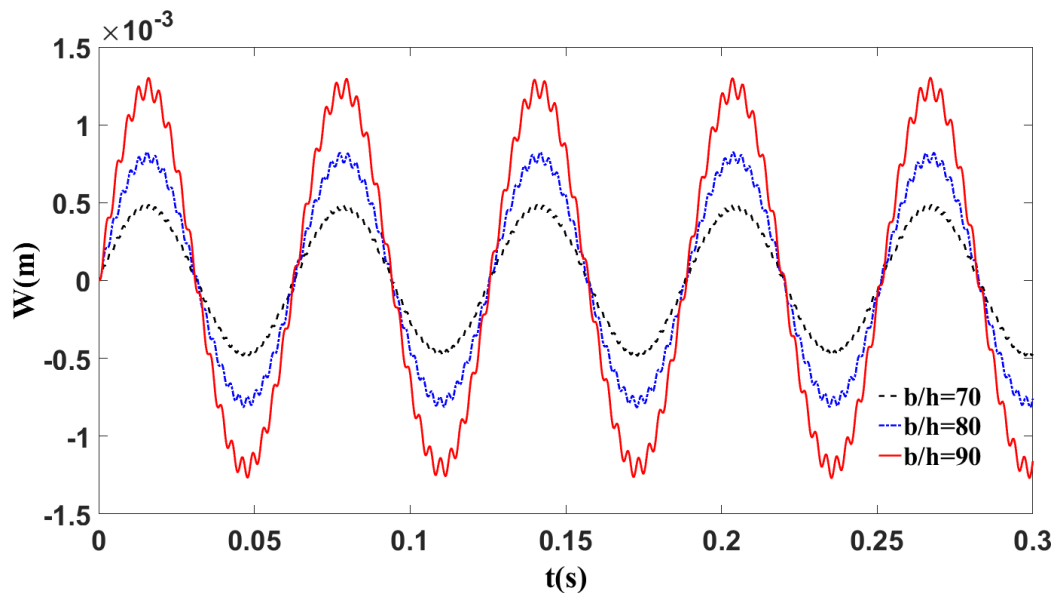


Figure 3.13. Effect of width to thickness ratio on the nonlinear response of stiffened cylindrical shell ($a/b=1$, $q(t)=10^5 \sin(100t)$, $h=0.01\text{m}$, $R_y=5\text{m}$, $K=1$).

Figure 3.14 depicts the effect of the length to width ratio on the time deflection curve. It can be seen that the deflection increase when the a/b ratio increases. Figure 3.15 shows the influence of increases the excitation loads on the time deflection curve. It is also seen that when the load increases the deflection imcreases.

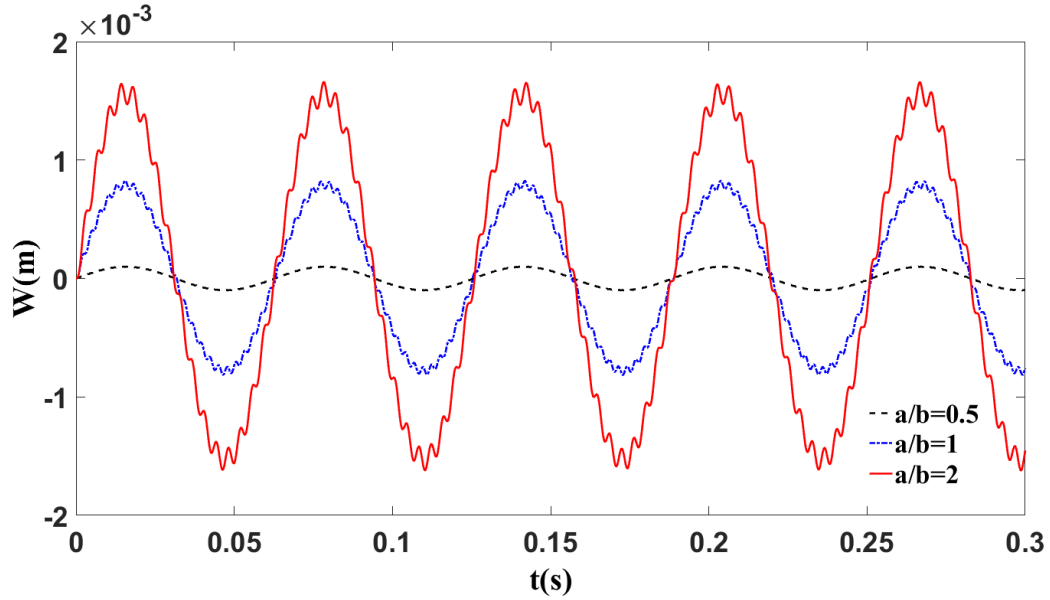


Figure 3.14. Effect of length to width ratio on the nonlinear response of stiffened cylindrical shell ($b/h=80$, $q(t)=10^5 \sin(100t)$, $h=0.01\text{m}$, $R_y=5\text{m}$, $K=1$).

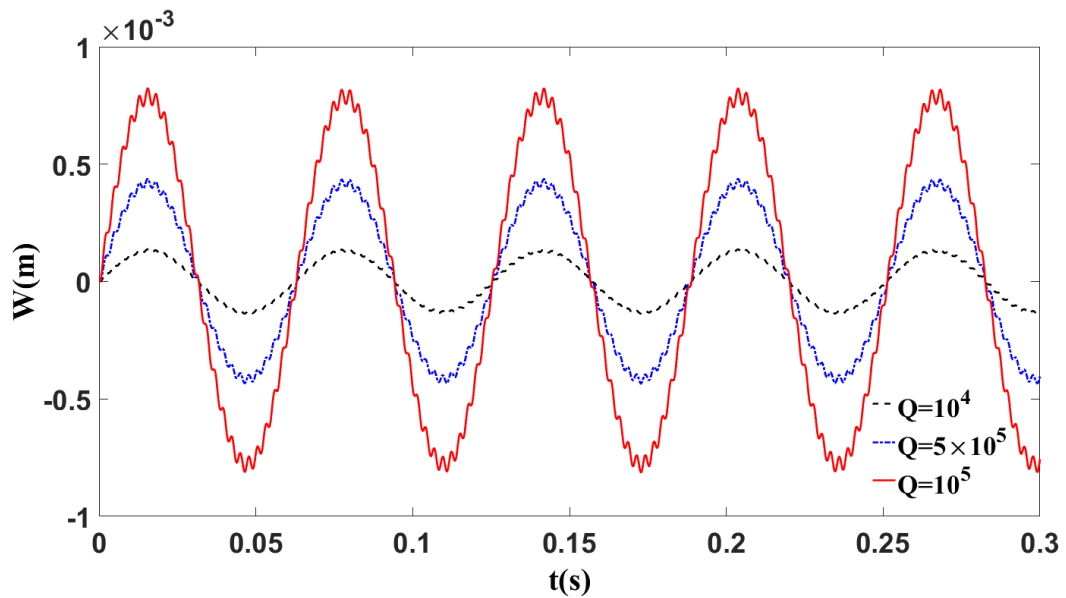


Figure 3.15. Effect of excitation loads on the nonlinear response of a stiffened cylindrical shell ($b/a=1$, $b/h=80$, $\Omega=100 \text{ rad/s}$, $h=0.01\text{m}$, $R_y=5\text{m}$, $K=1$).

3.5.4 Nonlinear Frequency Response

To validate the present solution technique, the results for nonlinear frequency-response obtained here, are compared with previously published papers in this area. For this purpose, several examples are considered here. The first study was performed for a simply supported Aluminum square plate with immovable edges. The so-called “backbone” obtained (frequency amplitude curve of nonlinear free vibration) is compared with the one obtained by Amabili (2004) and an excellent agreement can be found in Figure 3.16 below.

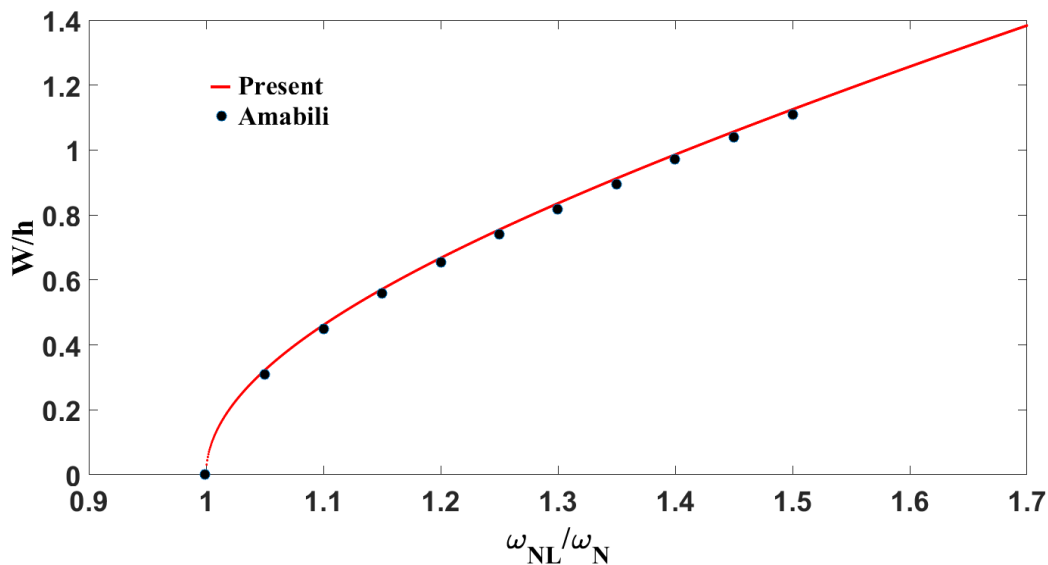


Figure 3.16. Backbone for a square simply supported immovable Aluminum plate ($a = b = 0.3\text{m}$, $h = 0.001\text{m}$, $E = 70\text{ GPa}$, $\rho = 2778\text{ kg/m}^3$, $\nu = 0.3$).

Next study was conducted on the same immovable Aluminum plate previously described, but under a concentrated harmonic force at the center of magnitude $F = 1.74\text{N}$ and modal damping ratio of $\zeta = 0.065$. As can be seen in Figure 3.17 below, the calculated results and the ones given by Amabili (2004) were in a good agreement.

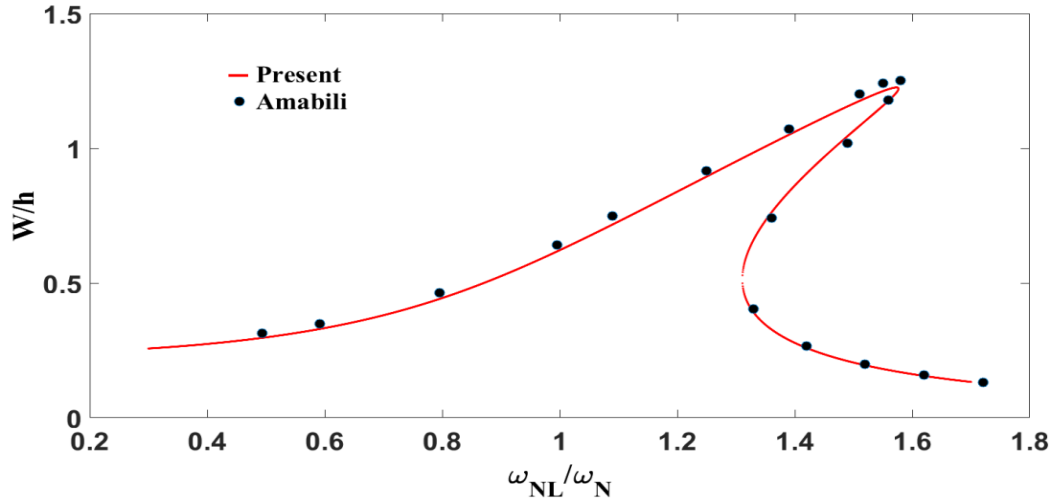


Figure 3.17. The frequency-amplitude curve of nonlinear vibration of an immovable Aluminum plate under $F = 1.74\text{N}$ and $\zeta = 0.065$.

For the case of functionally graded material plate, both quadratic and cubic nonlinear terms exist. Therefore, to validate the present formulation, frequency-response curves for nonlinear free and forced vibration are calculated and compared with previously published works.

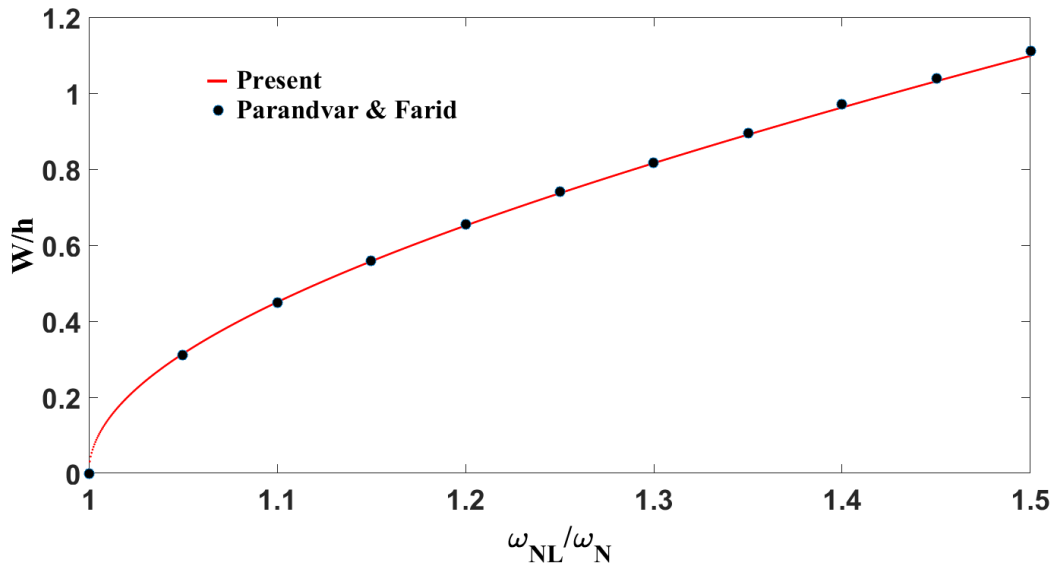


Figure 3.18. Backbone curve for simply supported immovable SUS304/SI₃N₄ plate.

A backbone curve for a simply supported square plate with immovable edges made of SUS304/Si₃N₄ was studied. The results obtained here were compared with Parandvar and Farid (2016) in Figure 3.18 above and a very good agreement was found.

Next, the calculation of the amplitude-frequency relationship for the same simply supported immovable FGM plate was done and compared to Alijani and Amabili (2014) in Figure 3.19. It shows the forced vibration frequency-response plot of SUS304/Si₃N₄. It can be seen that the present results are in good agreement with those of Alijani and Amabili.

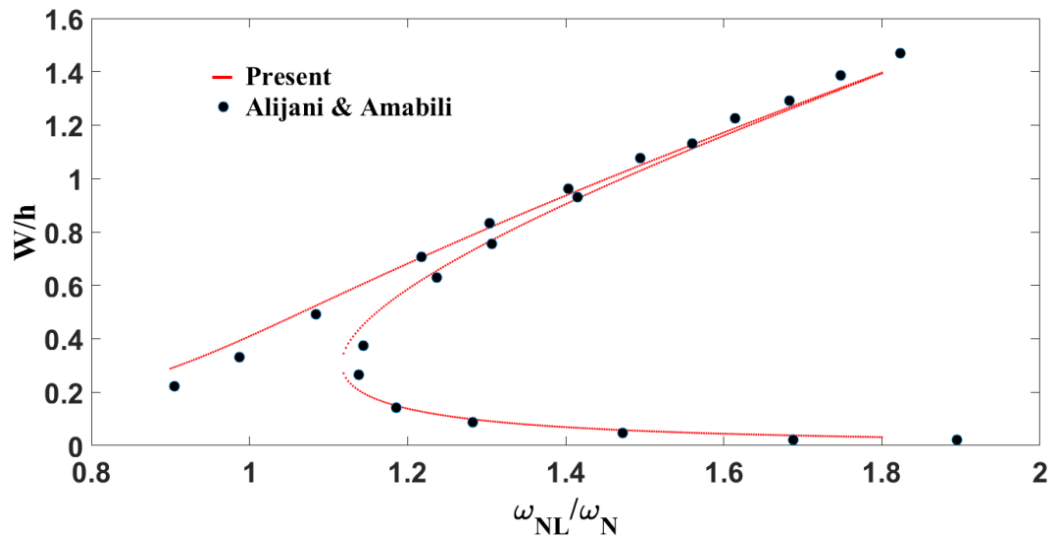


Figure 3.19. The frequency-amplitude curve of nonlinear vibration of immovable SUS304/Si₃N₄ plate under $\bar{f} = f_b/h\omega^2 = 0.03$ and $\zeta = 0.01$.

After validating the adopted method, the frequency-response of functionally graded stiffened spherical shell is considered. The structure is made of Aluminum (Al) and Alumina (Al₂O₂).

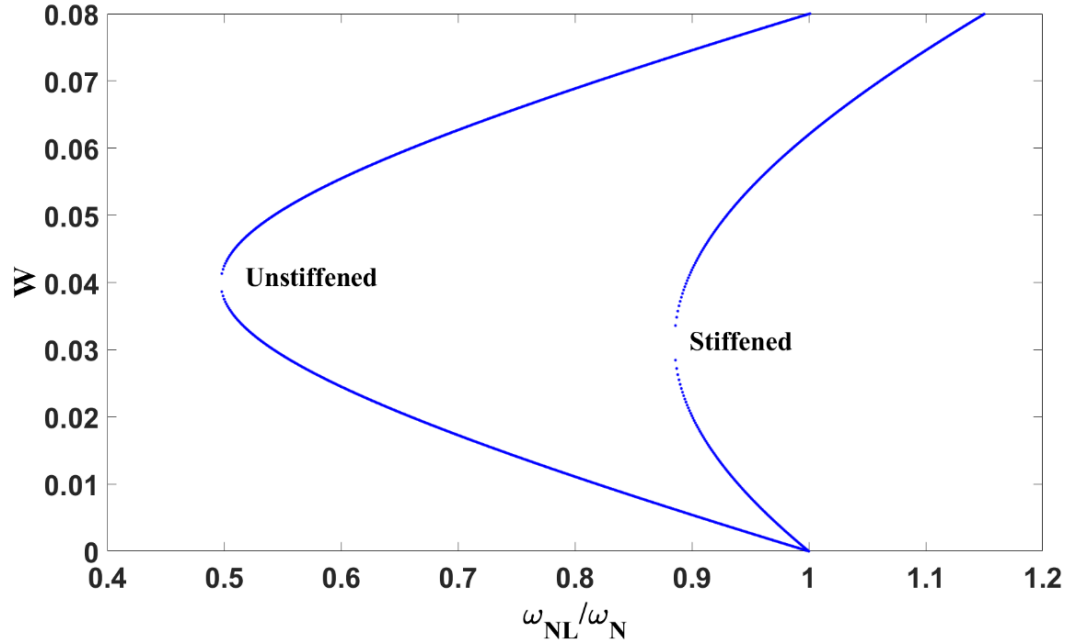


Figure 3.20. The frequency-amplitude curve of free nonlinear vibration of stiffened and unstiffened Al/Al₂O₂ spherical shell $R_x = R_y = 5\text{m}$, $a = b = 0.8\text{m}$, $h = 0.025\text{m}$, $K = 1$.

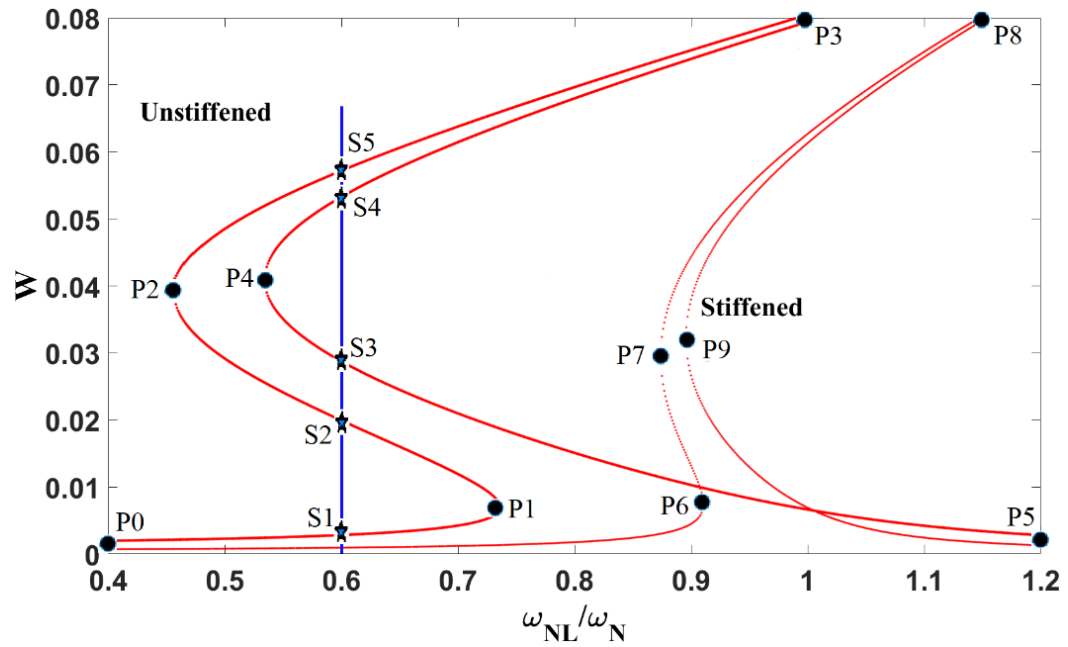


Figure 3.21. The frequency-amplitude curve of forced nonlinear vibration of stiffened and unstiffened Al/Al₂O₂ spherical shell $R_x = R_y = 5\text{m}$, $a = b = 0.8\text{m}$, $h = 0.025\text{m}$, $K = 1$ and $\zeta = 0.01$ under uniformly distributed load $Q = 10^5\text{Pa}$.

It can be seen from both plots (Figure 3.21) that the frequency-amplitude curves of the forced vibration responses are asymptotic to the free vibration responses. Here both cases display an initial softening behavior followed by hardening. This is due to very high excitation leading to the geometric nonlinearity of stretching type.

The points at which the motion changes its behavior, from stable to unstable and vice versa, are called Saddle-node Bifurcations. P1, P2, P3 and P4 for the un-stiffened spherical shell and P6, P7, P8 and P9 for stiffened one are called bifurcation points. Table 3.9 shows the change of motion between two consecutive bifurcation points as well as the change of behavior. For the unstiffened curve in Figure 3, one can observe that, at some dimensionless frequency ratios ($\omega_{NL}/\omega_L = 0.6$), five solutions exist theoretically (S1, S2, S3, S4, and S5). However, this is practically not possible.

Table 3.9

Practical Behavior of Amplitude-Frequency Curve of Forced Nonlinear Vibration of Stiffened and Unstiffened FGM Spherical Shell.

Curves	Bifurcation (saddle) Point		Motion	Behavior
Unstiffened	P0	→ P1	Stable	
	P1	→ P2	Unstable	Softening
	P2	→ P3	Stable	Hardening
	P3	→ P4	Unstable	
	P4	→ P5	Stable	
Stiffened	P0	→ P6	Stable	
	P6	→ P7	Unstable	Softening
	P7	→ P8	Stable	Hardening
	P8	→ P9	Unstable	
	P9	→ P5	Stable	

Based on the motion behavior in Table 3.9, solution S2 and S4 belong to two unstable regions, therefore, they are considered unstable points and can't be achieved practically.

It can be seen that the unstable region and the softening behavior of the unstiffened

spherical shell are much bigger than the stiffened one. And this highlights one of the advantages of using stiffeners.

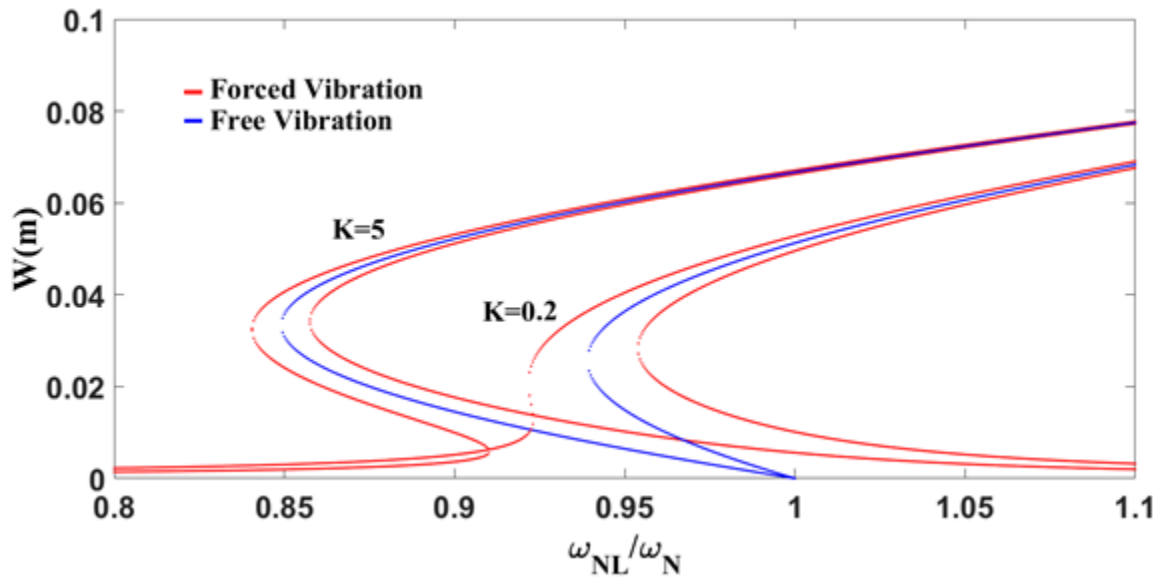


Figure 3.22. Effect of volume fraction exponent K on the frequency-amplitude curves of stiffened spherical panels ($R_x = R_y = 5\text{m}$, $a = b = 0.8\text{m}$, $h = 0.025\text{m}$, $Q = 10^5\text{Pa}$).

Figure 3.22 shows the effect of volume fraction index on the frequency-amplitude curve. It can be seen that the peak amplitude decreased as the volume fraction decreases and this is because the young's modulus of the functionally graded materials increases by increasing the concentration of ceramic. Hence the hardness behavior increases. In Figure 3.23 the effect of the radii of curvature of a stiffened cylindrical shell on the amplitude Frequency-Response curves is investigated. It is obvious that as the radius of curvature increases, the shell becomes flatter and therefore stiffer. Hence, the peak amplitude decreases and a better hardening behavior is observed.

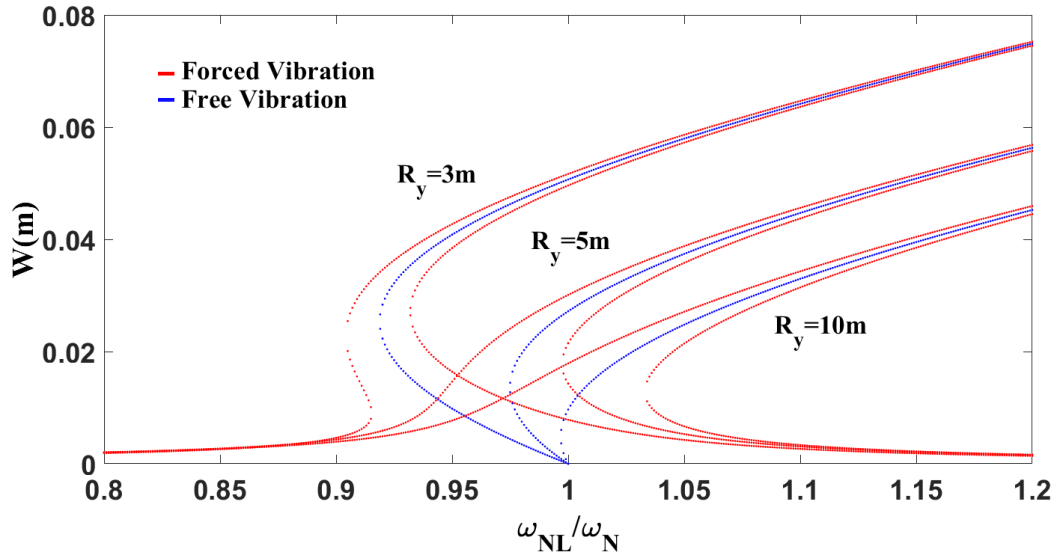


Figure 3.23. Effect of radii R_y on the frequency-amplitude curves of a stiffened cylindrical shell ($R_x = \infty$, $a = b = 0.8\text{m}$, $h = 0.025\text{m}$, $K = 1$, $Q = 10^5\text{Pa}$).

Figure 3.24 shows the effect of the magnitude of loading amplitude on the Frequency-response curve. It can be seen that when the loading amplitude decreases, the nonlinear forced vibration response becomes closer to the free vibration response.

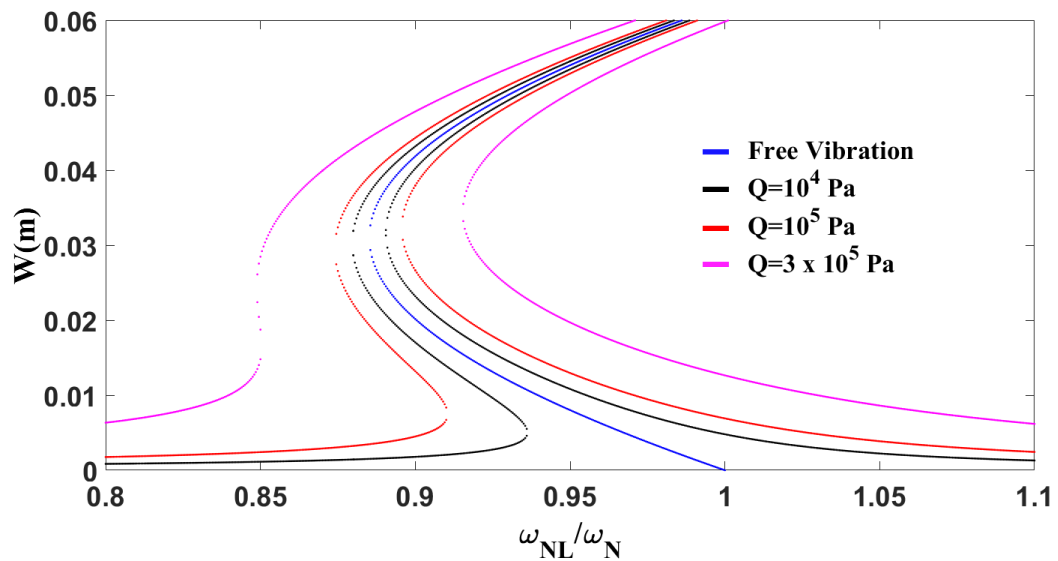


Figure 3.24. Effect of excitation loads Q on the frequency-amplitude curves of stiffened spherical shells ($R_x = R_y = 5\text{m}$, $a = b = 0.8\text{m}$, $h = 0.025\text{m}$, $K = 1$).

4. Temperature Variation And Thermal Buckling

In this chapter, the temperature variation across the thickness of the simply-supported stiffened functionally graded double-curved is discussed. Also, the critical buckling temperature variation is analyzed and a closed-form solution was found.

4.1 Temperature Variation

Consider a stiffened FGM double- curved shallow shell to be subjected to a very high thermal effect. Three types of temperature distribution are considered in this study: uniform, linear and nonlinear temperature rise.

4.1.1 Uniform Temperature Rise

The temperature field is assumed to change uniformly through the thickness of the stiffened shell, and this variation of temperature is expressed as:

$$\Delta T(z) = T_f - T_i = T_f - T_0 \quad (41)$$

where the temperature of the top surface (metal-rich surface) is similar to the ambient temperature ($T_{top} = T_m = T_0 = 300K$) unless mentioned otherwise. At the initial temperature T_i , the shell is thermal stress-free. The final value T_f is, in fact, the temperature at which the shell buckles. Hence the thermal stresses in both the shell and the stiffeners are found by substituting equation (41) into equations (17 a-f).

4.1.2 Linear Temperature Rise

The temperature distribution is assumed to vary linearly through the thickness of the shell and for the stiffeners as well, as follows:

$$T(z) = T_0 + \Delta T \left(\frac{z}{h} + \frac{1}{2} \right), \quad \text{where } T_0 = T_m \text{ for shell} \quad (42a)$$

$$T_{sx}(z) = T_0 - \Delta T \left(\frac{2z - h}{2h_x} \right), \quad \text{where } T_0 = T_c \text{ for stiff in } x \text{ dir} \quad (42b)$$

$$T_{sy}(z) = T_0 - \Delta T \left(\frac{2z - h}{2h_y} \right), \text{ where } T_0 = T_c \text{ for stiff in } y \text{ dir} \quad (42c)$$

where $T_m = T_0 = 300K$ and $\Delta T = T\left(\frac{h}{2}\right) - T\left(-\frac{h}{2}\right) = T_b - T_t = T_c - T_m$. Hence the thermal parameters in the shell and the stiffeners can be expressed by substituting equations (42 a-c) into $T(z) = T_m + \Delta T(z)$, then the results into equations (17 a-f).

4.1.3 Nonlinear Temperature Rise

The temperature gradient is assumed to vary nonlinearly through the thickness of the shell and the stiffeners. It can be governed by the mono-dimensional steady-state heat conduction using the Fourier equations (Hetnarski, 1987) as follows:

$$-\frac{d}{dz} \left(k(z, T) \frac{dT}{dz} \right) = 0, \quad T\left(-\frac{h}{2}\right) = T_m \quad T\left(\frac{h}{2}\right) = T_c, \text{ for shell} \quad (43a)$$

$$-\frac{d}{dz} \left(k_{sx}(z, T) \frac{dT}{dz} \right) = 0, \quad T\left(\frac{h}{2}\right) = T_c \quad T\left(\frac{h}{2} + h_x\right) = T_m, \text{ for stiff in } x \text{ dir} \quad (43b)$$

$$-\frac{d}{dz} \left(k_{sy}(z, T) \frac{dT}{dz} \right) = 0, \quad T\left(\frac{h}{2}\right) = T_c \quad T\left(\frac{h}{2} + h_y\right) = T_m, \text{ for stiff in } y \text{ dir} \quad (43c)$$

The analytical solutions to equations (43 a-c) for the shell, and x-y stiffeners respectively are expressed as follow:

$$T(z) = T_c - (T_c - T_m) \frac{\int_{-\frac{h}{2}}^z \frac{1}{k(z, T)} dz}{\int_{-\frac{h}{2}}^{\frac{h}{2}} \frac{1}{k(z, T)} dz}, \quad \text{for shell} \quad (44a)$$

$$T_{sx}(z) = T_m + (T_c - T_m) \frac{\int_{\frac{h}{2}}^z \frac{1}{k_{sx}(z, T)} dz}{\int_{\frac{h}{2}}^{\frac{h}{2} + h_x} \frac{1}{k_{sx}(z, T)} dz}, \quad \text{for stiff in } x \text{ dir} \quad (44b)$$

$$T_{sy}(z) = T_m + (T_c - T_m) \frac{\int_{\frac{h}{2}}^z \frac{1}{k_{sy}(z, T)} dz}{\int_{\frac{h}{2}}^{\frac{h}{2} + h_y} \frac{1}{k_{sy}(z, T)} dz}, \quad \text{for stiff in } y \text{ dir} \quad (44c)$$

Now, substituting equations (5c) and equations (6 e-f) into equations (43a) and using the mentioned boundary conditions, the solution is obtained employing polynomial series. Hence the solution for nonlinear temperature distribution across the shell and stiffeners thicknesses becomes:

$$T(z) = T_m + \Delta T \frac{\sum_{i=0}^{\infty} \frac{1}{iK+1} \left(-\frac{k_{cm}}{k_m}\right)^i \left(\frac{2z+h}{2h}\right)^{iK+1}}{\sum_{i=0}^{\infty} \frac{1}{iK+1} \left(-\frac{k_{cm}}{k_m}\right)^i} \text{ for shell} \quad (45a)$$

$$T_{sx}(z) = T_c - \Delta T \frac{\sum_{i=0}^{\infty} \frac{1}{iK+1} \left(-\frac{k_{mc}}{k_c}\right)^i \left(\frac{2z-h}{2h_x}\right)^{iK+1}}{\sum_{i=0}^{\infty} \frac{1}{iK+1} \left(-\frac{k_{mc}}{k_c}\right)^i} \text{ for stiff in } x \text{ dir} \quad (45b)$$

$$T_{sy}(z) = T_c - \Delta T \frac{\sum_{i=0}^{\infty} \frac{1}{iK+1} \left(-\frac{k_{mc}}{k_c}\right)^i \left(\frac{2z-h}{2h_y}\right)^{iK+1}}{\sum_{i=0}^{\infty} \frac{1}{iK+1} \left(-\frac{k_{mc}}{k_c}\right)^i} \text{ for stiff in } y \text{ dir} \quad (45c)$$

The first eight terms of the series were taken for the solution to convert. Then the thermal stresses in the shell and the stiffeners under nonlinear temperature distribution can be expressed by substituting $T(z)$ from equations (45 a-c) into $(z) = T_m + \Delta T(z)$, then the results into equations (17 a-f). It can be seen that the temperature distribution in the functionally graded shell and stiffeners $T(z)$, $T_{sx}(z)$ and $T_{sy}(z)$ are nonlinear functions of thickness z . Hence, in the case of isotropic shells and stiffener equations (45 a-c) become equations of linear temperature distribution as equations (42 a-c).

4.2 Thermal Buckling

To study the thermal buckling, let's consider a stiffened shell to be simply-supported along all four edges. When the structure is subjected to a uniform temperature rise, the initial temperature is raised to a final value where the plate buckles. Therefore, it is very

important to find the critical buckling temperature difference. To do that, the pre-buckling thermal stresses should be determined.

4.2.1 Buckling Under Uniform Temperature Rise

From the expression of the force resultants, equations (18 a-c), the pre buckling resultant forces are found to be:

$$\begin{aligned} N_{x0} &= -\Phi_{1x}^{T/Shell} - \Phi_{1x}^{T/Stiff} \\ N_{y0} &= -\Phi_{1y}^{T/Shell} - \Phi_{1y}^{T/Stiff} \\ N_{xy0} &= 0 \end{aligned} \quad (46)$$

Substituting equations (17a), (17b), (17e), and (17f) in the pre-buckling resultant forces from equation (46), then the result into the linear operator l_{33} , and solving $\det[l_{ij}] = 0$, where

$$[l_{ij}] = \begin{bmatrix} l_{11} & l_{12} & l_{13} & l_{14} & l_{15} \\ l_{21} & l_{22} & l_{23} & l_{24} & l_{25} \\ l_{31} & l_{32} & l_{33} & l_{34} & l_{35} \\ l_{41} & l_{42} & l_{43} & l_{44} & l_{45} \\ l_{51} & l_{52} & l_{53} & l_{54} & l_{55} \end{bmatrix}$$

The buckling temperature change ΔT is obtained as:

$$\Delta T = -\frac{l_d}{l_c \left\{ (L_1 + L_2) \left(\frac{m\pi}{a} \right)^2 + (L_1 + L_3) \left(\frac{n\pi}{b} \right)^2 \right\}} \quad (47)$$

where

$$L_1 = \frac{h}{(1-\nu)} \left(E_m \alpha_m + \frac{1}{K+1} (E_m \alpha_{cm} + E_{cm} \alpha_m) + \frac{1}{2K+1} E_{cm} \alpha_{cm} \right) \quad (48a)$$

$$L_2 = \frac{d_x h_x \left(E_c \alpha_c + \frac{1}{K+1} (E_c \alpha_{mc} + E_{mc} \alpha_c) + \frac{1}{2K+1} E_{mc} \alpha_{mc} \right)}{d_x} \quad (48b)$$

$$L_3 = \frac{d_y h_y \left(E_c \alpha_c + \frac{1}{K+1} (E_c \alpha_{mc} + E_{mc} \alpha_c) + \frac{1}{2K+1} E_{mc} \alpha_{mc} \right)}{d_y} \quad (48c)$$

$$l_d = \text{Det}[l_{ij}] \quad \text{for } i, j = 1, 2, 3, 4, 5 \text{ and } N_{x0} = N_{y0} = 0 \quad (48d)$$

$$l_c = \text{Det}[l_{ij}] \quad \text{for } i, j = 1, 2, 4, 5 \quad (48e)$$

The critical buckling temperature difference ΔT_{cr} is obtained by giving values to m and n that makes equation (48) a minimum and this is accomplished for $m = n = 1$. It should be noted that equation (48) is an explicit expression of buckling temperature change ΔT when the functionally graded material properties are independent of the temperature. However, when they are entirely dependent on the temperature, equation (48) becomes an implicit expression. To determine the critical buckling temperature, the following iterative algorithm is adopted:

1. Temperature independent material properties are obtained at the initial temperature $T_0 = 300K$ unless otherwise specified.
2. Using the obtained material properties from step 1, the critical buckling temperature difference ΔT_{cr}^1 is calculated using equation (48).
3. The materials properties are found again using $T = T_0 + \Delta T_{cr}^1$, then the new buckling temperature difference ΔT_{cr}^2 is calculated.
4. Step 3 is repeated until the critical buckling temperature converges to a specific

$$\text{error tolerance} \left| \frac{\Delta T_{cr}^{i+1} - \Delta T_{cr}^i}{\Delta T_{cr}^i} \right| \leq \varepsilon.$$

4.2.2 Buckling Under Linear Temperature Change Across The Thickness

To find $\Delta T(z)$ for the shell and the stiffeners, we substitute equations (42 a-c) into $(z) = T_m + \Delta T(z)$, then the results into equations (17a), (17b), (17e), and (17f). Replacing the thermal stresses into equation (46), then the result into the linear operator l_{33} , and solving $\det|l_{ij}| = 0$, the buckling temperature change ΔT is obtained as:

$$\Delta T = - \frac{l_d}{l_c \left\{ (H_1 + H_2) \left(\frac{m\pi}{a} \right)^2 + (H_1 + H_3) \left(\frac{n\pi}{b} \right)^2 \right\}} \quad (50)$$

where

$$H_1 = \frac{h}{(1-\nu)} \left(\frac{E_m \alpha_m}{2} + \frac{(E_m \alpha_{cm} + E_{cm} \alpha_m)}{K+2} + \frac{E_{cm} \alpha_{cm}}{2K+2} \right) \quad (51a)$$

$$H_2 = \frac{b_x h_x}{2d_x} \frac{\left\{ E_c(1+2K)\{(1+K)(2+K)\alpha_c + 2\alpha_{mc}\} + E_{mc}\{(2+4K)\alpha_c + (2+K)\alpha_{mc}\} \right\}}{(1+K)(2+K)(1+2K)} \quad (51b)$$

$$H_3 = \frac{b_y h_y}{2d_y} \frac{\left\{ E_c(1+2K)\{(1+K)(2+K)\alpha_c + 2\alpha_{mc}\} + E_{mc}\{(2+4K)\alpha_c + (2+K)\alpha_{mc}\} \right\}}{(1+K)(2+K)(1+2K)} \quad (51c)$$

$$l_d = \text{Det}[l_{ij}] \quad \text{for } i, j = 1, 2, 3, 4, 5 \text{ and } N_{x0} = N_{y0} = 0 \quad (51d)$$

$$l_c = \text{Det}[l_{ij}] \quad \text{for } i, j = 1, 2, 4, 5 \quad (51f)$$

In case of functional graded temperature-dependent material properties, the same algorithm is used for the case of linear temperature variation through the thickness.

4.2.3 Buckling Under Nonlinear Temperature Change Across the Thickness

To find $\Delta T(z)$ for the shell and the stiffeners in this case, we substitute equations (45 a-c) into $T(z) = T_m + \Delta T(z)$, then the results into equations (17a), (17b), (17e), and (17f). In this case we replace the thermal stresses into equation (27) then the results into the linear operator l_{33} , and solving $\det|l_{ij}| = 0$, the buckling temperature change ΔT is obtained as:

$$\Delta T = - \frac{l_d}{l_c \left\{ (G_1 + G_2) \left(\frac{m\pi}{a} \right)^2 + (G_1 + G_3) \left(\frac{n\pi}{b} \right)^2 \right\}} \quad (52)$$

where

$$G_1 = \frac{\sum_{i=0}^{\infty} \frac{1}{iK+1} \left(-\frac{k_{cm}}{k_m}\right)^i \left(\frac{E_m \alpha_m}{iK+2} + \frac{E_m \alpha_{cm} + E_{cm} \alpha_m}{iK+K+2} + \frac{E_{cm} \alpha_{cm}}{iK+2K+2}\right)}{(1-\nu) \sum_{i=0}^{\infty} \frac{1}{iK+1} \left(-\frac{k_{cm}}{k_m}\right)^i} \quad (53a)$$

$$G_2 = \frac{d_x h_x \left(E_c \alpha_c + \frac{1}{K+1} (E_c \alpha_{mc} + E_{mc} \alpha_c) + \frac{1}{2K+1} E_{mc} \alpha_{mc}\right)}{d_x} - \frac{b_x h_x \sum_{i=0}^{\infty} \frac{1}{iK+1} \left(-\frac{k_{cm}}{k_m}\right)^i \left(\frac{E_c \alpha_c}{iK+2} + \frac{E_c \alpha_{mc} + E_{mc} \alpha_c}{iK+K+2} + \frac{E_{mc} \alpha_{mc}}{iK+2K+2}\right)}{d_x \sum_{i=0}^{\infty} \frac{1}{iK+1} \left(-\frac{k_{cm}}{k_m}\right)^i} \quad (53b)$$

$$G_3 = \frac{d_y h_y \left(E_c \alpha_c + \frac{1}{K+1} (E_c \alpha_{mc} + E_{mc} \alpha_c) + \frac{1}{2K+1} E_{mc} \alpha_{mc}\right)}{d_y} - \frac{b_y h_y \sum_{i=0}^{\infty} \frac{1}{iK+1} \left(-\frac{k_{cm}}{k_m}\right)^i \left(\frac{E_c \alpha_c}{iK+2} + \frac{E_c \alpha_{mc} + E_{mc} \alpha_c}{iK+K+2} + \frac{E_{mc} \alpha_{mc}}{iK+2K+2}\right)}{d_y \sum_{i=0}^{\infty} \frac{1}{iK+1} \left(-\frac{k_{cm}}{k_m}\right)^i} \quad (53c)$$

In case of functional graded temperature-dependent material properties, the same algorithm is used for the case of nonlinear temperature variation through the thickness.

4.3 Numerical Results

To calculate the nonlinear vibration of a functionally graded stiffened double-curved shell under thermal effect, the critical buckling temperature variation should be evaluated first. Once the critical buckling temperature, in either case, is defined, the applied temperature is taken to be less than the critical buckling temperature to prevent the stiffened shell from buckling.

4.3.1 Critical Buckling Temperature Variation

As an example, consider a functionally graded simply-supported cylindrical shell that consists of Stainless Steel and Silicon Nitride mixture ($SUS304/Si_3N_4$) with temperature-independent materials listed above. The critical buckling temperature under a uniform, linear, and nonlinear temperature rise with respect to the aspect ratios (b/a) for different volume fraction indices are plotted in Figure 4.1

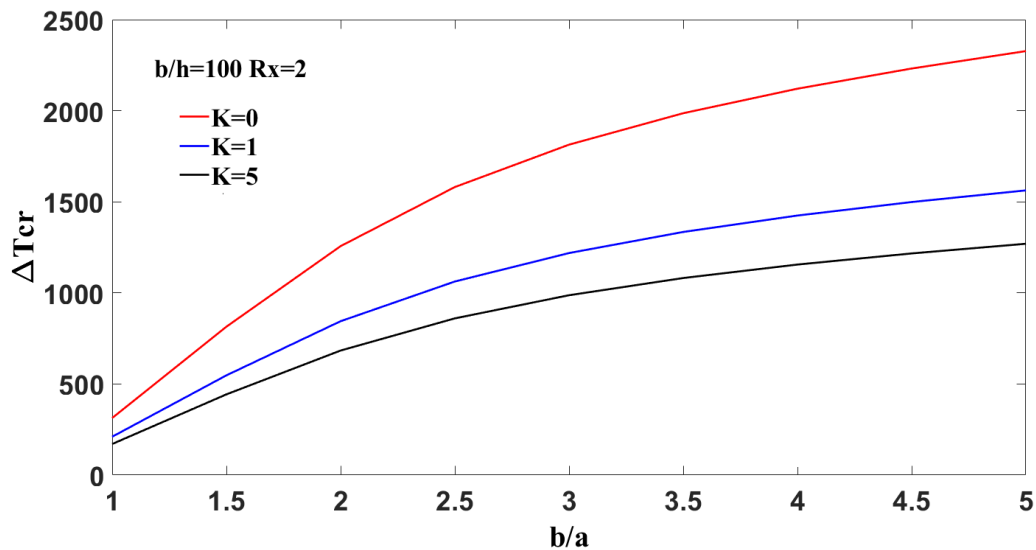


Figure 4.1. Critical buckling under uniform temperature rise vs b/a for $Si_3N_4/SUS304$.

It can be seen that when the length is equal to the width, the critical buckling temperatures for all three cases are the lowest for linear or nonlinear temperature rise. However, they are significantly higher than the ones of uniform temperature rise. Moreover, the critical buckling temperature change increases as the aspect ratio (width to length ratio) increase for all of the three cases. Also, ΔT_{cr} increases as the volume fraction K decreases, and this is because when K approached zero, the shell becomes more ceramic, hence stiffer. This will lead to a higher critical temperature change. However, the critical temperature change decreases rapidly, when the geometric

parameter b/h is increased. Thus, when the plates are thicker, the critical temperature change becomes higher.

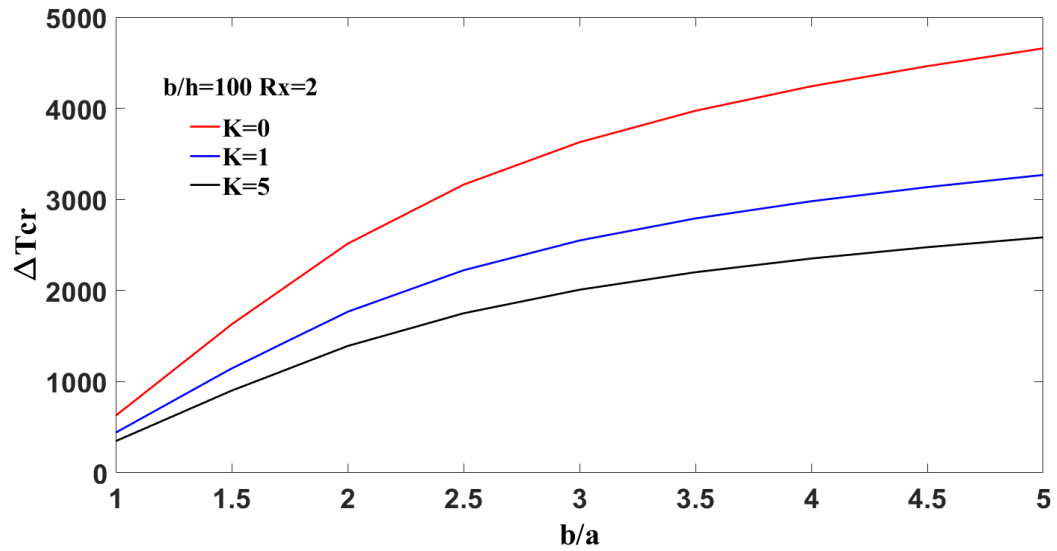


Figure 4.2. Critical buckling under linear temperature rise vs b/a for $\text{Si}_3\text{N}_4/\text{SUS304}$.

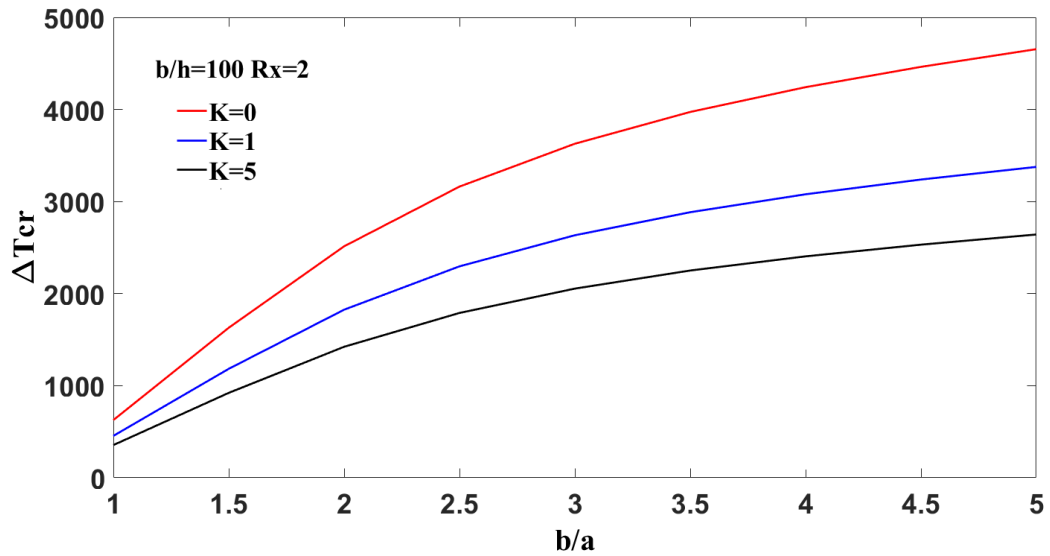


Figure 4.3. Critical buckling under Nonlinear temperature rise vs b/a for $\text{Si}_3\text{N}_4/\text{SUS304}$

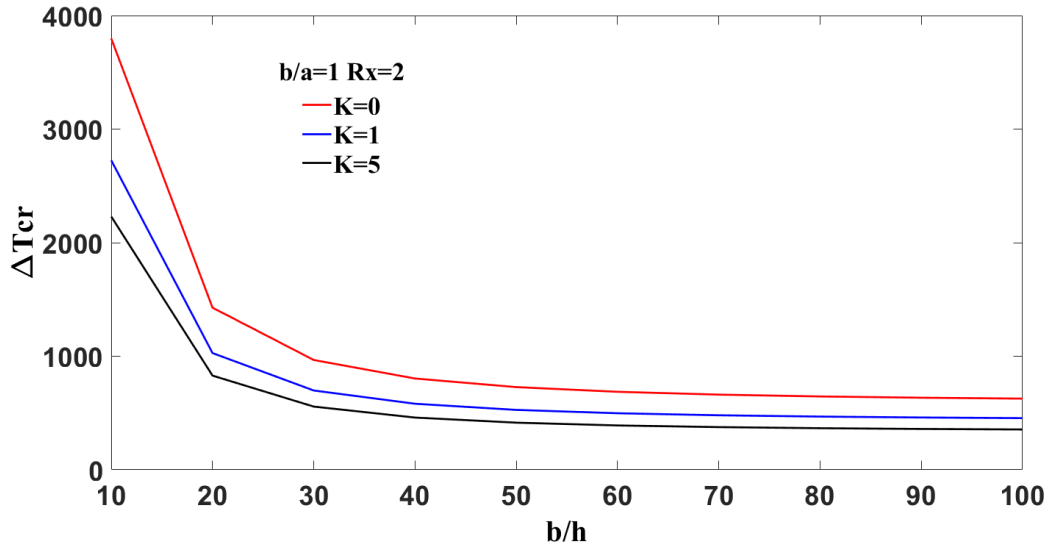


Figure 4.4. Critical buckling under linear temperature rise vs b/h for $\text{Si}_3\text{N}_4/\text{SUS304}$.

The variation of ΔT_{cr} versus the width to thickness ratio, is plotted in Figure 4.4 below for the three types of thermal loadings. It can be seen from the three plots above, that the critical buckling was very high when b/h was equal to 10 (thick shell). Also, when this ratio increases, the critical buckling temperature change decreases rapidly. This is because the thickness decreases with higher width to thickness ratio. Consequently, the shell becomes weaker and more flexible, which leads to less critical buckling temperature. Similar to the previously discussed case, when the volume fraction index K increases, the concentration of metal increases and the shell stiffness decreases.

The effect of the longitudinal and transverse stiffeners on the critical buckling variation of a stiffened FGM cylindrical shell under nonlinear thermal load is studied in Table 4.1 below. Both cases temperature-dependent and temperature-independent materials are considered. In this table, ΔT_{cr} was calculated for different volume fraction indices and length to width ratios.

Table 4.1

Critical Buckling Thermal Load for Stiffened FGM Cylindrical Shell Subjected to Nonlinear Temperature Rise with Temperature-Dependent Properties ($R_x=2$, $h=0.01m$).

a/b	K	No Stiffeners		5 Stiffeners in x-Direction		5 Stiffeners in y-Direction		5 by 5 Orthogonal Stiffeners	
		T-ID	T-D	T-ID	T-D	T-ID	T-D	T-ID	T-D
0.75	0	746.58	538.99	907.02	635.5	3309.2	2135	6593.0	3431.5
	1	541.88	451.39	264.08	235.8	2240.2	1574	3160.6	1947.1
	5	423.11	358.1	143.79	136.6	1730.8	1263	1993.6	1387.3
1	0	626.89	470.0	1195.4	727.7	1530.3	957.8	3388.5	1931.5
	1	455.07	383.7	582.75	457.9	1062.5	742.5	1817.2	859.7
	5	355.12	304.25	202.20	191.5	824.57	667.4	1174.6	758.43
1.5	0	335.41	275.54	1082.24	648.57	503.239	370.03	1469.91	897.2
	1	243.411	219.68	704.814	518.43	357.828	309.28	956.771	604.91
	5	190.181	173.55	473.623	378.77	277.33	260.96	698.731	547.46

It can be seen that when the number of stiffeners increases, the shell becomes stiffer and hence, a higher critical buckling temperature is achieved. Also, if the temperature-dependent materials are used, the thermal expansion as well as the stiffness increases.

4.3.2 Natural Frequency Results in Thermal Environment

In this section, the dimensionless frequency of the FGM plate is calculated and compared with the theoretical results of Huang and Shen (2004) based on the higher-order shear deformation theory. The FGM plate is made of Stainless Steel and Silicon Nitride ($SUS304/Si_3N_4$) with the temperature-dependent material properties listed in Table 4.2. Two different thermal loadings are considered: Case 1, $T_b = T_t = 300$ K and

Case 2, T-ID $T_b = 300$ K and $T_t = 600$ K. Note that in this table, ρ_0 and E_0 are the density and the young's modulus of ceramic reach surface at $T_0 = 300$ K.

Table 4.2

Comparison of Dimensionless Frequencies ($\Omega = \omega_L(a^2/h)[\rho_0(1 - \nu^2)/E_0]^{1/2}$ for $Si_3N_4/SUS304$ Plate Under Thermal Load ($a=b=0.2$ m, $h=0.3$ m).

Temperature	K		Mode					
			(1,1)	(1,2)	(2,2)	(1,3)	(2,3)	
$T_b = 300$ K $T_t = 300$ K	Si_3N_4	Present	12.506	29.249	44.206	53.410	66.292	
		HSDT	12.495	29.131	43.845	52.822	65.281	
	0.5	Present	8.622	20.197	30.557	36.941	45.885	
		HSDT	8.675	20.262	30.359	36.819	45.546	
	1.0	Present	7.560	17.713	26.802	32.402	40.246	
		HSDT	7.555	17.649	26.606	32.081	39.692	
	2.0	Present	6.786	15.885	24.019	29.025	36.031	
		HSDT	6.777	15.809	23.806	28.687	35.466	
	SUS304	SUS304	5.413	12.662	19.141	23.124	28.698	
		HSDT	5.405	12.602	18.967	22.850	28.239	
	$T_b = 300$ K $T_t = 600$ K	Si_3N_4	Present	11.714	28.675	43.807	53.117	66.143
			HSDT	11.984	28.504	43.107	51.998	64.358
0.5		Present	8.196	19.475	29.909	36.335	45.036	
		HSDT	8.269	19.783	29.998	36.239	44.901	
1.0		Present	6.929	16.953	26.083	31.706	39.579	
		HSDT	7.171	17.213	26.109	31.557	39.114	
2.0		Present	6.261	15.108	23.259	28.273	35.127	
		HSDT	6.398	15.384	23.327	28.185	34.918	
SUS304		Present	4.743	11.978	18.246	22.210	27.655	
		HSDT	4.971	12.089	18.392	22.221	27.557	

It can be seen that both, the temperature and volume fraction index rise, decrease the natural frequency. A good agreement with the results obtained by Huang and Shen (2004) can be observed between the present results and the one based on HSDT.

4.3.3 Thermomechanical Static Analysis Results

In this section, an FGM cylindrical shell consisting of a mixture of Aluminum (Al) and Zirconia (ZrO_2) is considered. All material properties are temperature-independent. The nonlinear response of a cylindrical shell under uniform temperature rise is calculated and compared with the previously published results. Then the effect of temperature distribution and imperfection are studied.

The nonlinear pressure deflection response of an FGM cylindrical shell is calculated for different uniform temperature rise ΔT . The results are compared with the results obtained by Duc and Tung (2010) based on the classical shell theory and temperature-independent material properties. An excellent agreement can be seen in Figure 4.5.

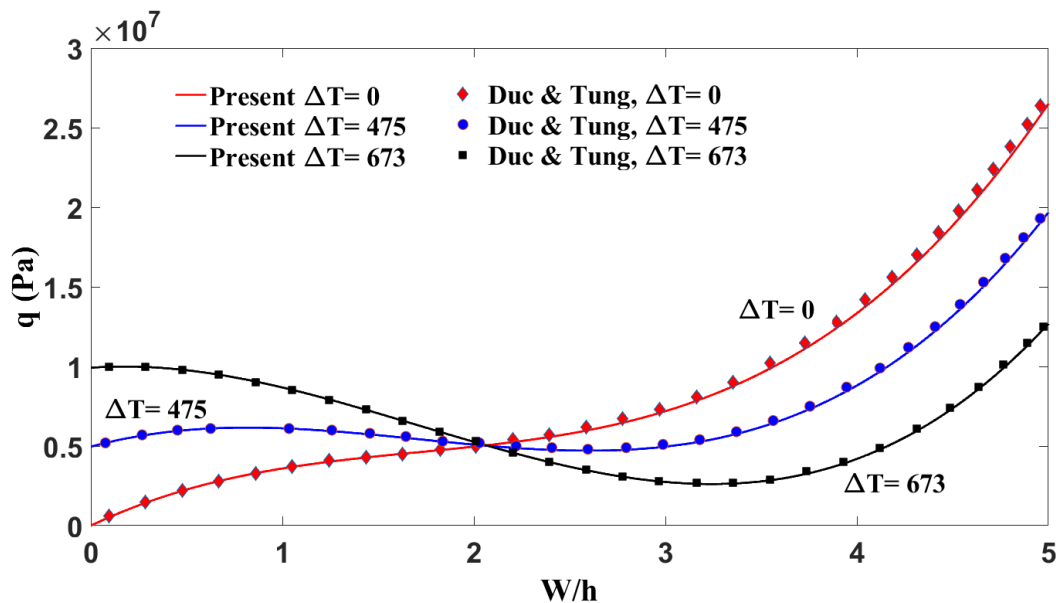


Figure 4.5. Effect of uniform temperature rise Δt on the nonlinear response of cylindrical panels ($a/b=1$, $b/h=50$, $a/Ry=0.5$, $K=1$).

As shown in the following figure, when $\Delta T = 0$ (the isothermal case), the load-deflection curve starts from the coordinate origin. When $\Delta T > 0$, the applied loads on the cylindrical shell exhibit a bifurcation behavior and no deflection occurs until a bifurcation behavior point is reached for $\Delta T = 475 K$ and $673 K$. This may be due to the

fact that when the thermal load was applied before the mechanical forces, the cylindrical shell deflected outward since the positive dimensional deflection is by deflecting inward. But after starting to apply the mechanical load, the outward deflection started to reduce and became zero when the applied load reached the bifurcation points ($0.5 * 10^7$ and $1 * 10^7$).

It can also be seen that, due to the existence of bifurcation behavior, both load-deflection curves become unstable and a snap through response was observed. The curves are more nonlinear and unstable when the temperature changes are higher. The effect of temperature variations on the nonlinear load-deflection curves is plotted in Figure 4.6 and Figure 4.7 below.

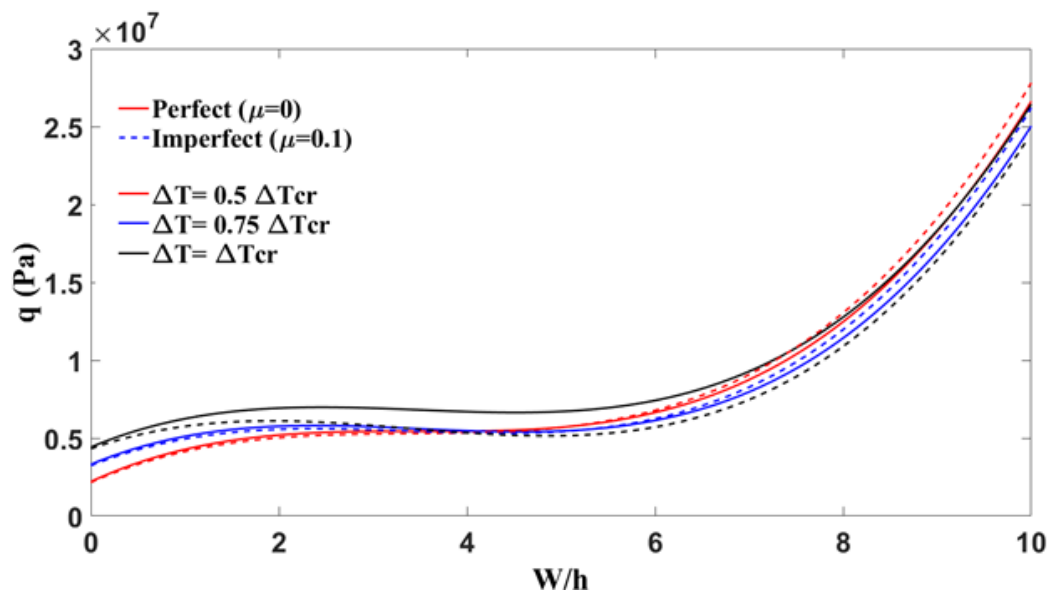


Figure 4.6. Effect of uniform temperature rise ΔT and imperfection μ on the nonlinear response of $\text{Si}_3\text{N}_4/\text{SUS304}$ cylindrical shell. ($a/b=1$, $b/h=50$, $a/Ry=0.5$, $k=1$).

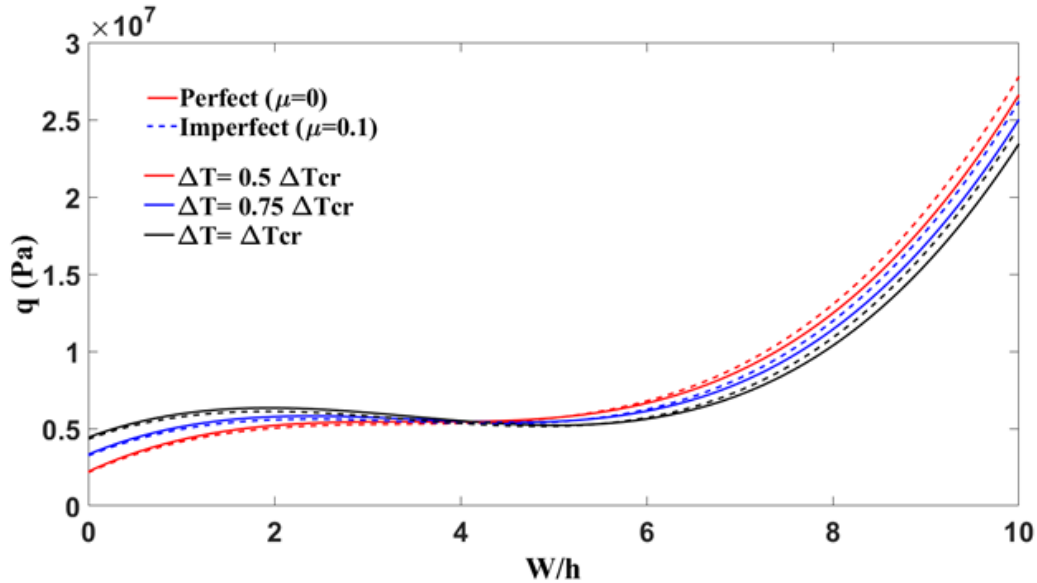


Figure 4.7. Effect of nonlinear temperature rise ΔT and imperfection μ on the nonlinear response of $\text{Si}_3\text{N}_4/\text{SUS304}$ cylindrical shell. ($a/b=1$, $b/h=50$, $a/Ry=0.5$, $k=1$).

It can be seen that, in contrary to the nonlinear temperature variation, the uniform temperature rise produces much smaller outward deflection and the shell is more stable. This is illustrated in Figure 4.6 where a smoother snap-through phenomenon can be observed.

4.3.4 Amplitude - Frequency Response Under Thermal Load

The amplitude-frequency response of the stiffened functionally graded plate under different ceramic temperature is investigated. The effect of the surface temperature on the Backbone curve is shown in *Figure 4.8* below.

It can be seen that when the temperature of the ceramic surface increases, the hardening behavior increases, therefore the curve tends to bend more to the right side. This is because the thermal load affects changed the stiffness matrix.

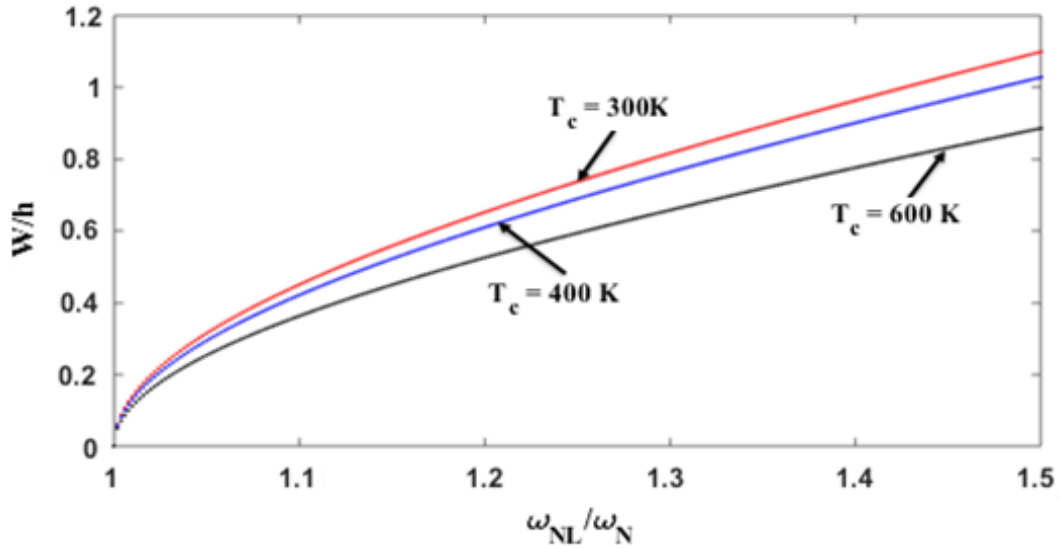


Figure 4.8. Backbone curve for square simply supported plate subjected to temperature variations through the thickness ($a = b = 0.2\text{m}$, $h = 0.025\text{m}$, $K = 2$).

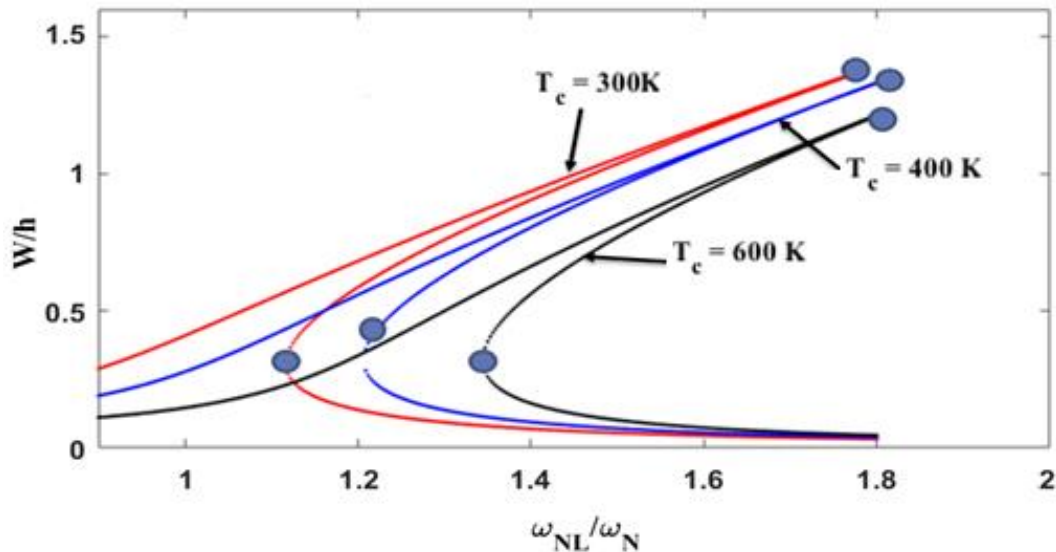


Figure 4.9. The frequency-amplitude curve of nonlinear vibration of simply-supported SUS304/ Si_3N_4 plate ($a = b = 0.2\text{m}$, $h = 0.025\text{m}$) under $F = 375\text{kN}$ and $\zeta = 0.01$ subjected to temperature variations through the thickness.

Finally, the effect of surface temperature on the amplitude-frequency response of the nonlinear vibration of simply-supported FGM plate is shown in Figure 4.9 above. Similar to the free vibration case, the higher the surface temperature is, the stiffer the plate become

5. Multimode Theoretical Formulation

In this chapter, the numerical analysis is based on the multi-modal energy method and nonlinear first order shear deformation theory (FSDT). The equations of motion are obtained based on Lagrange's Method.

5.1 Kinetic and Elastic Strain Energy

The kinetic energy of the stiffened functionally graded double curved shell including rotary inertia is given by:

$$T_p = \frac{1}{2} \int_{-h/2}^{h/2} \int_0^a \int_0^b \rho(z) \{ \dot{u}^2 + \dot{v}^2 + \dot{w}^2 \} dx dy dz \quad (54)$$

The dot indicates the differentiation of the displacements with respect to time.

Substituting equation (7) into equation (54), the kinetic energy becomes:

$$T_p = \frac{I_0}{2} \int_0^a \int_0^b (\dot{u}_0^2 + \dot{v}_0^2 + \dot{w}_0^2) dx dy + I_1 \int_0^a \int_0^b (\dot{\psi}_x \dot{u}_0 + \dot{\psi}_y \dot{v}_0) dx dy + \frac{I_2}{2} \int_0^a \int_0^b (\dot{\psi}_x^2 + \dot{\psi}_y^2) dx dy \quad (55)$$

where

$$I_0 = \int_{-h/2}^{h/2} \rho(z) dz \quad I_1 = \int_{-h/2}^{h/2} \rho(z) z dz \quad I_2 = \int_{-h/2}^{h/2} \rho(z) z^2 dz$$

The expression for the elastic strain energy of a stiffened functionally graded double curved shells under thermal effect is given by:

$$\begin{aligned} U_S^{Total} &= U_{s,Shell} + U_{s,Stiff} \\ &= \frac{1}{2} \int_0^a \int_0^b \int_{-\frac{h}{2}}^{\frac{h}{2}} \{ \sigma_x(z, T)^{Shell+T} \{ \varepsilon_x - \alpha_x(z, T) \Delta T(z) \} \\ &\quad + \sigma_y(z, T)^{Shell+T} \{ \varepsilon_y - \alpha_y(z, T) \Delta T(z) \} + \tau_{xy}(z, T)^{Shell+T} (\gamma_{xy}) \\ &\quad + \tau_{yz}(z, T)^{Shell+T} (\gamma_{yz}) + \tau_{xz}(z, T)^{Shell+T} (\gamma_{xz}) \} dx dy dz \end{aligned}$$

$$\begin{aligned}
& + \frac{1}{2} \int_0^a \int_0^b \int_{\frac{h}{2}}^{\frac{h}{2}+h_{x,y}} \{ \sigma_x(z, T)^{Stiff+T} \{ \varepsilon_x - \alpha_{sx}(z, T) \Delta T(z) \} \\
& \quad + \sigma_y(z, T)^{Stiff+T} \{ \varepsilon_y - \alpha_{sy}(z, T) \Delta T(z) \} + \tau_{xy}(z, T)^{Stiff+T} (\gamma_{xy}) \\
& \quad + \tau_{yz}(z, T)^{Stiff+T} (\gamma_{yz}) + \tau_{xz}(z, T)^{Stiff+T} (\gamma_{xz}) \} dx dy dz
\end{aligned} \tag{56}$$

Assuming Poisson ratio variation is constant across the thickness ($\nu(z) = \nu_m = \nu_c$)

$\alpha_x(z) = \alpha_y(z) = \alpha(z)$ and $E_x(z) = E_y(z)$. Substituting equation (9) into equation (10)

and (11), then the result into equation (56) and integrating over the thickness, the above expression of elastic strain energy became:

$$\begin{aligned}
U_S^{Total} = & \frac{E_1}{2(1-\nu^2)} \int_0^a \int_0^b \{ (\varepsilon_x^0)^2 + (\varepsilon_y^0)^2 + 2\nu\varepsilon_x^0\varepsilon_y^0 \} dx dy \\
& + \frac{E_1}{4(1+\nu)} \int_0^a \int_0^b \{ (\gamma_{xy}^0)^2 + (\gamma_{xz}^0)^2 + (\gamma_{yz}^0)^2 \} dx dy \\
& + \frac{E_2}{(1-\nu^2)} \int_0^a \int_0^b \{ \kappa_x \varepsilon_x^0 + \kappa_y \varepsilon_y^0 + \nu(\kappa_x \varepsilon_y^0 + \kappa_y \varepsilon_x^0) \} dx dy \\
& + \frac{E_2}{2(1+\nu)} \int_0^a \int_0^b \{ \kappa_{xy} \gamma_{xy}^0 \} dx dy \\
& + \frac{E_3}{2(1-\nu^2)} \int_0^a \int_0^b \{ (\kappa_x)^2 + (\kappa_y)^2 + 2\nu\kappa_x \kappa_y \} dx dy \\
& + \frac{E_3}{4(1+\nu)} \int_0^a \int_0^b \{ (\kappa_{xy})^2 \} dx dy \\
& + \frac{F_1}{4(1+\nu)} \int_0^a \int_0^b [(\gamma_{xz}^0)^2 + (\gamma_{yz}^0)^2 + 2(1+\nu) \{ (\varepsilon_x^0)^2 + (\varepsilon_y^0)^2 \}] dx dy \\
& + F_2 \int_0^a \int_0^b \{ \kappa_x \varepsilon_x^0 + \kappa_y \varepsilon_y^0 \} dx dy + \frac{F_3}{2} \int_0^a \int_0^b \{ (\kappa_x)^2 + (\kappa_y)^2 \} dx dy \\
& - \frac{G_1}{(1-\nu)} \int_0^a \int_0^b \{ \varepsilon_x^0 + \varepsilon_y^0 \} dx dy - \frac{G_2}{(1-\nu)} \int_0^a \int_0^b \{ \kappa_x + \kappa_y \} dx dy \\
& - H_1 \int_0^a \int_0^b \{ \varepsilon_x^0 + \varepsilon_y^0 \} dx dy - H_2 \int_0^a \int_0^b \{ \kappa_x + \kappa_y \} dx dy
\end{aligned} \tag{57}$$

where

$$\begin{aligned}
 E_1 &= \int_{-h/2}^{h/2} E(z, T) dz & E_2 &= \int_{-h/2}^{h/2} E(z, T) z dz \\
 E_3 &= \int_{-h/2}^{h/2} E(z, T) z^2 dz & F_1 &= \int_{h/2+hx,y}^{h/2+hx,y} E(z, T) dz \\
 F_2 &= \int_{h/2+hx,y}^{h/2+hx,y} E(z, T) z dz & F_3 &= \int_{h/2+hx,y}^{h/2+hx,y} E(z, T) z^2 dz \\
 G_1 &= \int_{-h/2}^{h/2} E(z, T) \alpha(z, T) \Delta T(z) dz & G_2 &= \int_{-h/2}^{h/2} E(z, T) \alpha(z, T) \Delta T(z) z dz \\
 H_1 &= \int_{h/2+hx,y}^{h/2+hx,y} E(z, T) \alpha(z, T) \Delta T(z) dz & H_2 &= \int_{h/2+hx,y}^{h/2+hx,y} E(z, T) \alpha(z, T) \Delta T(z) z dz
 \end{aligned}$$

The energy dissipation, due to viscous friction, are taken into account by using the Rayleigh's dissipation function is expressed as follows (Amabili, 2004):

$$D = \frac{1}{2} c \int_0^a \int_0^b \left(\dot{u}_0^2 + \dot{v}_0^2 + \dot{w}_0^2 + \dot{\psi}_x^2 + \dot{\psi}_y^2 \right) dx dy \quad (58)$$

where c is the viscous damping coefficient and related to the damping ratio by $c = 2\zeta\omega$.

The virtual work done by an external concentrated harmonic force acting at the point (\tilde{x}, \tilde{y}) , is expressed as follows (Amabili, 2004):

$$\begin{aligned}
 W &= \int_0^a \int_0^b \tilde{f} w \delta(x - \tilde{x}) \delta(y - \tilde{y}) \cos(\Omega t) dx dy = \tilde{f} \cos(\Omega t) w|_{x = \tilde{x}, y} \\
 &= \tilde{y}
 \end{aligned} \quad (59)$$

where \tilde{f} is the harmonic force amplitude, δ is the Dirac delta function and Ω is the forcing excitation frequency.

5.2 Boundary Conditions

In this section, the displacement and rotation fields are represented by a combination of boundary functions, mode shapes and harmonic time function where the shape functions are written in terms of Chebyshev polynomials as follows (Kiani, 2016):

$$u_0(x, y, t) = U(x, t)g(t) = R^u(x, y) \sum_{m=0}^{M_U} \sum_{n=0}^{N_U} U_{m,n} T_m(x) T_n(y) g(t) \quad (60a)$$

$$v_0(x, y, t) = V(x, t)g(t) = R^v(x, y) \sum_{m=0}^{M_V} \sum_{n=0}^{N_V} V_{m,n} T_m(x) T_n(y) g(t) \quad (60b)$$

$$w_0(x, y, t) = W(x, t)g(t) = R^w(x, y) \sum_{m=0}^{M_W} \sum_{n=0}^{N_W} W_{m,n} T_m(x) T_n(y) g(t) \quad (60c)$$

$$\psi_x(x, y, t) = \Psi_x(x, t)g(t) = R^{\psi_x}(x, y) \sum_{m=0}^{M_{\Psi_x}} \sum_{n=0}^{N_{\Psi_x}} \Psi_{x,m,n} T_m(x) T_n(y) g(t) \quad (60d)$$

$$\psi_y(x, y, t) = \Psi_y(x, t)g(t) = R^{\psi_y}(x, y) \sum_{m=0}^{M_{\Psi_y}} \sum_{n=0}^{N_{\Psi_y}} \Psi_{y,m,n} T_m(x) T_n(y) g(t) \quad (60e)$$

where $g(t) = \cos(\omega t)$. The Chebyshev polynomials of the first kind of order n and m

$\{T_m(x) \text{ and } T_n(y)\}$ are obtained from the following three-term recurrence relation

(Franklin, 2007):

$$T_{m+1}(x) = 2xT_m(x) - T_{m-1}(x), \quad -1 \leq x \leq 1, \quad m = 1, 2, 3, 4, 5, ..$$

$$T_{n+1}(y) = 2yT_n(y) - T_{n-1}(y), \quad -1 \leq y \leq 1, \quad n = 1, 2, 3, 4, 5, ..$$

$$\text{with starting values } T_0(x) = T_0(y) = 1, T_1(x) = x, T_1(y) = y \quad (61)$$

Since the Chebyshev polynomials of the first kind are nonzero at x and $y = \pm 1$, the boundary functions $R^{u,v,w,\psi_x,\psi_y}(x, y)$ should be chosen to satisfy the essential boundary conditions. The general expression of the auxiliary functions is written as (Kiani, 2016):

$$R^{u,v,w,\psi_x,\psi_y}(x, y) = (x)^p (x - a)^q (y)^r (y - b)^s \quad (62)$$

where the superscripts p , q , r , and s are either zero or one depending on the essential boundary conditions. Suppose that all four edges are simply supported and restrained from moving, in other words, all edges are immovable, the auxiliary functions are expressed as follows:

$$\begin{aligned}
R^u(x, y) &= (x)^1(x - a)^1(y)^1(y - b)^1 \\
R^v(x, y) &= (x)^1(x - a)^1(y)^1(y - b)^1 \\
R^w(x, y) &= (x)^1(x - a)^1(y)^1(y - b)^1 \\
R^{\psi_x}(x, y) &= (x)^0(x - a)^0(y)^0(y - b)^0 = 1 \\
R^{\psi_y}(x, y) &= (x)^0(x - a)^0(y)^0(y - b)^0 = 1
\end{aligned} \tag{63}$$

It should be noted that the range of the independent variables x and y is $[-1, 1]$, but for analytical and numerical work, it is often more convenient to shift the range of the variables to $[0, 1]$. Therefore shifted Chebyshev polynomials from x and y to $2x-1$ and $2y-1$ are used and expressed as follows (Gil, Segura & Temme, 2007):

$$\begin{aligned}
T_{m+1}(2x - 1) &= 2(2x - 1)T_m(2x - 1) - T_{m-1}(2x - 1), & 0 \leq x \leq 1, \\
& m = 1, 2, 3, \dots \\
T_{n+1}(2y - 1) &= 2(2y - 1)T_n(2y - 1) - T_{n-1}(2y - 1), & 0 \leq y \leq 1, \\
& n = 1, 2, 3, \dots
\end{aligned} \tag{64}$$

with $T_0(2x - 1) = T_0(2y - 1) = 1$, $T_1(x) = 2x - 1$, $T_1(y) = 2y - 1$

Let $\xi = \frac{x}{a}$ and $\eta = \frac{y}{b}$ be the dimensionless coordinates. Using the shifted Chebyshev polynomials and auxiliary functions for an immovable simple supported shell, the displacement and rotation fields are written as follows:

$$u_0(\xi, \eta, t) = (\xi)(\xi - 1)(\eta)(\eta - 1) \sum_{m=0}^{M_U} \sum_{n=0}^{N_U} U_{m,n} T_m(2\xi - 1) T_n(2\eta - 1) g(t) \tag{65a}$$

$$v_0(\xi, \eta, t) = (\xi)(\xi - 1)(\eta)(\eta - 1) \sum_{m=0}^{M_V} \sum_{n=0}^{N_V} V_{m,n} T_m(2\xi - 1) T_n(2\eta - 1) g(t) \tag{65b}$$

$$w_0(\xi, \eta, t) = (\xi)(\xi - 1)(\eta)(\eta - 1) \sum_{m=0}^{M_W} \sum_{n=0}^{N_W} W_{m,n} T_m(2\xi - 1) T_n(2\eta - 1) g(t) \tag{65c}$$

$$\psi_x(\xi, \eta, t) = \sum_{m=0}^{M_{\Psi_x}} \sum_{n=0}^{N_{\Psi_x}} \Psi_{x_{m,n}} T_m(2\xi - 1) T_n(2\eta - 1) g(t) \quad (65d)$$

$$\psi_y(\xi, \eta, t) = \sum_{m=0}^{M_{\Psi_y}} \sum_{n=0}^{N_{\Psi_y}} \Psi_{y_{m,n}} T_m(2\xi - 1) T_n(2\eta - 1) g(t) \quad (65e)$$

$$w^*(\xi, \eta) = (\xi)(\xi - 1)(\eta)(\eta - 1) \sum_{m=0}^{M_W} \sum_{n=0}^{N_W} W^* T_m(2\xi - 1) T_n(2\eta - 1) \quad (65f)$$

In which W^* is the amplitude of the imperfection.

5.3 Linear Analysis

To calculate the linear vibration of a perfect stiffened FGM double-curved shell, the nonlinear parts of the strain-displacement relationship in equation (9) are neglected.

Using the Lagrange's equations of motion expressed below:

$$\frac{d}{dt} \left(\frac{\partial L}{\partial \dot{q}_k} \right) - \frac{\partial L}{\partial q_k} = 0, \quad k = 1, 2, \dots, N_{max} \quad (66)$$

Where

$$L = T_p - U_s^{Total}$$

$$g(t) = q \cos(\omega t)$$

$$N_{max} = (M_U + 1)(N_U + 1) + (M_V + 1)(N_V + 1) + (M_W + 1)(N_W + 1)$$

$$+ (M_{\Psi_x} + 1)(M_{\Psi_x} + 1)$$

$$+ (M_{\Psi_y} + 1)(M_{\Psi_y} + 1) \text{ is the total number of degree of freedom}$$

$$q = \{U_{m,n}, V_{m,n}, W_{m,n}, \Psi_{x_{m,n}} \text{ and } \Psi_{y_{m,n}}\}$$

with $m = 0, \dots, M_U$ or M_V or M_W or M_{Ψ_x} or M_{Ψ_y}

$n = 0, \dots, N_U$ or N_V or N_W or N_{Ψ_x} or N_{Ψ_y}

Substituting equation (55), equation (57) and $g(t) = q \cos(\omega t)$ into equation (66) results to an eigenvalue problem as:

$$(K - \omega^2 M)q = 0 \quad (67)$$

Where M is the mass matrix and K is the stiffness matrix. The element of the mass and stiffness matrices for a perfect stiffened shell are found using Mathematica software.

Equation (67) is written as follows:

$$\begin{pmatrix}
 \sum_l \sum_k \int_0^1 \int_0^1 \begin{pmatrix}
 (K_{UU})_{m,..,k}^{Total} & (K_{UV})_{m,..,k} & (K_{UW})_{m,..,k} & (K_{U\Psi_x})_{m,..,k} & (K_{U\Psi_y})_{m,..,k} \\
 (K_{VU})_{m,..,k} & (K_{VV})_{m,..,k}^{Total} & (K_{VW})_{m,..,k} & (K_{V\Psi_x})_{m,..,k} & (K_{V\Psi_y})_{m,..,k} \\
 (K_{WU})_{m,..,k} & (K_{WV})_{m,..,k} & (K_{WW})_{m,..,k}^{Total} & (K_{W\Psi_x})_{m,..,k} & (K_{W\Psi_y})_{m,..,k} \\
 (K_{\Psi_x U})_{m,..,k} & (K_{\Psi_x V})_{m,..,k} & (K_{\Psi_x W})_{m,..,k} & (K_{\Psi_x \Psi_x})_{m,..,k}^{Total} & (K_{\Psi_x \Psi_y})_{m,..,k} \\
 (K_{\Psi_y U})_{m,..,k} & (K_{\Psi_y V})_{m,..,k} & (K_{\Psi_y W})_{m,..,k} & (K_{\Psi_y \Psi_x})_{m,..,k} & (K_{\Psi_y \Psi_y})_{m,..,k}^{Total}
 \end{pmatrix} abd\xi d\eta \\
 - \sum_l \sum_k \omega^2 \int_0^1 \int_0^1 \begin{pmatrix}
 (M_{UU})_{m,..,k} & 0 & 0 & (M_{U\Psi_x})_{m,..,k} & 0 \\
 0 & (M_{VV})_{m,..,k} & 0 & 0 & (M_{V\Psi_y})_{m,..,k} \\
 0 & 0 & (M_{WW})_{m,..,k} & 0 & 0 \\
 (M_{\Psi_x U})_{m,..,k} & 0 & 0 & (M_{\Psi_x \Psi_x})_{m,..,k} & 0 \\
 0 & (M_{\Psi_y V})_{m,..,k} & 0 & 0 & (M_{\Psi_y \Psi_y})_{m,..,k}
 \end{pmatrix} abd\xi d\eta
 \end{pmatrix} q_{l,k} \\
 = 0 \\
 m, l = 0, \dots, M_U \text{ or } M_v \text{ or } M_w \text{ or } M_{\Psi_x} \text{ or } M_{\Psi_y} \\
 n, k = 0, \dots, N_U \text{ or } N_v \text{ or } N_w \text{ or } N_{\Psi_x} \text{ or } N_{\Psi_y} \tag{68}$$

where

$$\begin{aligned}
 (K_{UU})_{m,..,k}^{Total} &= (K_{UU})_{m,..,k} + (K_U)_{m,n}^T \\
 (K_{VV})_{m,..,k}^{Total} &= (K_{VV})_{m,..,k} + (K_V)_{m,n}^T \\
 (K_{WW})_{m,..,k}^{Total} &= (K_{WW})_{m,..,k} + (K_W)_{m,n}^T \\
 (K_{\Psi_x \Psi_x})_{m,..,k}^{Total} &= (K_{\Psi_x \Psi_x})_{m,..,k} + (K_{\Psi_x})_{m,n}^T \\
 (K_{\Psi_y \Psi_y})_{m,..,k}^{Total} &= (K_{\Psi_y \Psi_y})_{m,..,k} + (K_{\Psi_y})_{m,n}^T
 \end{aligned}$$

Solving the determinant of equation (67) gives the eigenvalues of the perfect stiffened shell. Eigenvectors are obtained by substituting each eigenvalue back into equation (67). The mode shapes corresponding to the eigenvectors are obtained by using equations (65 a-f) after neglecting the time function $g(t)$ and substituting the unknown coefficients

$U_{m,n}$, $V_{m,n}$, $W_{m,n}$, $\Psi_{x_{m,n}}$ and $\Psi_{y_{m,n}}$ with $U_{m,n}^{(i)}$, $V_{m,n}^{(i)}$, $W_{m,n}^{(i)}$, $\Psi_{x_{m,n}}^{(i)}$ and $\Psi_{y_{m,n}}^{(i)}$ which are the coefficient of the i^{th} eigenvector previously obtained as follows:

$$U^{(i)}(\xi, \eta) = \sum_{m=0}^{M_U} \sum_{n=0}^{N_U} U_{m,n}^{(i)}(\xi)(\xi-1)(\eta)(\eta-1)T_m(2\xi-1)T_n(2\eta-1) \quad (69a)$$

$$V^{(i)}(\xi, \eta) = \sum_{m=0}^{M_V} \sum_{n=0}^{N_V} V_{m,n}^{(i)}(\xi)(\xi-1)(\eta)(\eta-1)T_m(2\xi-1)T_n(2\eta-1) \quad (69b)$$

$$W^{(i)}(\xi, \eta) = \sum_{m=0}^{M_W} \sum_{n=0}^{N_W} W_{m,n}^{(i)}(\xi)(\xi-1)(\eta)(\eta-1)T_m(2\xi-1)T_n(2\eta-1) \quad (69c)$$

$$\Psi_x^{(i)}(\xi, \eta) = \sum_{m=0}^{M_{\Psi_x}} \sum_{n=0}^{N_{\Psi_x}} \Psi_{x_{m,n}}^{(i)} T_m(2\xi-1)T_n(2\eta-1) \quad (69d)$$

$$\Psi_y^{(i)}(\xi, \eta) = \sum_{m=0}^{M_{\Psi_y}} \sum_{n=0}^{N_{\Psi_y}} \Psi_{y_{m,n}}^{(i)} T_m(2\xi-1)T_n(2\eta-1) \quad (69e)$$

5.4 Nonlinear Analysis

To study the multi-mode nonlinear analysis of the stiffened double-curved shell, the mode shapes obtained by linear analysis should be used. Therefore, the displacements and rotations in the function of mode shapes obtained previously are expressed as follows:

$$u_0(\xi, \eta, t) = \sum_{i=1}^{\bar{M}_u} u_i(t)U^{(i)}(\xi, \eta) \quad (70a)$$

$$v_0(\xi, \eta, t) = \sum_{i=1}^{\bar{M}_v} v_i(t)V^{(i)}(\xi, \eta) \quad (70b)$$

$$w_0(\xi, \eta, t) = \sum_{j=1}^{\bar{N}_w} w_j(t)W^{(j)}(\xi, \eta) \quad (70c)$$

$$w^*(\xi, \eta) = \sum_{j=1}^{\bar{N}_w} w^* W^{(j)}(\xi, \eta) \quad (70d)$$

$$\psi_x(\xi, \eta, t) = \sum_{j=1}^{\bar{N}_{\psi_x}} \psi_{x_j}(t) \Psi_x^{(j)}(\xi, \eta) \quad (70e)$$

$$\psi_y(\xi, \eta, t) = \sum_{j=1}^{\bar{N}_{\psi_y}} \psi_{y_j}(t) \Psi_y^{(j)}(\xi, \eta) \quad (70f)$$

where the terms $u_i(t)$, $v_i(t)$, $w_i(t)$, $\psi_{x_j}(t)$ and $\psi_{y_j}(t)$ are the generalized coordinates, which are the unknown functions of time, “t”. It should be noted that the index “j” is used for the out of plane displacement and rotations and it starts from the first transverse natural frequency (j=1). As for the in-plane displacements, index “I” is used and it starts from the first in-plane mode.

The Lagrange equations of motion, in terms of virtual work and energy dissipation, is written as follows:

$$\frac{d}{dt} \left(\frac{\partial L}{\partial \dot{q}_s} \right) - \frac{\partial L}{\partial q_s} + \frac{\partial D}{\partial q_s} = \frac{\partial W}{\partial q_s}, \quad s = 1, 2, \dots, \bar{N}_{max} \quad (71)$$

where

$$q_s = \{u_i(t), v_i(t), w_j(t), \psi_{x_j}(t) \text{ and } \psi_{y_j}(t)\}$$

$$i = 1, \dots, \bar{M}_u \text{ or } \bar{M}_v \text{ and } j = 1, \dots, \bar{N}_w \text{ or } \bar{N}_{\psi_x} \text{ or } \bar{N}_{\psi_y}$$

$$\bar{N}_{max} = \bar{M}_u + \bar{M}_v + \bar{N}_w + \bar{N}_{\psi_x} + \bar{N}_{\psi_y}$$

Substituting equation (70 a-f) into equation (55), (57), (58) and (59), without neglecting the nonlinear terms of the stain-displacement relationship, then the results into equation (71). This leads to a strongly nonlinear duffing equation, which can be written in matrix form as follows:

$$M\ddot{q} + C\dot{q} + K_1q + K_2(q)q + K_3(q, q)q = F \cos(\Omega t) \quad (72)$$

where M is the mass matrix, C is the damping matrix, K_1 is the linear stiffness matrix of the imperfect stiffened shell which includes the effect of temperature, K_2 and K_3 are the nonlinear quadratic and cubic matrices, respectively. F is the vector of excitation amplitude. Matrices M, C, K_1, K_2, K_3, F and F^T are expressed as follows:

$$M = \left\{ \sum_k \int_0^1 \int_0^1 \begin{pmatrix} (M_{UU})_{s,k} & 0 & 0 & (M_{U\Psi_x})_{s,k} & 0 \\ 0 & (M_{VV})_{s,k} & 0 & 0 & (M_{V\Psi_y})_{s,k} \\ 0 & 0 & (M_{WW})_{s,k} & 0 & 0 \\ (M_{\Psi_x U})_{s,k} & 0 & 0 & (M_{\Psi_x \Psi_x})_{s,k} & 0 \\ 0 & (M_{\Psi_y V})_{s,k} & 0 & 0 & (M_{\Psi_y \Psi_y})_{s,k} \end{pmatrix} abd\xi d\eta \right\} \quad (73)$$

$$C = \left\{ \sum_k \int_0^1 \int_0^1 c \begin{pmatrix} (C_{UU})_{s,k} & 0 & 0 & 0 & 0 \\ 0 & (C_{VV})_{s,k} & 0 & 0 & 0 \\ 0 & 0 & (C_{WW})_{s,k} & 0 & 0 \\ 0 & 0 & 0 & (C_{\Psi_x \Psi_x})_{s,k} & 0 \\ 0 & 0 & 0 & 0 & (C_{\Psi_y \Psi_y})_{s,k} \end{pmatrix} abd\xi d\eta \right\} \quad (74)$$

$$K_1 = \left\{ \sum_k \int_0^1 \int_0^1 \begin{pmatrix} (K_{1UU})_{s,k}^{Total} & (K_{1UV})_{s,k} & (K_{1UW})_{s,k} & (K_{1U\Psi_x})_{s,k} & (K_{1U\Psi_y})_{s,k} \\ (K_{1VU})_{s,k} & (K_{1VV})_{s,k}^{Total} & (K_{1VW})_{s,k} & (K_{1V\Psi_x})_{s,k} & (K_{1V\Psi_y})_{s,k} \\ (K_{1WU})_{s,k} & (K_{1WV})_{s,k} & (K_{1WW})_{s,k}^{Total} & (K_{1W\Psi_x})_{s,k} & (K_{1W\Psi_y})_{s,k} \\ (K_{1\Psi_x U})_{s,k} & (K_{1\Psi_x V})_{s,k} & (K_{1\Psi_x W})_{s,k} & (K_{1\Psi_x \Psi_x})_{s,k}^{Total} & (K_{1\Psi_x \Psi_y})_{s,k} \\ (K_{1\Psi_y U})_{s,k} & (K_{1\Psi_y V})_{s,k} & (K_{1\Psi_y W})_{s,k} & (K_{1\Psi_y \Psi_x})_{s,k} & (K_{1\Psi_y \Psi_y})_{s,k}^{Total} \end{pmatrix} abd\xi d\eta \right\} q_k \quad (75)$$

Where

$$\begin{aligned} (K_{1UU})_{s,k}^{Total} &= (K_{1UU})_{s,k} + (K_{1U})_s^T \\ (K_{1VV})_{s,k}^{Total} &= (K_{1VV})_{s,k} + (K_{1V})_s^T \\ (K_{1WW})_{s,k}^{Total} &= (K_{1WW})_{s,k} + (K_{1W})_s^T \\ (K_{1\Psi_x \Psi_x})_{m,..,k}^{Total} &= (K_{1\Psi_x \Psi_x})_{s,k} + (K_{\Psi_x})_s^T \\ (K_{1\Psi_y \Psi_y})_{m,..,k}^{Total} &= (K_{1\Psi_y \Psi_y})_{s,k} + (K_{1\Psi_y})_s^T \end{aligned}$$

$$K_2(q)q = \left\{ \sum_l \sum_k \int_0^1 \int_0^1 \begin{pmatrix} 0 & 0 & (K_{2UW})_{s,k,l} & 0 & 0 \\ 0 & 0 & (K_{2VW})_{s,k,l} & 0 & 0 \\ (K_{2WU})_{s,k,l} & (K_{2WV})_{s,k,l} & (K_{2WW})_{s,k,l} & (K_{2W\Psi_x})_{s,k,l} & (K_{2W\Psi_y})_{s,k,l} \\ 0 & 0 & (K_{2\Psi_x W})_{s,k,l} & 0 & 0 \\ 0 & 0 & (K_{2\Psi_y W})_{s,k,l} & 0 & 0 \end{pmatrix} abd\xi d\eta \right\} q_k q_l \quad (76)$$

$$K_3(q, q)q = \left\{ \sum_p \sum_l \sum_k \int_0^1 \int_0^1 \begin{pmatrix} 0 & 0 & 0 & 0 & 0 \\ 0 & 0 & 0 & 0 & 0 \\ 0 & 0 & (K_{3WW})_{s,k,l,p} & 0 & 0 \\ 0 & 0 & 0 & 0 & 0 \\ 0 & 0 & 0 & 0 & 0 \end{pmatrix} abd\xi d\eta \right\} q_k q_l q_p \quad (77)$$

$$F = \begin{pmatrix} W^{(j)}(\xi, \eta) \\ W^{(j+1)}(\xi, \eta) \\ W^{(j+2)}(\xi, \eta) \\ \vdots \\ W^{(\bar{N}_w)}(\xi, \eta) \end{pmatrix}^T \tilde{f} \cos(\Omega t) \quad (78)$$

It should be noted that Matrix M and K_1 are going to be diagonalized because of modal analysis. For numerical implementation, the set of equations of motion above is reconstructed in the form of a state space modal by multiplying it by the inverse of the mass matrix which gives:

$$\begin{aligned} \dot{q} &= y, \\ \dot{y} &= -M^{-1}C\dot{q} - M^{-1}K_1q - M^{-1}K_2(q)q - M^{-1}K_3(q, q)q - M^{-1}F\cos(\Omega t) \end{aligned} \quad (79)$$

5.5 Numerical Results

This section is divided into two main parts. The first part consists of the validation of the multimodal formulation explained in the previous section. The nonlinear amplitude-frequency response of a thin Stainless steel rectangular plate with free edges and a simply-supported double-curved shells with movable edges under dimensionless concentrated force and damping are considered here. In the second part, the nonlinear frequency response of a functionally graded stiffened cylindrical shell is studied under mechanical and thermal load

5.5.1 Validation of the Multimodal Formulation

To study the large amplitude vibration of a rectangular plate, linear analysis is carried out first to find the transverse and rotational modes as well as the in-plane modes. These mode shapes are going to be used in order to discretize the energy functional. The Stainless steel plate has $a = 0.3m$, $b = 0.45m$, $E = 198GPa$, $\rho = 7850kg/m^3$ and $\nu = 0.3$. It should be noted that in order to satisfy the necessary boundary conditions for free edges, the superscripts p, q, r, and s are taken to be zero in equation (63). To reach convergence, Chebyshev polynomials of order 8 were enough. This made the total number of the degree of freedoms $N_{max} = 405$. The transverse and rotational dimensionless frequencies for the stainless steel rectangular plate are calculated and listed in Table 5.1.

Table 5.1

Comparison of Dimensionless Transverse and Rotational Frequency $\varpi = \omega_{mn}a^3\sqrt{\rho h/D}$ for Isotropic Rectangular Plate ($h=0.001$, $R/b=10$).

a/h	Theory	Transverse and Rotational Modes			
		1	2	3	4
300	HSDT	8.9314	9.5169	20.598	22.1822
	Present	8.9305	9.5168	20.5965	22.1812
100	HSDT	8.9273	9.5148	20.5844	22.1743
	Present	8.9240	9.5150	20.5781	22.1729
30	HSDT	8.8825	9.4983	20.4425	22.088
	Present	8.8277	9.4626	20.3186	22.000

In addition, the dimensionless in-plane modes are illustrated in Table 5.2 below. A very good agreement can be witnessed with the comparison to those obtained based on the higher-order shear deformation theory.

Table 5.2

Comparison of Dimensionless In-Plane frequency $\bar{\omega} = \omega_{mn} a^3 \sqrt{\rho h / D}$ for Isotropic Rectangular Plate ($h=0.001$, $R/b=10$)

a/h	Theory	In-Plane Modes			
		1	2	3	4
300	HSDT	1521.712 ⁽⁴⁶⁾	1996.159 ⁽⁴⁷⁾	2019.403 ⁽⁴⁸⁾	2728.038 ⁽⁵⁰⁾
	Present	1521.670 ⁽⁶⁷⁾	1995.917 ⁽⁶⁹⁾	2019.391 ⁽⁷⁰⁾	2727.981 ⁽⁸⁰⁾
100	HSDT	507.237 ⁽³⁷⁾	665.386 ⁽³⁹⁾	673.134 ⁽⁴⁰⁾	909.346 ⁽⁴⁷⁾
	Present	507.215 ⁽⁵²⁾	665.294 ⁽⁵⁷⁾	673.119 ⁽⁵⁸⁾	909.311 ⁽⁶²⁾
30	HSDT	152.171 ⁽²¹⁾	199.615 ⁽²⁵⁾	201.940 ⁽²⁶⁾	272.803 ⁽²⁹⁾
	Present	152.146 ⁽²⁴⁾	199.561 ⁽³¹⁾	201.911 ⁽³²⁾	272.761 ⁽³⁹⁾

Note: In Table 5.2, the numbers given in the superscript represent the eigenvalue number.

Table 5.3

Dimensionless In Plane Frequency $\bar{\omega} = \omega_{mn} a^3 \sqrt{\rho h / D}$ for Isotropic Rectangular Plate ($h=0.001$, $R/b=10$, $a/h=30$).

In-Plane Modes					
5	6	7	8	9	10
275.187 ⁽⁴⁰⁾	303.574 ⁽⁴³⁾	313.808 ⁽⁴⁴⁾	318.465 ⁽⁴⁵⁾	328.130 ⁽⁴⁶⁾	470.563 ⁽⁵⁴⁾
11	12	13	14	15	16
425.977 ⁽⁵⁵⁾	429.436 ⁽⁵⁶⁾	432.970 ⁽⁵⁷⁾	441.564 ⁽⁵⁸⁾	491.784 ⁽⁶⁰⁾	515.351 ⁽⁶¹⁾
17	18	19			
519.408 ⁽⁶³⁾	529.212 ⁽⁶⁵⁾	542.61 ⁽⁶⁶⁾			

It can be seen from Table 5.2 and Table 5.3 that the in-plane modes occur at a higher frequency for the thin plate rather than for the thick one. In previously published papers, it was concluded that the accuracy of the nonlinear vibration is related to the in-plane mode rather than the transverse and rotational modes. To validate the discussed

formulation, and to compare it with Alijani and Amabili (2011), more dimensionless in-plane modes are needed. After obtaining the mode shapes from linear analysis, the energy functional is discretized by including several combinations of generalized coordinates.

These combinations are shown in Table 5.4 below.

Table 5.4

Generalized Coordinates Combination.

Models	Generalized Coordinates
24 dof	$u_{24}, u_{31}, u_{32}, u_{39}, u_{40}, u_{43}, v_{24}, v_{31}, v_{32}, v_{39}, v_{40}, v_{43}$ $w_1, w_2, w_3, w_4, \psi_{x_1}, \psi_{x_2}, \psi_{x_3}, \psi_{x_4}, \psi_{y_1}, \psi_{y_2}, \psi_{y_3}, \psi_{y_4}$
36 dof	$u_{24}, u_{31}, u_{32}, u_{39}, u_{40}, u_{43}, u_{44}, u_{45}, u_{46}, u_{54}, u_{55}, u_{56}$ $v_{24}, v_{31}, v_{32}, v_{39}, v_{40}, v_{43}, v_{44}, v_{45}, v_{46}, v_{54}, v_{55}, v_{56}$ $w_1, w_2, w_3, w_4, \psi_{x_1}, \psi_{x_2}, \psi_{x_3}, \psi_{x_4}, \psi_{y_1}, \psi_{y_2}, \psi_{y_3}, \psi_{y_4}$
44 dof	$u_{24}, u_{31}, u_{32}, u_{39}, u_{40}, u_{43}, u_{44}, u_{45}, u_{46}, u_{54}, u_{55}, u_{56}, u_{57}, u_{58}, u_{60}, u_{61}$ $v_{24}, v_{31}, v_{32}, v_{39}, v_{40}, v_{43}, v_{44}, v_{45}, v_{46}, v_{54}, v_{55}, v_{56}, v_{57}, v_{58}, v_{60}, v_{61}$ $w_1, w_2, w_3, w_4, \psi_{x_1}, \psi_{x_2}, \psi_{x_3}, \psi_{x_4}, \psi_{y_1}, \psi_{y_2}, \psi_{y_3}, \psi_{y_4}$

It can be seen from the generalized coordinates combination that the transverse and rotation modes numbers are similar for the three cases. On the other hand, the in-plane modes increased from 12 in the case of 24 dof to 24 in the case of 36 dof to 32 for the 44 dof case and finally 38 for the 50 dof case. This is due to the significance of in-plane mode on nonlinear vibration response.

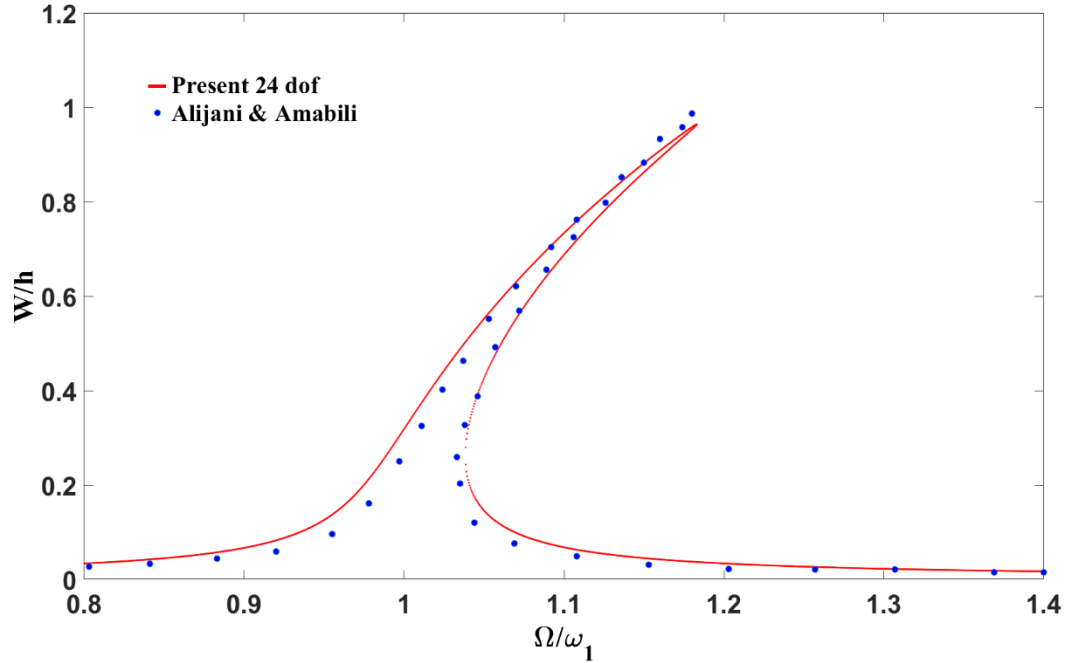


Figure 5.1. The frequency amplitude curve of nonlinear vibration of free edges stainless steel rectangular plate ($b/a = 1.5$, $a/h = 30$) under dimensionless $f = 0.03$ and damping ratio $\zeta = 0.004$ using 24 dof model.

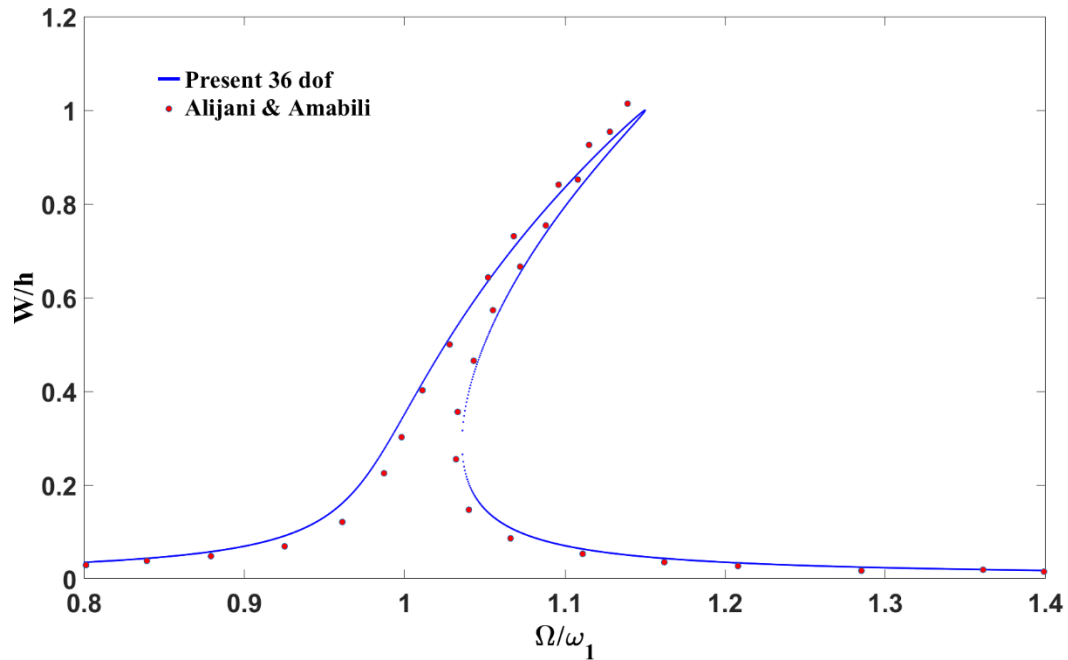


Figure 5.2. The frequency amplitude curve of nonlinear vibration of free edges stainless steel rectangular plate ($b/a = 1.5$, $a/h = 30$) under dimensionless $f = 0.03$ and damping ratio $\zeta = 0.004$ using 36 dof model.

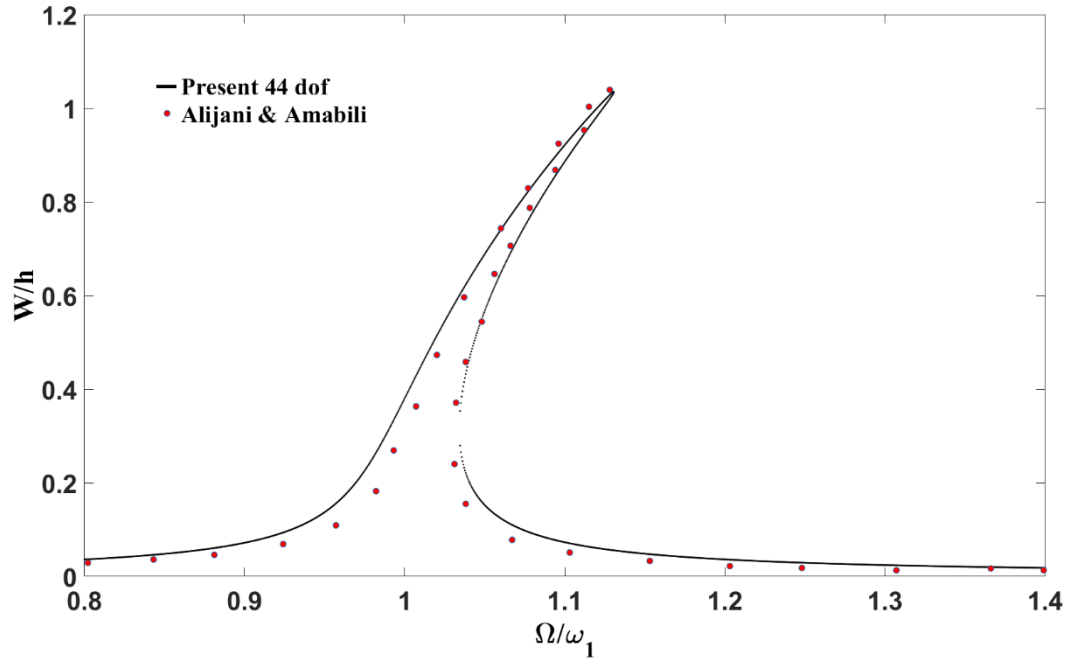


Figure 5.3. The frequency amplitude curve of nonlinear vibration of the free edges stainless steel rectangular plate ($b/a = 1.5$, $a/h = 30$) under dimensionless $f = 0.03$ and damping ratio $\zeta = 0.004$ using 44 dof model.

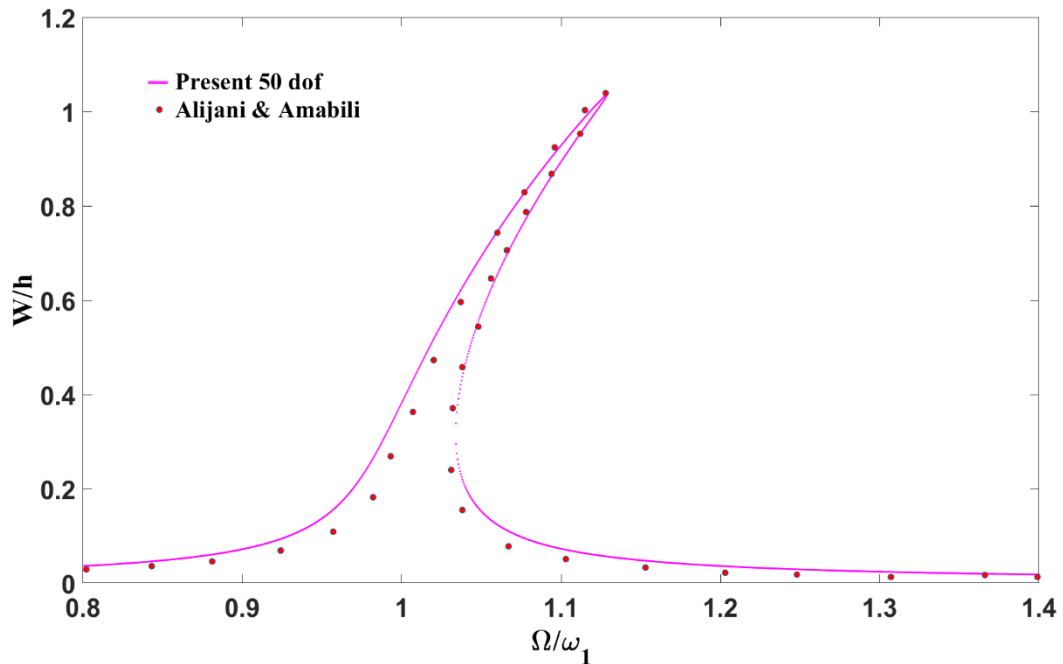


Figure 5.4. The frequency amplitude curve of nonlinear vibration of the free edges stainless steel rectangular plate ($b/a = 1.5$, $a/h = 30$) under dimensionless $f = 0.03$ and damping ratio $\zeta = 0.004$ using 50 dof model.

Now the nonlinear frequency responses are plotted using the software XPPAUT which contains the popular bifurcation program AUTO. First, the set of nonlinear ordinary differential equations is solved using the numerical software XPP, then the amplitude-frequency response was obtained by using the built-in software AUTO. The Stainless Steel rectangular plate is subjected to a dimensionless force $f = 0.03$ and damping ratio $\zeta = 0.004$. A very good agreement can be observed in Figure 5.1, Figure 5.2, Figure 5.3 and Figure 5.4. It can be seen from Figure 5.5 that the variation of the number of dof model has a significant effect on the nonlinear response of the rectangular plate. In this example, the increase the number of dof, decreases hardening behavior. It can also be seen that for 44 and 50 dof, the nonlinear response has completely converged. Therefore, a 44 dof model can be adopted to decrease the computational cost.

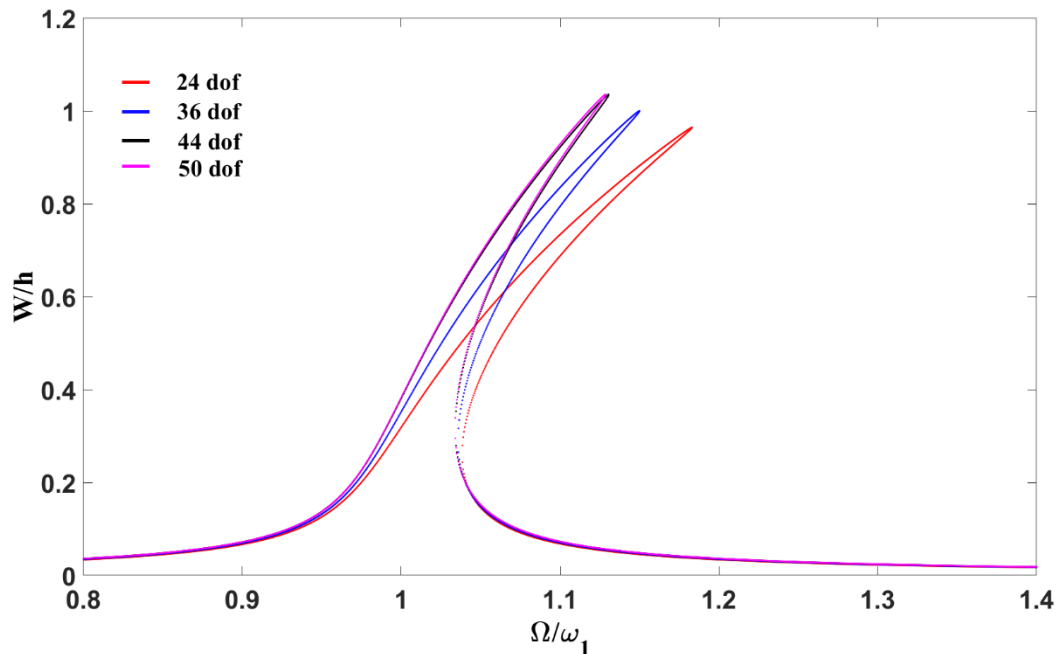


Figure 5.5. Effect of the number of dof model on the nonlinear frequency amplitude response of the free edges stainless steel rectangular plate ($b/a = 1.5$, $a/h = 30$) under dimensionless $f = 0.03$ and damping ratio $\zeta = 0.004$.

Now a simply-supported movable functionally graded double curved shell studied and compared with results obtained by Amabili et al. (2011). For the movable edges, the auxiliary functions that satisfy the boundary conditions are given as follows:

$$R^u(x, y) = (x)^0(x - a)^0(y)^1(y - b)^1$$

$$R^v(x, y) = (x)^1(x - a)^1(y)^0(y - b)^0$$

$$R^w(x, y) = (x)^1(x - a)^1(y)^1(y - b)^1$$

$$R^{\psi_x}(x, y) = (x)^0(x - a)^0(y)^0(y - b)^0 = 1$$

$$R^{\psi_y}(x, y) = (x)^0(x - a)^0(y)^0(y - b)^0 = 1$$

and the generalized coordinated are found in Table 5.5 below:

Table 5.5

Generalized Coordinated Combination for the FGM Double Curved Shell.

Models	Generalized Coordinates
15 dof	$u_{14}, u_{19}, u_{20}, u_{28}, u_{31}, u_{34}, v_{14}, v_{19}, v_{20}, v_{28}, v_{31}, v_{34}, w_1, \psi_{x_1}, \psi_{y_1}$

Figure 5.6 shows the nonlinear amplitude-frequency response of the simply supported functionally graded double curved shell under dimensionless force and damping. The results are obtained using only 15 dof models. It can be seen that the present results are in acceptable agreement with those of Amabili et al. (2011), and the slight difference is due to the fact that Amabili used the higher order shear deformation theory. In addition, he didn't assume the shell to be shallow.

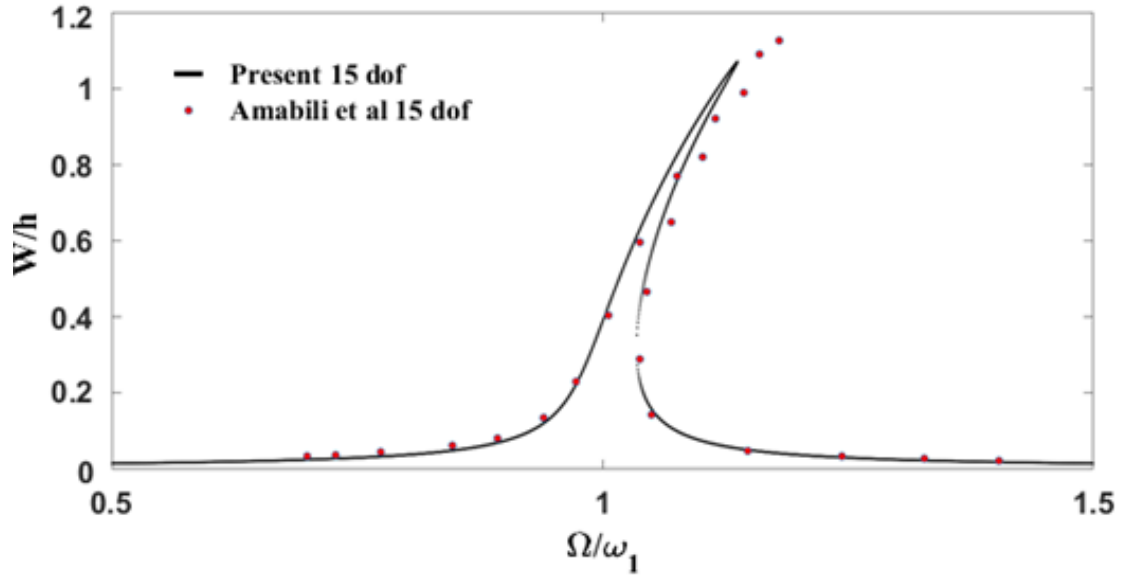


Figure 5.6. The frequency amplitude curve of nonlinear vibration of the simply supported double curved shells with movable edges ($a/b = 1$, $a/R_x = b/R_y = 10$, $a/h = 10$) under dimensionless $f = 0.0155$ and damping ratio $\zeta = 0.004$.

Now, after validating the multimodal formulation that is adopted in this chapter, a more complicated problem can be considered.

5.5.2 Results and Discussions

To show the significance of multimodal analysis on the nonlinear response, a previously studied problem based on the single-mode Galerkin's method is reevaluated using the new formulation. A functionally graded stiffened spherical shell made of Aluminum and Alumina mixture is considered. The frequency-amplitude curve of the forced nonlinear vibration under distributed load was investigated in Chapter 3 (Figure 3.21).

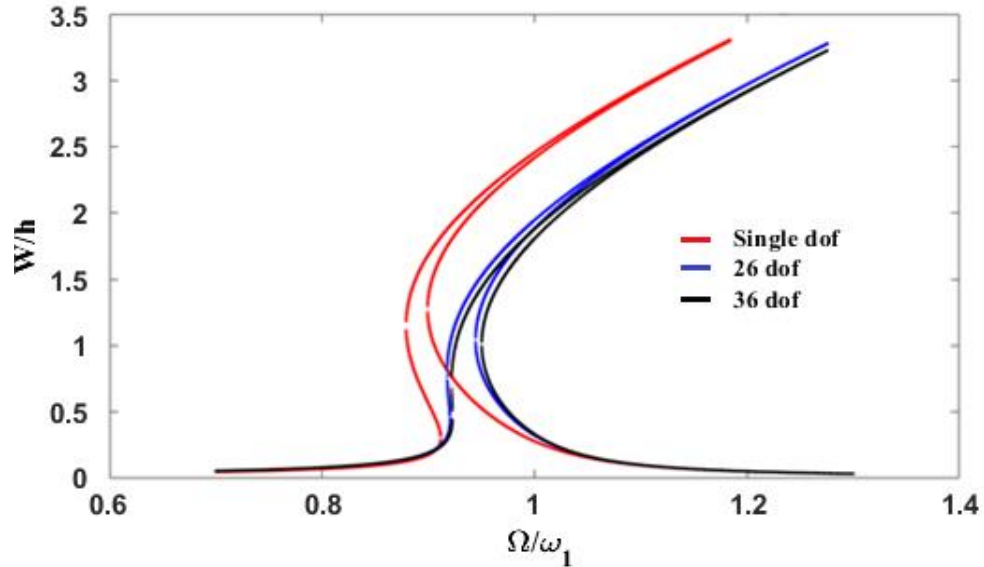


Figure 5.7. The effect of the number of dof on the frequency-amplitude curve of forced nonlinear vibration of stiffened Al/Al₂O₂ spherical shell $R_x = R_y = 5\text{m}$, $a = b = 0.8\text{m}$, $h = 0.025\text{m}$, $K = 1$ and $\zeta = 0.01$ under uniformly distributed load $Q = 10^5\text{Pa}$.

Following the same procedure discussed in the validation part of Chapter 5, the frequency response is plotted in Figure 5.7. The convergence of the solution can be seen when the number of dof modal was increased from a single-mode, solved previously, to 26 dof then to 36 dof models. It can be seen that the difference of the nonlinear response between one mode solution and the 26 dof modal solution is much higher than the ones between 26 and 36 dof models. Hence, it can be concluded from this example that the single-mode solution gives a general nonlinear solution but not necessarily the accurate. This solution is not accurate enough because of the lack of transverse, rotational and in-plane mode.

In the second example, the same stiffened spherical FGM shell is considered under uniform temperature rise. In Figure 5.8, 36 dof models were used since they lead to a fast convergence. Also, the material properties are temperature-dependent. Figure 5.8 also shows that as the temperature rise increases, the deflection slightly increase for the same

frequency ratio. This can be seen that the initial curve has shifted to the left side. Hence, more softening behavior can be noticed.

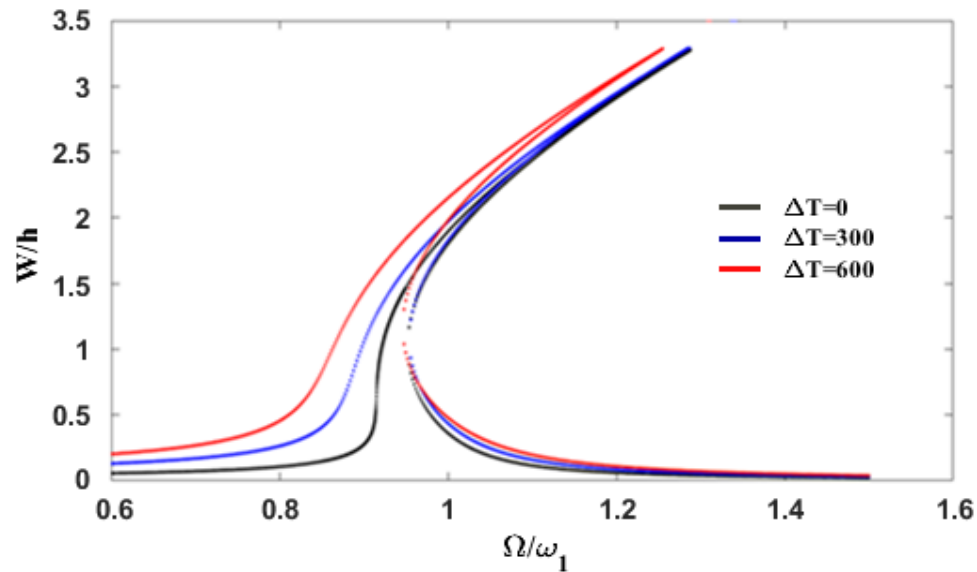


Figure 5.8. Effect of uniform temperature rise on the frequency response curve of a stiffened spherical shell ($R_x = R_y = 5\text{m}$, $a = b = 0.8\text{m}$, $h = 0.025\text{m}$, $K = 1$ and $\zeta = 0.01$) under uniformly distributed load $Q = 10^5\text{Pa}$.

Generally, it is hardly possible to manufacture a structure without any initial geometric imperfections. Therefore, it is imperative to evaluate the effect of imperfection on the selected spherical shell. Figure 5.9 below illustrates the nonlinear response of the stiffened spherical shell under three different imperfection amplitudes. It can be seen that the geometric imperfection has a significant effect on the nonlinear response of the structure. A softening behavior was observed for the imperfect spherical shell. This is because adding imperfection makes the structure weaker. Also, the variation of the nonlinear response between $W^* = 0$ and $W^* = 0.5h$ is much smaller than that of between $W^* = 0.5h$ and $W^* = h$. This is may be due to the fact that adding an imperfection of the size of the shell thickness surpasses the limit of this structure to hold a specific imperfection.

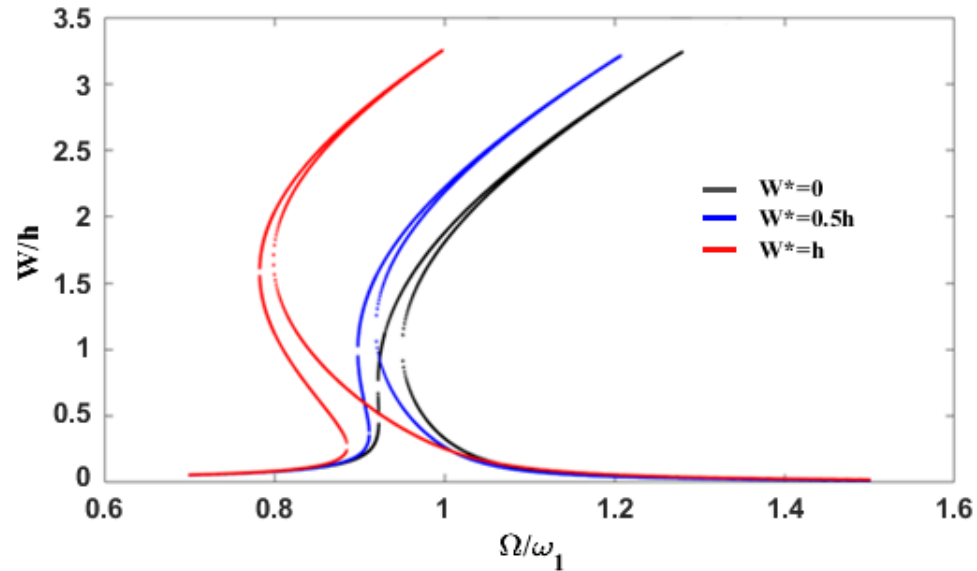


Figure 5.9. Effect of geometrical imperfection on the frequency response curve of a stiffened spherical shell ($R_x = R_y = 5\text{m}$, $a = b = 0.8\text{m}$, $h = 0.025\text{m}$, $K = 1$ and $\zeta = 0.01$) under uniformly distributed load $Q = 10^5\text{Pa}$.

In the first part of Chapter 5, the formulation of the problem was validated by Alijani and Amabili (2011), and an excellent agreement was obtained. Then a convergence study was done to highlight the importance of using multimode over the single-mode solution. The difference in the nonlinear response was remarkable. This chapter was ended by evaluating the effect of the uniform temperature rise and the influence of the geometrical imperfection of the amplitude-frequency curve.

6. Conclusion And Future Work

6.1 Conclusion

This dissertation consisted mainly of two parts. The first part was concerned with the nonlinear static and dynamic analysis of the imperfect stiffened functionally graded double-curved shell in a thermal environment using a single-mode solution. The nonlinear equations of motion were derived using a single-mode analysis in conjunction with the Galerkin's method. Closed-form solution of the amplitude-frequency response of an extended duffing equation with strong quadratic and cubic nonlinearities was obtained using He's method. Also, Lekhnitsky's technique was used to smear the effect of the stiffeners over the thickness of the shell. The influence of the imperfection, stiffeners, geometric parameters and power index variations was also studied. Since the shell was subjected to a thermal load, a pre buckling thermal analysis was done to calculate the critical temperature difference. Three types of temperature functions: uniform temperature; linear; and nonlinear temperature rise through the thickness were studied. All the results obtained here were compared and validated with previously published papers.

For the second part, the same problem was considered using multimode analysis. Chebyshev polynomials used to satisfy the essential boundary conditions. The energy functional was discretized by including several combinations of generalized coordinates. To solve the discretized equations of motion, the numerical XPPAUT software was used. Then a convergence study was done to highlight the importance of using multimode over the single-mode solution. It is, therefore, concluded that the nonlinear study of problems of thin-walled structures with even stiffeners is of paramount importance. We can also conclude that the difference between single-mode and multi-mode analyses could be very

significant for nonlinear problems in a thermal environment. Hence, multimode vibration analysis is necessary for structures of this nature. In addition, it is concluded that further study of FGM structures and the effect of temperature variations and imperfections on the nonlinear response of such structures are notable for the following two reasons. The first reason is that FGM structures are inherently nonlinear. The second reason is, due to the existence of the coupling between extension and bending, the FGM structures cannot be constructed flat; thus, it is necessary to consider the effect of imperfection.

6.2 Future Work

This dissertation can be extended, by perhaps using a higher-order shear deformation theory which may give more accuracy when it comes to thick double-curved shells. Airy stress functions can also be used to decrease the number of unknowns in the equations of motion.

Another extension of this work could be using isogrid and orthogrid stiffeners and finding a way to apply Lekhnitsky smeared technique to deal with structures that consist of these kinds of stiffeners. Also, the current thesis/project could be extended to different kinds of FGM structures, for example, considering those for which material properties vary in two different directions (x, y) or three different directions (x, y, z) than just along with the thickness (only z) direction.

Distribution of the material properties can be extended to change with respect to the length and width. Other future work would be studying the shell response to an impulsive load. In addition, an experimental test could also be considered as a future work to validate the numerical results. To perform any kind of experiments on functionally graded structures, 3D printing might be used. Furthermore, flutter analysis, fracture, fatigue, failure, and optimization of structures made of FGM could be studied.

REFERENCES

- Abe, A., Kobayashi, Y., & Yamada, G. (2019). One-to-One Internal Resonance of Symmetric Crossply Laminated Shallow Shells. *Journal of Applied Mechanics*, 68(4), 640-649.
- Alhazza, K. A. (2002). *Nonlinear Vibrations of Doubly Curved Cross-Ply Shallow Shells* (Doctoral Dissertation). Blacksburg, VA: Virginia Polytechnic Institute and State University.
- Alijani, F., Amabili, M., & Nejad, B. F. (2011). Thermal Effects on Nonlinear Vibrations of Functionally Graded Doubly Curved Shells Using Higher Order Shear Deformation Theory. *Composite Structures*, 93(10), 2541–53.
- Alijani, F., Amabili, M., Karagiozis, K., & Nejad, B. F. (2011). Nonlinear Vibrations of Functionally Graded Doubly Curved Shallow Shells. *Journal of Sound and Vibration* 330(7), 1432–54.
- Alijani, F., & Amabili, M. (2014). Effect of Thickness Deformation on Large-Amplitude Vibrations of Functionally Graded Rectangular Plates. *Composite Structures*, 113(1), 89–107.
- Amabili, M. (2004). Nonlinear Vibrations of Rectangular Plates with Different Boundary Conditions: Theory and Experiments. *Computers and Structures*, 82(31–32), 2587–2605.
- Bich, D. H., Dung, D. V., & Nam, V. H. (2012). Nonlinear Dynamical Analysis of Eccentrically Stiffened Functionally Graded Cylindrical Panels. *Composite Structures*, 94(8), 2465–73.
- Bich, D. H., Dung, D. V., & Nam, V. H. (2013). Nonlinear Dynamic Analysis of Eccentrically Stiffened Imperfect Functionally Graded Doubly Curved Thin Shallow Shells. *Composite Structures*, 96(3) 384–95.
- Bich, D. H. & Long, V. D. (2010). Non-Linear Dynamical Analysis of Imperfect Functionally Graded. *Vietnam Journal of Mechanics*, 32(1), 1–14.
- Bich, D. H., & Xuan, N. N. (2012). Nonlinear Vibration of Functionally Graded Circular Cylindrical Shells Based on Improved Donnell Equations. *Journal of Sound and Vibration*, 331(25), 5488–5501.
- Birman, V. (2011). *Plate Structures* (p. 65). Dordrecht: Springer Science & Business Media.

- Brush, D. O., & Almroth, B. O. (1975). *Buckling of Bars, Plates, and Shells*. New York, NY: McGraw-Hill.
- Bui, T. Q. et al. (2016). On the High Temperature Mechanical Behaviors Analysis of Heated Functionally Graded Plates Using FEM and a New Third-Order Shear Deformation Plate Theory. *Composites Part B: Engineering*, 92(6), 218–41.
- Cao, Z., & Tang, S. (2012). Natural Vibration of Functionally Graded Cylindrical Shells With Infinite and Finite Lengths. *Journal of Vibration and Acoustics*, 134(1), 67–78.
- Carrera, E., Brischetto, S., Cinefra, M., & Soave, M. (2011). Effects of Thickness Stretching in Functionally Graded Plates and Shells. *Composites Part B: Engineering*, 42(2), 123–33.
- Chern, Y. C., & Chao, C. C. (2000). Comparison of Natural Frequencies of Laminates By 3-D Theory, Part Ii: Curved Panels. *Journal of Sound and Vibration*, 230(5), 1009–30.
- Chia, C. Y. (1980). *Nonlinear Analysis of Plates*. New York, NY: McGraw-Hill.
- Chorfi, S. M., & Houmat, A. (2010). Non-Linear Free Vibration of a Functionally Graded Doubly-Curved Shallow Shell of Elliptical Plan-Form. *Composite Structures*, 92(10), 2573–81.
- Duc, D., Nguyen, & Khoa, N. D. (2017). Nonlinear Dynamic Analysis and Vibration of Eccentrically Stiffened S-FGM Elliptical Cylindrical Shells Surrounded on Elastic Foundations in Thermal Environments. *Thin-Walled Structures*, 117(4), 178–89.
- Duc, D., & Tung, H. V. (2010). Nonlinear Response of Pressure-Loaded Functionally Graded Cylindrical Panels with Temperature Effects. *Composite Structures*, 92(7), 1664–72.
- Duc, D. et al. (2016). Nonlinear Vibration and Dynamic Response of Imperfect Eccentrically Stiffened Shear Deformable Sandwich Plate with Functionally Graded Material in Thermal Environment. *Journal of Sandwich Structures and Materials*, 18(4), 445–73.
- Duc, D. (2013). Corrigendum to Nonlinear Dynamic Response of Imperfect Eccentrically Stiffened FGM Double Curved Shallow Shells on Elastic Foundation. *Composite Structures*, 102(99), 306–14.
- Duc, D., Bich, D. H., & Cong, P. H. (2016). Nonlinear Thermal Dynamic Response of Shear Deformable FGM Plates on Elastic Foundations. *Journal of Thermal Stresses*, 39(3), 278–97.

- Duc, D., & Quan, T. Q. (2012). Nonlinear Stability Analysis of Double-Curved Shallow Fgm Panels on Elastic Foundations in Thermal Environments. *Mechanics of Composite Materials*, 48(4), 435–48.
- Duc, D., & Quan, T. Q. (2013a). Nonlinear Dynamic Analysis of Imperfect Functionally Graded Material Double Curved Thin Shallow Shells with Temperature-Dependent Properties on Elastic Foundation. *Journal of Vibration and Control*, 21(4), 637–46.
- Duc, D., & Quan, T. Q. (2013b). Nonlinear Postbuckling of Imperfect Eccentrically Stiffened P-FGM Double Curved Thin Shallow Shells on Elastic Foundations in Thermal Environments. *Composite Structures*, 106, 590–600.
- Duc, D., & Quan, T. Q. (2014). Nonlinear Response of Imperfect Eccentrically Stiffened FGM Cylindrical Panels on Elastic Foundation Subjected to Mechanical Loads. *European Journal of Mechanics and Solids*, 46, 60–71.
- Dung, D. V., Duc, D., & Thiem, H. T. (2017). Dynamic Analysis of Imperfect FGM Circular Cylindrical Shells Rein- Forced by FGM Stiffener System Using Third Order Shear Deforma- Tion Theory in Term of Displacement Components. *Latin American Journal of Solids and Structures* 14(13), 1–39.
- Gil, A., Segura, J., & Temme, N. (2007). Chebyshev Expansions. In *Numerical Methods for Special Functions* (p. 51-70). Philadelphia, PA: Society for Industrial and Applied Mathematics.
- Gulshantaj, M. N.A., & Chakrabarti, A. (2013). Dynamic Response of Functionally Graded Skew Shell Panel. *Latin American Journal of Solids and Structures*, 10(6), 1243–66.
- Haddadpour, H., Mahmoudkhani, S., & Navazi, H. M. (2007). Free Vibration Analysis of Functionally Graded Cylindrical Shells Including Thermal Effects. *Thin-Walled Structures*, 45(6), 591–99.
- He, J. H. (2006). Some Asymptotic Methods For Strongly Nonlinear Equations. *International Journal of Modern Physics B*, 20(10), 1141–99.
- Hetnarski, R. B., (1987). *Thermal Stresses*. Amsterdam: North-Holland
- Cong, P. H., Anh, V. M., & Duc, D. (2017). Nonlinear Dynamic Response of Eccentrically Stiffened FGM Plate Using Reddy's TSDT in Thermal Environment. *Journal of Thermal Stresses*, 40(6), 704–32.
- Hashemi, H. S., Taher, H. R. D., Akhavan, H. & Omid, M. (2010). Free Vibration of Functionally Graded Rectangular Plates Using First-Order Shear Deformation Plate Theory. *Applied Mathematical Modelling*, 34(5), 1276–91.

- Huang, X. L., & Shen, H. S. (2004). Nonlinear Vibration and Dynamic Response of Functionally Graded Plates in Thermal Environments. *International Journal of Solids and Structures*, 41(9–10), 2403–27.
- Bich, H. D., Duc, D., & Quan, T. Q. (2014). Nonlinear Vibration of Imperfect Eccentrically Stiffened Functionally Graded Double Curved Shallow Shells Resting on Elastic Foundation Using the First Order Shear Deformation Theory. *International Journal of Mechanical Sciences*, 80, 16–28.
- Kar, V. R., & Panda, S. K. (2016). Geometrical Nonlinear Free Vibration Analysis of FGM Spherical Panel under Nonlinear Thermal Loading with TD and TID Properties. *Journal of Thermal Stresses*, 39(8), 942–59.
- Kar, V. R., & Panda, S. K. (2015). Free Vibration Responses of Temperature Dependent Functionally Graded Curved Panels under Thermal Environment. *Latin American Journal of Solids and Structures*, 12(11), 2006–24.
- Kar, V. R., & Panda, S. K. (2017). Large-Amplitude Vibration of Functionally Graded Doubly-Curved Panels Under Heat Conduction. *AIAA Journal*, 55(12), 1–11.
- Kawasaki, A., & Watanabe, R. (1997). Concept and P/M Fabrication of Functionally Gradient Materials. *Ceramics International*, 23(1), 73–83.
- Kiani, Y. (2016). Free Vibration of Functionally Graded Carbon Nanotube Reinforced Composite Plates Integrated with Piezoelectric Layers. *Computers and Mathematics with Applications*, 72(9), 2433–49.
- Kobayashi, Y., & Leissa, A. W. (1995). Large Amplitude Free Vibration of Thick Shallow Shells Supported by Shear Diaphragms. *International Journal of Non-Linear Mechanics*, 30(1), 57–66.
- Koizumi, M. (1997). FGM Activities in Japan. *Composites Part B: Engineering*, 28(1–2), 1–4.
- Lee, Y. Y., Zhao, X., & Reddy, J. N. (2010). Postbuckling Analysis of Functionally Graded Plates Subject to Compressive and Thermal Loads. *Computer Methods in Applied Mechanics and Engineering*, 199(25–28), 1645–53.
- Li, Q., Iu, V. P., & Kou, K. P. (2009). Three-Dimensional Vibration Analysis of Functionally Graded Material Plates in Thermal Environment. *Journal of Sound and Vibration*, 324(3–5), 733–50.
- Liew, K. M., Yang, J. & Wu, Y. F. (2006). Nonlinear Vibration of a Coating-FGM-Substrate Cylindrical Panel Subjected to a Temperature Gradient. *Computer Methods in Applied Mechanics and Engineering*, 195(9–12), 1007–26.

- Matsunaga, H. (2009). Free Vibration and Stability of Functionally Graded Circular Cylindrical Shells According to a 2D Higher-Order Deformation Theory. *Composite Structures*, 88(4), 519–31.
- Najafizadeh, M. M., Hasani, A., and Khazaeinejad, P. (2009). Mechanical Stability of Functionally Graded Stiffened Cylindrical Shells. *Applied Mathematical Modelling*, 33(2), 1151–57.
- Nemeth, M. P. (2011). *A Treatise on Equivalent-Plate Stiffnesses for Stiffened Laminated-Composite Plates and Plate-Like Lattices* (Report No. TP-216882). Hampton, VA: NASA Langley Research Center.
- Parandvar, H., & Farid, M. (2016). Large Amplitude Vibration of FGM Plates in Thermal Environment Subjected to Simultaneously Static Pressure and Harmonic Force Using Multimodal FEM. *Composite Structures*, 141, 163–71.
- Patel, B. P., Gupta, S. S., Loknath, M. S., & Kadu, C. P. (2005). Free Vibration Analysis of Functionally Graded Elliptical Cylindrical Shells Using Higher-Order Theory. *Composite Structures*, 69(3), 259–70.
- Pradhan, S. C., Loy, C. T., Lam, K. Y., & Reddy, J. N. (2000). Vibration Characteristics of Functionally Graded Cylindrical Shells under Various Boundary Conditions. *Applied Acoustics*, 61(1), 111–29.
- Pradyumna, S., & Nanda, N. (2013). Geometrically Nonlinear Transient Response of Functionally Graded Shell Panels with Initial Geometric Imperfection. *Mechanics of Advanced Materials and Structures*, 20(3), 217–26.
- Pradyumna, S., Nanda, N., & Bandyopadhyay, J. N. (2010). Geometrically Nonlinear Transient Analysis of Functionally Graded Shell Panels Using a Higher-Order Finite Element Formulation. *Mechanical Engineering*, 2(3), 39–51.
- Quan, T. Q., & Duc, N. D. (2017). Nonlinear Thermal Stability of Eccentrically Stiffened FGM Double Curved Shallow Shells. *Journal of Thermal Stresses*, 40(2), 211–36.
- Quan, T. Q., & Duc, N. D. (2016). Nonlinear Vibration and Dynamic Response of Shear Deformable Imperfect Functionally Graded Double-Curved Shallow Shells Resting on Elastic Foundations in Thermal Environments. *Journal of Thermal Stresses*, 39(4), 437–59.
- Rafiee, M., Mohammadi, M., Sobhani B. A., & Yaghoobi, M. (2013). Nonlinear Free and Forced Thermo-Electro-Aero-Elastic Vibration and Dynamic Response of Piezoelectric Functionally Graded Laminated Composite Shells, Part I: Theory and Analytical Solutions. *Composite Structures*, 103, 179–87.

- Rahimi, G. H., Ansari, R., & Hemmatnezhad, M. (2011). Vibration of Functionally Graded Cylindrical Shells with Ring Support. *Scientia Iranica*, 18(6), 1313–20.
- Reddy, J. N., & Chin, C. D. (1998). Thermomechanical Analysis of Functionally Graded Cylinders and Plates. *Journal of Thermal Stresses*, 21(6), 593–626.
- Reddy, J. N. (2000). Analysis of Functionally Graded Plates. *International Journal For Numerical Methods In Engineering*, 47(6), 663–84.
- Reddy, J. N. (2003). *Mechanics of Laminated Composite Plates and Shells: Theory and Analysis*. New York, NY: CRC Press.
- Santos, H., Soares, C. M. M., & Reddy, J. N. (2009). A Semi-Analytical Finite Element Model for the Analysis of Cylindrical Shells Made of Functionally Graded Materials. *Composite Structures*, 91(4), 427–32.
- Sepiani, H. A., Rastgoo, A., Ebrahimi, F., & Arani, A. G. (2010). Vibration and Buckling Analysis of Two-Layered Functionally Graded Cylindrical Shell, Considering the Effects of Transverse Shear and Rotary Inertia. *Materials and Design*, 31(3), 1063–69.
- Shah, A. G., Mahmood, T., & Naeem, M. N. (2009). Vibrations of FGM Thin Cylindrical Shells with Exponential Volume Fraction Law. *Applied Mathematics and Mechanics*, 30(5), 607–15.
- Shen, H., et al. (2015). Nonlinear Vibration of FGM Doubly Curved Panels Resting on Leastic Foundations in Thermla Environments. *Aerospace Science and Technology*, 47, 434–46.
- Shen, H., & Wang, H. (2013). Thermal Postbuckling of Functionally Graded Fiber Reinforced Composite Cylindrical Shells Surrounded by an Elastic Medium. *Composite Structures*, 102(8), 250–60.
- Shen, H. (2012). Nonlinear Vibration of Shear Deformable FGM Cylindrical Shells Surrounded by an Elastic Medium. *Composite Structures*, 94(3), 1144–54.
- Shen, H., & Wang, H. (2014). Nonlinear Vibration of Shear Deformable FGM Cylindrical Panels Resting on Elastic Foundations in Thermal Environments. *Composites Part B: Engineering*, 60, 167–77.
- Sheng, G. G., & Wang, X. (2013). Nonlinear Vibration Control of Functionally Graded Laminated Cylindrical Shells. *Composites Part B: Engineering*, 52, 1–10.
- Singh, V. K., & Panda, S. K. (2014). Nonlinear Free Vibration Analysis of Single/Doubly Curved Composite Shallow Shell Panels. *Thin-Walled Structures*, 85, 341–49.

- Strozzi, M., & Pellicano, F. (2013). Nonlinear Vibrations of Functionally Graded Cylindrical Shells. *Thin-Walled Structures*, 67, 63–77.
- Sundararajan, N., Prakash, T., & Ganapathi, M. (2005). Nonlinear Free Flexural Vibrations of Functionally Graded Rectangular and Skew Plates under Thermal Environments. *Finite Elements in Analysis and Design*, 42(2), 152–68.
- Tornabene, F., Liverani, A., & Caligiana, G. (2011). FGM and Laminated Doubly Curved Shells and Panels of Revolution with a Free-Form Meridian: A 2-D GDQ Solution for Free Vibrations. *International Journal of Mechanical Sciences*, 53(6), 446–70.
- Tornabene, F., Viola, E., & Inman, D. J. (2009). 2-D Differential Quadrature Solution for Vibration Analysis of Functionally Graded Conical, Cylindrical Shell and Annul Plate Structures. *Journal of Sound and Vibration*, 328(3), 259–90.
- Tung, H. V., & Duc, N. D. (2010). Nonlinear Analysis of Stability for Functionally Graded Plates under Mechanical and Thermal Loads. *Composite Structures*, 92(5), 1184–91.
- Tung, H. V., & Duc, N. D. (2014). Nonlinear Response of Shear Deformable FGM Curved Panels Resting on Elastic Foundations and Subjected to Mechanical and Thermal Loading Conditions. *Applied Mathematical Modelling*, 38(11–12), 2848–66.
- Wattanasakulpong, N., & Chaikittiratana, A. (2015). An Analytical Investigation on Free Vibration of FGM Doubly Curved Shallow Shells with Stiffeners under Thermal Environment. *Aerospace Science and Technology*, 40, 181–90.
- Xiang, S., Kang, G., & Liu, Y. (2014). A Nth-Order Shear Deformation Theory for Natural Frequency of the Functionally Graded Plates on Elastic Foundations. *Composite Structures*, 111, 224–31.
- Yang, J., & Shen, H. (2002). Vibration Characteristics and Transient Response of Shear-Deformable Functionally Graded Plates in Thermal Environments. *Journal of Sound and Vibration*, 255(3), 579–602.
- Yang, J., & Shen, H. (2003). Free Vibration and Parametric Resonance of Shear Deformable Functionally Graded Cylindrical Panels. *Journal of Sound and Vibration*, 261(5), 871–93.
- Zhang, W., Hao, Y. X., & Yang, J. (2012). Nonlinear Dynamics of FGM Circular Cylindrical Shell with Clamped-Clamped Edges. *Composite Structures*, 94(3), 1075–86.

Zhao, X., & Liew, K. M. (2009). Geometrically Nonlinear Analysis of Functionally Graded Shells. *International Journal of Mechanical Sciences*, 51(2), 131–44.

Zhu, P., Zhang, L. W., & Liew, K. M. (2014). Geometrically Nonlinear Thermomechanical Analysis of Moderately Thick Functionally Graded Plates Using a Local Petrov-Galerkin Approach with Moving Kriging Interpolation. *Composite Structures*, 107(1), 298–314.

APPENDIX

L_{ij} ($i = 1, 2, 3, 4, 5; j = 1, 2, 3, 4, 5, 6$) are the linear operator and NL_i ($i = 1, 2, \dots, 18$), are the nonlinear operators of the governing equations and are listed below:

$$L_{11}(u_0) = (A_{66} + C_0 B_{66}) \frac{\partial^2 u_0}{\partial y^2} + \left(A_{11} + \frac{E_x A}{d_x} \right) \frac{\partial^2 u_0}{\partial x^2} - \left(A_{55} + \frac{G_x A_x}{d_x} \right) \frac{k_s u_0}{R_x^2}$$

$$L_{12}(v_0) = (A_{12} + A_{66} + C_0 B_{66}) \frac{\partial^2 v_0}{\partial x \partial y}$$

$$L_{13}(w_0) = \frac{1}{R_x} \left(A_{11} + \frac{E_x A_x}{d_x} \right) \frac{\partial w_0}{\partial x} + \frac{A_{12}}{R_y} \frac{\partial w_0}{\partial x} + \left(A_{55} + \frac{G_x A_x}{d_x} \right) \frac{k_s}{R_x} \frac{\partial w_0}{\partial x}$$

$$L_{14}(\psi_x) = (B_{66} + C_0 D_{66}) \frac{\partial^2 \psi_x}{\partial y^2} + \left(B_{11} + \frac{E_x A e_x}{d_x} \right) \frac{\partial^2 \psi_x}{\partial x^2} + \left(A_{55} + \frac{G_x A_x}{d_x} \right) \frac{k_s \psi_x}{R_x} \\ + \frac{C_0}{2} \left(\frac{G_x J_x}{d_x} + \frac{G_y J_y}{d_y} \right) \frac{\partial^2 \psi_x}{\partial y^2}$$

$$L_{15}(\psi_y) = (B_{12} + B_{66} + C_0 D_{66}) \frac{\partial^2 \psi_y}{\partial x \partial y} + \frac{C_0}{2} \left(\frac{G_x J_x}{d_x} + \frac{G_y J_y}{d_y} \right) \frac{\partial^2 \psi_y}{\partial x \partial y}$$

$$L_{16}(w^*) = \left(A_{55} + \frac{G_x A_x}{d_x} \right) \frac{k_s}{R_x} \frac{\partial w^*}{\partial x}$$

$$NL_1(w_0) = (A_{66} + C_0 B_{66}) \frac{\partial w_0}{\partial x} \frac{\partial^2 w_0}{\partial y^2} + (A_{12} + A_{66} + C_0 B_{66}) \frac{\partial w_0}{\partial y} \frac{\partial^2 w_0}{\partial x \partial y} \\ + \left(A_{11} + \frac{E_x A_x}{d_x} \right) \frac{\partial w_0}{\partial x} \frac{\partial^2 w_0}{\partial x^2}$$

$$NL_2(w_0, w^*) = (A_{66} + C_0 B_{66}) \left(\frac{\partial^2 w^*}{\partial y^2} \frac{\partial w_0}{\partial x} + \frac{\partial^2 w_0}{\partial y^2} \frac{\partial w^*}{\partial x} \right) \\ + (A_{12} + A_{66} + C_0 B_{66}) \left(\frac{\partial w_0}{\partial y} \frac{\partial^2 w^*}{\partial x \partial y} + \frac{\partial w^*}{\partial y} \frac{\partial^2 w_0}{\partial x \partial y} \right) \\ + \left(A_{11} + \frac{E_x A_x}{d_x} \right) \left(\frac{\partial w_0}{\partial x} \frac{\partial^2 w^*}{\partial x^2} + \frac{\partial w^*}{\partial x} \frac{\partial^2 w_0}{\partial x^2} \right)$$

$$L_{21}(u_0) = (A_{21} + A_{66} - C_0 B_{66}) \frac{\partial^2 u_0}{\partial x \partial y}$$

$$L_{22}(v_0) = (A_{66} - C_0 B_{66}) \frac{\partial^2 v_0}{\partial x^2} + \left(A_{22} + \frac{E_y A_y}{d_y} \right) \frac{\partial^2 v_0}{\partial y^2} - \left(A_{44} + \frac{G_y A_y}{d_y} \right) \frac{k_s v_0}{R_y^2}$$

$$L_{23}(w_0) = \frac{1}{R_y} \left(A_{22} + \frac{E_y A_y}{d_y} \right) \frac{\partial w_0}{\partial y} + \frac{A_{21}}{R_x} \frac{\partial w_0}{\partial y} + \left(A_{44} + \frac{G_y A_y}{d_y} \right) \frac{k_s}{R_y} \frac{\partial w_0}{\partial y}$$

$$L_{24}(\psi_x) = (B_{21} + B_{66} - C_0 D_{66}) \frac{\partial^2 \psi_x}{\partial x \partial y} - \frac{C_0}{2} \left(\frac{G_x J_x}{d_x} + \frac{G_y J_y}{d_y} \right) \frac{\partial^2 \psi_x}{\partial x \partial y}$$

$$L_{25}(\psi_y) = (B_{66} - C_0 D_{66}) \frac{\partial^2 \psi_y}{\partial x^2} + \left(B_{22} + \frac{E_y A_y e_y}{d_y} \right) \frac{\partial^2 \psi_y}{\partial y^2} + \left(A_{44} + \frac{G_y A_y}{d_y} \right) \frac{k_s \psi_y}{R_y} \\ - \frac{C_0}{2} \left(\frac{G_x J_x}{d_x} + \frac{G_y J_y}{d_y} \right) \frac{\partial^2 \psi_y}{\partial x^2}$$

$$L_{26}(w^*) = \left(A_{44} + \frac{G_y A_y}{d_y} \right) \frac{k_s}{R_y} \frac{\partial w^*}{\partial y}$$

$$NL_3(w_0) = (A_{66} - C_0 B_{66}) \frac{\partial w_0}{\partial y} \frac{\partial^2 w_0}{\partial x^2} + (A_{21} + A_{66} - C_0 B_{66}) \frac{\partial w_0}{\partial x} \frac{\partial^2 w_0}{\partial x \partial y} \\ + \left(A_{22} + \frac{E_y A_y}{d_y} \right) \frac{\partial w_0}{\partial y} \frac{\partial^2 w_0}{\partial y^2}$$

$$NL_4(w_0, w^*) = (A_{66} - C_0 B_{66}) \left(\frac{\partial w^*}{\partial y} \frac{\partial^2 w_0}{\partial x^2} + \frac{\partial w_0}{\partial y} \frac{\partial^2 w^*}{\partial x^2} \right) \\ + (A_{21} + A_{66} - C_0 B_{66}) \left(\frac{\partial w^*}{\partial x} \frac{\partial^2 w_0}{\partial x \partial y} + \frac{\partial w_0}{\partial x} \frac{\partial^2 w^*}{\partial x \partial y} \right) \\ \left(A_{22} + \frac{E_y A_y}{d_y} \right) \left(\frac{\partial w_0}{\partial y} \frac{\partial^2 w^*}{\partial y^2} + \frac{\partial w^*}{\partial y} \frac{\partial^2 w_0}{\partial y^2} \right)$$

$$L_{31}(u_0) = -\frac{1}{R_x} \left(A_{11} + \frac{E_x A_x}{d_x} \right) \frac{\partial u_0}{\partial x} - \left(\frac{k_s A_{55}}{R_x} + \frac{k_s G_x A_x}{R_x d_x} + \frac{A_{21}}{R_y} \right) \frac{\partial u_0}{\partial x}$$

$$L_{32}(v_0) = -\frac{1}{R_y} \left(A_{22} + \frac{E_y A_y}{d_y} \right) \frac{\partial v_0}{\partial y} - \left(\frac{k_s A_{44}}{R_y} + \frac{k_s G_y A_y}{R_y d_y} + \frac{A_{12}}{R_x} \right) \frac{\partial v_0}{\partial y}$$

$$L_{33}(w_0) = -\left(A_{11} + \frac{E_x A_x}{d_x} \right) \frac{w_0}{R_x^2} - \left(A_{22} + \frac{E_y A_y}{d_y} \right) \frac{w_0}{R_y^2} - 2 \frac{A_{12} w_0}{R_x R_y} \\ + \left(k_s A_{44} + \frac{k_s G_y A_y}{d_y} \right) \frac{\partial^2 w_0}{\partial y^2} + \left(k_s A_{55} + \frac{k_s G_x A_x}{d_x} \right) \frac{\partial^2 w_0}{\partial x^2} \\ - (\Phi_{1x}^{Shell+T} + \Phi_{1x}^{Stiff+T}) \frac{\partial^2 w_0}{\partial x^2} - (\Phi_{1y}^{Shell+T} + \Phi_{1y}^{Stiff+T}) \frac{\partial^2 w_0}{\partial y^2}$$

$$L_{34}(\psi_x) = \left(k_s A_{55} + \frac{k_s G_x A_x}{d_x} \right) \frac{\partial \psi_x}{\partial x} - \left(\frac{B_{11}}{R_x} + \frac{E_x A_x e_x}{R_x d_x} + \frac{B_{21}}{R_y} \right) \frac{\partial \psi_x}{\partial x}$$

$$L_{35}(\psi_y) = \left(k_s A_{44} + \frac{k_s G_y A_y}{d_y} \right) \frac{\partial \psi_y}{\partial y} - \left(\frac{B_{22}}{R_y} + \frac{E_y A_y e_y}{R_y d_y} + \frac{B_{12}}{R_x} \right) \frac{\partial \psi_y}{\partial y}$$

$$L_{36}(w^*) = \left(k_s A_{44} + \frac{k_s G_y A_y}{d_y} \right) \frac{\partial^2 w^*}{\partial y^2} + \left(k_s A_{55} + \frac{k_s G_x A_x}{d_x} \right) \frac{\partial^2 w^*}{\partial x^2} \\ - (\Phi_{1x}^{Shell+T} + \Phi_{1x}^{Stiff+T}) \frac{\partial^2 w^*}{\partial x^2} - (\Phi_{1y}^{Shell+T} + \Phi_{1y}^{Stiff+T}) \frac{\partial^2 w^*}{\partial y^2}$$

$$L_{37}(\Phi) = \frac{\Phi_{1x}^{Shell+T}}{R_x} + \frac{\Phi_{1y}^{Shell+T}}{R_y} + \frac{\Phi_{1x}^{Stiff+T}}{R_x} + \frac{\Phi_{1y}^{Stiff+T}}{R_y}$$

$$NL_5(w_0) = \frac{A_{21} w_0}{R_x} \frac{\partial^2 w_0}{\partial y^2} + \frac{w_0}{R_y} \left(A_{22} + \frac{E_y A_y}{d_y^T} \right) \frac{\partial^2 w_0}{\partial y^2} + \frac{3}{2} \left(A_{22} + \frac{E_y A_y}{d_y} \right) \frac{\partial^2 w_0}{\partial y^2} \left(\frac{\partial w_0}{\partial y} \right)^2 \\ + (2A_{12} + 4A_{66}) \frac{\partial w_0}{\partial x} \frac{\partial w_0}{\partial y} \frac{\partial^2 w_0}{\partial x \partial y} + \frac{3}{2} \left(A_{11} + \frac{E_x A_x}{d_x} \right) \frac{\partial^2 w_0}{\partial x^2} \left(\frac{\partial w_0}{\partial x} \right)^2 \\ + \left(\frac{1}{2} A_{21} + A_{66} \right) \frac{\partial^2 w_0}{\partial y^2} \left(\frac{\partial w_0}{\partial x} \right)^2 + \frac{w_0}{R_x} \left(A_{11} + \frac{E_x A_x}{d_x} \right) \frac{\partial^2 w_0}{\partial x^2} \\ + \frac{A_{12} w_0}{R_y} \frac{\partial^2 w_0}{\partial x^2} + \left(\frac{1}{2} A_{12} + A_{66} \right) \frac{\partial^2 w_0}{\partial x^2} \left(\frac{\partial w_0}{\partial y} \right)^2 + \frac{A_{12}}{2R_x} \left(\frac{\partial w_0}{\partial y} \right)^2 \\ + \frac{1}{2R_y} \left(A_{22} + \frac{E_y A_y}{d_y} \right) \left(\frac{\partial w_0}{\partial y} \right)^2 + \frac{1}{2R_x} \left(A_{11} + \frac{E_x A_x}{d_x} \right) \left(\frac{\partial w_0}{\partial x} \right)^2 \\ + \frac{A_{12}}{2R_y} \left(\frac{\partial w_0}{\partial x} \right)^2$$

$$NL_6(w_0, u_0) = A_{21} \frac{\partial u_0}{\partial x} \frac{\partial^2 w_0}{\partial y^2} + A_{66} \frac{\partial w_0}{\partial x} \frac{\partial^2 u_0}{\partial y^2} + (A_{21} + A_{66}) \frac{\partial w_0}{\partial y} \frac{\partial^2 u_0}{\partial x \partial y} \\ + 2A_{66} \frac{\partial u_0}{\partial y} \frac{\partial^2 w_0}{\partial x \partial y} + \left(A_{11} + \frac{E_x A_x}{d_x} \right) \left(\frac{\partial u_0}{\partial x} \frac{\partial^2 w_0}{\partial x^2} + \frac{\partial w_0}{\partial x} \frac{\partial^2 u_0}{\partial x^2} \right)$$

$$NL_7(w_0, v_0) = A_{21} \frac{\partial v_0}{\partial y} \frac{\partial^2 w_0}{\partial x^2} + A_{66} \frac{\partial w_0}{\partial y} \frac{\partial^2 v_0}{\partial x^2} + (A_{12} + A_{66}) \frac{\partial w_0}{\partial x} \frac{\partial^2 v_0}{\partial x \partial y} \\ + 2A_{66} \frac{\partial v_0}{\partial x} \frac{\partial^2 w_0}{\partial x \partial y} + \left(A_{22} + \frac{E_y A_y}{d_y} \right) \left(\frac{\partial v_0}{\partial y} \frac{\partial^2 w_0}{\partial y^2} + \frac{\partial w_0}{\partial y} \frac{\partial^2 v_0}{\partial y^2} \right)$$

$$NL_8(w_0, \psi_x) = B_{21} \frac{\partial \psi_x}{\partial x} \frac{\partial^2 w_0}{\partial y^2} + B_{66} \frac{\partial w_0}{\partial x} \frac{\partial^2 \psi_x}{\partial y^2} + 2B_{66} \frac{\partial \psi_x}{\partial y} \frac{\partial^2 w_0}{\partial x \partial y}$$

$$\begin{aligned}
& + (B_{21} + B_{66}) \frac{\partial w_0}{\partial y} \frac{\partial^2 \psi_x}{\partial x \partial y} + \left(B_{11} + \frac{E_x A_x e_x}{d_x} \right) \left(\frac{\partial \psi_x}{\partial x} \frac{\partial^2 w_0}{\partial x^2} + \frac{\partial w_0}{\partial x} \frac{\partial^2 \psi_x}{\partial x^2} \right) \\
NL_9(w_0, \psi_y) = & B_{12} \frac{\partial \psi_y}{\partial y} \frac{\partial^2 w_0}{\partial x^2} + B_{66} \frac{\partial w_0}{\partial y} \frac{\partial^2 \psi_y}{\partial x^2} + 2B_{66} \frac{\partial \psi_y}{\partial x} \frac{\partial^2 w_0}{\partial x \partial y} \\
& + (B_{12} + B_{66}) \frac{\partial w_0}{\partial x} \frac{\partial^2 \psi_y}{\partial x \partial y} \\
& + \left(B_{22} + \frac{E_y A_y e_y}{d_y} \right) \left(\frac{\partial \psi_y}{\partial y} \frac{\partial^2 w_0}{\partial y^2} + \frac{\partial w_0}{\partial y} \frac{\partial^2 \psi_y}{\partial y^2} \right)
\end{aligned}$$